

The Stability of Monoclonal Antibodies

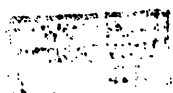
Andrew David Heron

Thesis presented for the degree of Doctor of Philosophy

Department of Chemistry

University of Glasgow

October, 1999



ProQuest Number: 13834088

All rights reserved

INFORMATION TO ALL USERS

The quality of this reproduction is dependent upon the quality of the copy submitted.

In the unlikely event that the author did not send a complete manuscript and there are missing pages, these will be noted. Also, if material had to be removed, a note will indicate the deletion.



ProQuest 13834088

Published by ProQuest LLC (2019). Copyright of the Dissertation is held by the Author.

All rights reserved.

This work is protected against unauthorized copying under Title 17, United States Code
Microform Edition © ProQuest LLC.

ProQuest LLC.
789 East Eisenhower Parkway
P.O. Box 1346
Ann Arbor, MI 48106 – 1346

GLASGOW
UNIVERSITY
LIBRARY

11762 (Copy 1)

Acknowledgements

I would like to thank my supervisors Alan Cooper and Ulla Lashmar for their help and guidance over the past three years. I must also thank Nick Price and Sharon Kelly at the University of Stirling for their circular dichroism work, without which the data presented in this thesis would not have been possible. Thanks to Sarah Barron, Lindsay McDermott, Margaret Nutley, Samantha Rutherford and Tennie Videler for their help, interest, friendship and laughs. Many thanks also to Glaxo Wellcome for generously funding my three years of research. And finally, to mum and Janey, thank you for your constant support, encouragement and of course patience.

Abstract

The Stability of Monoclonal Antibodies

Monoclonal antibodies (mAbs) are antibodies which are homogeneous and are of constant specificity and affinity. These properties make them ideal targets for rational drug design as molecular biology techniques allows the therapy to be genetically designed to fit the disease or condition, but, the inherent instability and aggregation propensity of such protein drugs poses serious problems for the pharmaceutical industry. With these problems in mind, the stability of mAbs in solution has been extensively studied using a range of biophysical techniques. With a view to correlating thermal unfolding data with protein drug shelf-life, differential scanning calorimetry (DSC) was used to study the thermal unfolding of three mAbs (Campath-1H, 4162W94 and 1209W95). It was found that each of the antibodies unfolds irreversibly and, by complementing DSC results with results from circular dichroism (CD) and intrinsic tryptophan fluorescence spectroscopy, we show all three mAbs unfold by firstly undergoing a small change in tertiary structure which is then followed by, at a higher temperature, major changes in both tertiary and secondary structure after which all structure is lost. Kinetic analysis of these irreversible processes over a range of pH and DSC scan rates resulted in the calculation of the activation energy (E_A) and rate constants of unfolding. Extrapolation of these rate constants to physiological conditions afforded an estimate of drug shelf-life which we have shown is relevant only when thermal unfolding is the only reaction resulting in protein denaturation. The effect of various additives on the thermal unfolding of the antibodies has also been studied using both DSC and fluorescence spectroscopy, in particular fluorescence quenching techniques and the use of the extrinsic fluorescent probe ANS (8-anilino-1-naphthalene sulfonic acid). These studies revealed that mannitol exerts a strong stabilising influence i.e. increases the mean unfolding temperature (T_m) whereas cyclodextrins decrease the T_m and are therefore considered destabilising additives. Cyclodextrins also prevent gross thermal aggregation of the mAbs possibly as a result of binding to exposed hydrophobic amino acid residues and masking hydrophobic patches which are indicated in aggregate formation.

Contents

Acknowledgements		i
Abstract		ii
Contents		iii
Tables		v
Figures		vi
Abbreviations		ix
Chapter 1	Introduction	1
	1.1 Aims of Thesis	2
	1.2 Introduction	3
	1.3 Summary of the Immune Response	3
	1.4 Structure of Antibodies	4
	1.5 What are Monoclonal Antibodies?	10
	1.6 Stability of Monoclonal Antibodies	14
	1.7 DSC and Pharmaceuticals	15
Chapter 2	Materials and Methods	17
	2.1 Reagents used	18
	2.2 Differential Scanning Calorimetry	20
	2.3 Protein analysis	29
	2.4 Fluorescence Spectroscopy	30
	2.5 Circular Dichroism	35
	2.6 Induced aggregation experiments	37
	2.7 Long-term storage sample preparation	38
	2.8 Isothermal Calorimetry	38
Chapter 3	Thermal Unfolding of Monoclonal Antibodies	40
	3.1 Introduction	41
	3.2 Results	42
	3.3 Discussion	47

Chapter 4	Kinetic Analysis of Unfolding	69
	4.1 Introduction	70
	4.2 Results	72
	4.3 Discussion	75
Chapter 5	Formulation and the Effects of Additives and Adjuvants	92
	5.1 Introduction	93
	5.2 Results	97
	5.3 Discussion	104
Chapter 6	Induction and Kinetics of mAb Aggregation	123
	6.1 Introduction	124
	6.2 Results	126
	6.3 Discussion	129
Chapter 7	Further Observations	137
	7.1 Introduction	138
	7.2 Results	140
	7.3 Discussion	143
Chapter 8	General conclusions	153
References		156

Tables

Table 2.1	Summary of extinction coefficients used	30
Table 3.1	T_m values for Campath-1H over the 3.0-8.0 pH range	50
Table 3.2	T_m values for 4162W94 over the 3.0-6.0 pH range	50
Table 3.3	T_m values for 1209W95 at pH 6.6 and 8.0	50
Table 4.1	DSC curve fitting data for Campath-1H (pH 3 CBS)	78
Table 4.2	DSC curve fitting data for Campath-1H (pH 4 ABS)	79
Table 4.3	DSC curve fitting data for Campath-1H (pH 5 CBS)	80
Table 4.4	DSC curve fitting data for 4162W94 (pH 3 CBS)	81
Table 4.5	DSC curve fitting data for 1209W95 (pH 6.6 ABS)	82
Table 4.6	Concentration dependence of DSC curve fitting data for Campath-1H (pH 6 CBS)	82
Table 4.7	Activation energies for the thermal denaturation of Campath-1H, 4162W94 and 1209W95	83
Table 5.1	Effect of buffer pH on accessibility of Trp residues	107
Table 5.2	Short-term effects of additives on the T_m of the main endothermic transition of Campath-1H, 4162W94 and 1209W95	108
Table 5.3	Long-term effects of additives on the T_m of the main endothermic transition of Campath-1H and 1209W95	109
Table 5.4	Long-term effect of formulation additives on the accessibility of Trp residues within Campath-1H and 1209W95	110
Table 5.5	Effect of additives on the ANS binding of Campath-1H and 1209W95	111
Table 5.6	Activation energies for the thermal denaturation of Campath-1H in the presence of methyl- β -cyclodextrin	112
Table 5.7	Effect of HPCD concentration on the T_m values of Campath-1H	113
Table 6.1	Activation energies for the thermal denaturation of Campath-1H in the absence and presence of preformed aggregate	131

Figures

Figure 1.1	Basic structure of an antibody molecule	5
Figure 1.2	The immunoglobulin fold	8
Figure 1.3	Cartoon illustrating the structure of the IgG molecule	9
Figure 3.1a	Raw DSC data for Campath-1H in a range of pH conditions	51
Figure 3.1b	Variation of Campath-1H T_m values with pH	52
Figure 3.2	Raw DSC data for 4162W94 in a range of pH conditions	53
Figure 3.3	Raw DSC data for 1209W95 in pH 6.6 and 8.0	54
Figure 3.4	Raw DSC results of successive annealing of Campath-1H	55
Figure 3.5	Raw DSC results of successive annealing of 4162W94	56
Figure 3.6	Three successive DSC scans of 4162W94	57
Figure 3.7a	Near-UV CD spectra of Campath-1H recorded at a range of temperatures	58
Figure 3.7b	Far-UV CD spectra of Campath-1H recorded at a range of temperatures	59
Figure 3.8a	Near-UV CD spectra of 4162W94 recorded at a range of temperatures	60
Figure 3.8b	Far-UV CD spectra of 4162W94 recorded at a range of temperatures	61
Figure 3.9a	Near-UV CD spectra of 1209W95 recorded at a range of temperatures	62
Figure 3.9b	Far-UV CD spectra of 1209W95 recorded at a range of temperatures	63
Figure 3.10	Fluorescence intensity of Campath-1H as a function of temperature	64
Figure 3.11	Fluorescence intensity of 4162W94 as a function of temperature	65
Figure 3.12a	Effect of Campath-1H thermal denaturation on fluorescence of ANS	66
Figure 3.12b	Effect of 4162W94 thermal denaturation on fluorescence of ANS	67

Figure 3.12c	Effect of 1209W95 thermal denaturation on fluorescence of ANS	68
Figure 4.1	Effect of scan rate on the DSC trace of Campath-1H	84
Figure 4.2	Effect of concentration on the thermal unfolding of Campath-1H	85
Figure 4.3	Plots corresponding to equations 2.15-2.17 for Campath-1H (pH 3)	86
Figure 4.4	Plot of extrapolated half-life of Campath-1H at 20 °C	87
Figure 4.5a	Plot of $\langle\Delta H\rangle$ calculated for Campath-1H (pH 3) at six different scan rates, as a function of temperature	88
Figure 4.5b	Exponential plots of $\langle\Delta H\rangle$ versus $1/v$	89
Figure 4.6	Plot of $\langle\Delta H\rangle_{rev}$ with respect to temperature for Campath-1H (pH 3)	90
Figure 4.7	$C_{p\ exc}$ profile of Campath-1H (pH 3) at infinite scanning rate with respect to temperature.	91
Figure 5.1	Stern-Volmer plot of results of succinimide quenching of Campath-1H (pH 6)	114
Figure 5.2a	Stern-Volmer plot of results of acrylamide quenching of Campath-1H (pH 6)	115
Figure 5.2b	Modified Stern-Volmer plot of results of acrylamide quenching of Campath-1H (pH 6)	116
Figure 5.3	Reducing 15% SDS PAGE of equimolar amounts of Campath-1H in pH 7.2 PBS and pH 3 CBS	117
Figure 5.4	Raw DSC data showing the effects of HPCD concentration on Campath-1H	118
Figure 5.5	Effect of scan rate on the DSC trace of Campath-1H (pH 6 CBS, 40% (w/w) HPCD)	119
Figure 5.6	Raw DSC data showing the effects of HPCD concentration on 4162W94	120
Figure 5.7a	Raw DSC data showing the effects of DEAE-dextran on the thermal unfolding of Campath-1H	121
Figure 5.7b	Raw DSC data showing the effects of DEAE-dextran/lactitol combinations on the thermal unfolding of Campath-1H	122

Figure 6.1a	Effect of 0.5 and 1.0% (v/v) preformed aggregate solution on the turbidity of Campath-1H solutions as measured by absorbance at 320 nm	132
Figure 6.1b	Effect of 0.5 and 1.0% (v/v) preformed aggregate solution on the turbidity of Campath-1H solutions as measured by absorbance at 400 nm	133
Figure 6.2a	Effect of 5.0 and 10.0% (v/v) preformed aggregate solution on the turbidity of Campath-1H solutions as measured by absorbance at 320 nm	134
Figure 6.2b	Effect of 5.0 and 10.0% (v/v) preformed aggregate solution on the turbidity of Campath-1H solutions as measured by absorbance at 400 nm	135
Figure 6.3	Effect of preformed aggregate on the rate constants for the thermal denaturation of Campath-1H	136
Figure 7.1	GdmHCl unfolding curves for Campath-1H, 4162W94 and 1209W95 as monitored by CD	145
Figure 7.2	GdmHCl unfolding curves for Campath-1H, 4162W94 and 1209W95 as monitored by fluorescence spectroscopy	146
Figure 7.3	Stern-Volmer plot of results of succinimide quenching of Campath-1H (pH 6) in the presence and absence of 0.5 M GdmHCl	147
Figure 7.4	Raw DSC data showing the effect of 0.5 M urea on the T_m of Campath-1H (pH 6)	148
Figure 7.5	Urea unfolding curve for Campath-1H (pH 6) as monitored by CD	149
Figure 7.6	Raw isothermal calorimetry data for Campath-1H (pH 6) showing temperature dependence of traces	150
Figure 7.7	Raw isothermal calorimetry data for Campath-1H (pH 6) showing concentration dependence of traces	151
Figure 7.8	Normalized isothermal calorimetry data for Campath-1H (pH 6) showing concentration dependence of traces	152

Abbreviations

ABS	acetate buffered saline
ANS	8-anilino-1-naphthalene-sulfonic acid
Asp	asparagine
CBS	citrate buffered saline
CD	circular dichroism
CD4	cluster differentiation 4
CDR	complementarity determining regions
DSC	differential scanning calorimetry
E_A	activation energy
EDTA	ethylenediaminetetraacetic acid
ELISA	enzyme-linked immunosorbent assay
FDA	Federal Drugs Administration
GdmHCl	guanidine hydrochloride
GPI	glycosylphosphatidylinositol
HAMA	human anti-mouse antibody
HPCD	hydroxypropyl- β -cyclodextrin
Ig	immunoglobulin
K_{sv}	Stern-Volmer constant
Lys	lysine
mAb	monoclonal antibody
MALDI TOF MS	matrix-assisted laser desorption ionization time-of-flight mass spectrometry
MCD	methyl- β -cyclodextrin
NHL	non-Hodgkin lymphoma
OD	optical density
P188	Ploxamer 188
PBS	phosphate buffered saline
$t_{1/2}$	half-life
Thr	threonine
TMT	terpyridine methylenetetraacid
Trp	tryptophan
SDS PAGE	sodium dodecylsulfate polyacrylamide gel

	electrophoresis
SPR	surface plasmon resonance
TBS	Tris buffered saline
UV	ultraviolet

CHAPTER 1

INTRODUCTION

1.1 Aims of Thesis

The aim of this project has been the extensive investigation of a wide range of factors affecting the stability of monoclonal antibodies (mAbs), as part of a general approach to formulation development of these molecules, using a range of biophysical techniques. The techniques used include fluorescence spectroscopy, circular dichroism and differential scanning calorimetry (DSC). The broad objectives were:

1. To determine the thermal stability characteristics of mAbs in solution under various conditions using sensitive DSC and related calorimetric techniques.
2. To compare the effects of pH, adjuvants and other additives on the reversibility of thermal denaturation and related coagulation/aggregation phenomena.
3. To study the dynamic accessibility of protein groups using fluorescence quenching and related spectroscopic techniques, in comparison with stability studies under similar conditions.
4. To relate calorimetric and dynamic parameters to long-term storage properties of these proteins.
5. To apply these biophysical techniques to appropriately aged samples to examine possible diagnostic/analytical/quality control applications.

1.2 Introduction

Antibodies (also referred to as immunoglobulins, Ig) are produced by an individual's immune response to a foreign substance or invading pathogen (antigen), and perform a crucial role in the individual's immune defence. Nature has designed these molecules to be bifunctional in that they bind their antigen with exquisite specificity and selectivity but their function is also to activate the wide range of effector functions which will ultimately lead to the inactivation and removal of the antigen. This bifunctionality is essential for the immune system of the host to function effectively but it has also meant that antibodies have become indispensable tools in the laboratory whether it be in experimental research, clinical investigation or diagnosis, or most recently as therapeutic agents.

The role of antibodies in the host immune response requires the host to produce a wide range of antibody molecules from a range of antibody producing cells to recognise and bind the array of antigenic determinants (epitopes) present on the surface of invading pathogens. These antibodies are known as polyclonal antibodies. However, the role of antibodies as laboratory reagents or therapeutic drugs usually requires them to recognise only one molecule or even a single epitope and such antibodies are known as monoclonal antibodies (mAbs). This thesis is concerned with investigations into the stability of mAbs which have been developed and produced as therapeutic agents.

1.3 Summary of the Immune Response

The human immune response is a vastly complex system on which many textbooks and literature can be found. This thesis is not concerned with the production of antibodies *in vivo* but rather the finished product of production *in vitro*, but to set the work in context, a summary of the immune response, much simplified, follows.

To invoke an immune response, a foreign substance or invading pathogen must be recognised by antigen-specific lymphocytes of which there are two types: B lymphocytes (B cells) and T lymphocytes (T cells). Activation of these lymphocytes can occur when antigen binds to the lymphocyte surface via specific cell surface receptors. In the case of B cells these receptors are membrane-bound antibody molecules. T cell activation results in the destruction

and removal of infected host cells whereas B cell activation results in two main events; firstly the activated B cell divides and multiplies producing a 'clone' of identical cells then secondly these clones differentiate into either plasma cells or memory B cells. Plasma cells are able to secrete large amount of soluble antibody of the same specificity as the original membrane-bound antibody which bound the original antigen whereas the function of memory B cells is to produce an enhanced immune response on subsequent re-exposure to the same antigen. Activation of memory B cells leads to the production of antibodies with a higher affinity for antigen than those produced by the primary immune response.

1.4 Structure of Antibodies

As a rule, antibody molecules are glycoproteins whose basic unit comprises two identical glycosylated heavy chains of relative molecular mass 50 000-75 000 and two identical, nonglycosylated light chains of molecular mass 25 000 (Figure 1.1) (Goding, 1996). These chains are arranged in a symmetrical fashion, the heavy chains joined by disulfide bonds to each other and each light chain joined to a heavy chain by a disulfide bond. This disulfide bonding arrangement characteristic of immunoglobulins although the exact number and the locations of the bonds is variable (Nisonoff, et al., 1975).

Each chain of the antibody molecule is composed of domains: heavy chains contain either four or five depending on their class (IgG, IgA and IgD contain four; IgM and IgE contain five) and light chains contain two domains. (The grouping of immunoglobulins into five main classes is a somewhat complex affair where the class depends on the heavy chain of the molecule. IgM, IgD, IgG, IgE and IgA possess μ , δ , γ , ϵ and α heavy chains respectively. Individual classes have distinctive structures and biological functions.) Further subgrouping of individual Ig classes occurs as although IgM and IgD have single genes, the remaining classes often do not and are subdivided into subclasses (for example, there are four subclasses of IgG in mouse rat and human (designated IgG1, IgG2, etc.) but only one in the rabbit), each with its own constant region gene. There are also two types of light chain (κ and λ), a fact which is used in this complex classification system. An expert and readable guide to this classification minefield is given in Goding, 1996.

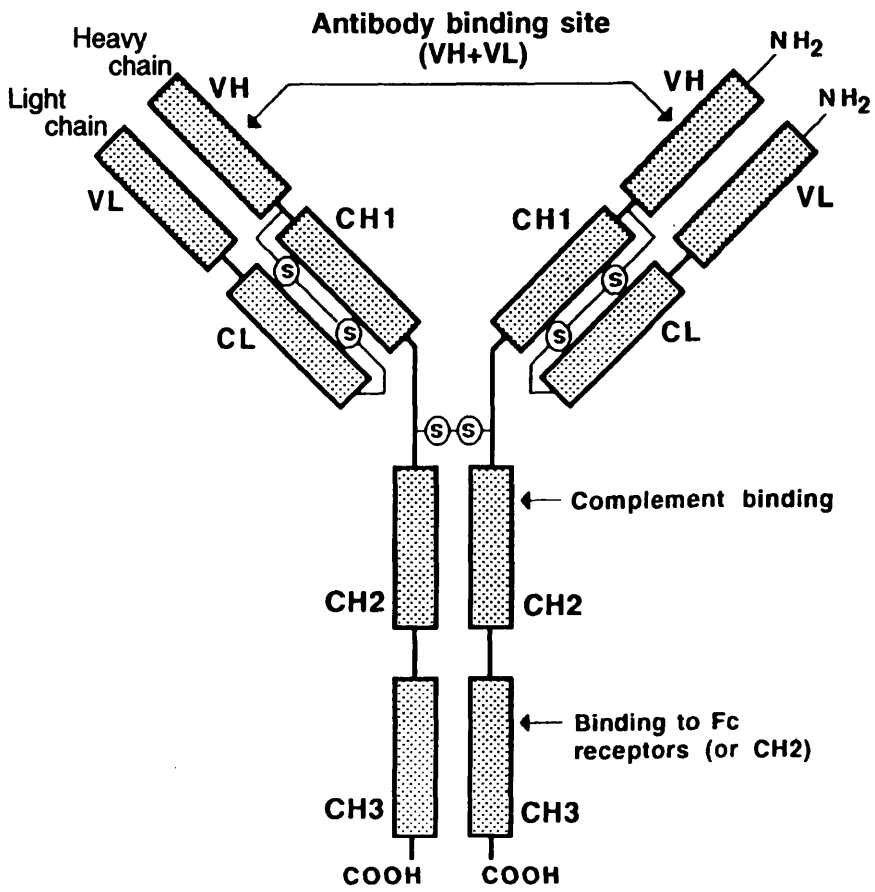


Figure 1.1: Basic structure of an antibody molecule (From Ritter and Ladyman, 1995)

The ability of the antibody to bind antigen is controlled by the N-terminal domains. Each antigen binding site is created by the combination of one domain from the heavy chain and one from the light chain with the remaining domains of the molecule required for the effector functions of the molecule. The N-terminal domains of the molecule are termed variable domains (V domains) as their primary structures vary considerably between antibodies of differing specificity whereas the primary structure of the other domains in the molecule is relatively constant and these are known as constant domains (C domains). Due to the symmetry of the molecule (the two heavy chains are identical and so are the two light chains), each antibody molecule contains two identical sites for antigen binding.

Despite the N-terminal domains of the molecule being labelled 'variable', the variability in primary structure is not spread throughout the domain but in fact it is focused in three main areas which are designated the hypervariable regions or complementarity determining regions (CDR). Changes in the amino acid sequence in these regions of the molecule alter the molecules specificity and affinity for antigen by changing the shape of the binding site and also altering potential interactions between antigen and antibody.

As mentioned previously, the general structure of Igs is a Y-shaped molecule composed of two heavy (H) chains and two light (L) chains. Within this structure there are well-defined domains: the L chain consists of V_L and C_L domains and the H chains comprise the V_H , C_{H1} , C_{H2} , and C_{H3} domains. Each of these domains consist of approximately 100 residues, are homologous in their primary structures, and are independent, stable structural units. On a secondary structural level, each domain is a compact, globular structure containing large amount of β -sheet. This motif has been termed the immunoglobulin fold (Poljak, et al., 1973) and consists of two layers of antiparallel β -sheets that are usually linked by a disulfide bond (fig. 1.2). Individual domains are rather resistant to proteolytic attack (Goding, 1996) in contrast to the short linking sequences joining individual domains. Some classes of antibody also contain an extra hinge region between the C_{H1} and C_{H2} domains. This region tends to have a more open and flexible structure and in hence is especially susceptible to proteolysis. The biological function of this hinge region, if any, is probably to allow the antibody to bind polymeric antigens which have a varying distance between epitopes. Recent work in solving the structure of an IgG molecule including the hinge region has revealed the

Chapter 1

conformation of this region (Harris, et al., 1992). A cartoon of the crystal structure of an IgG molecule is given in figure 1.3.



Figure 1.2: The immunoglobulin fold. This fold comprises two layers of antiparallel β -sheet folded on top of each other to form a sandwich-like structure. Located between the two layers are hydrophobic residues and the indicated disulfide bond linking two cysteine residues which are about 60 residues apart. The V_L domain is illustrated here and the loops containing the hypervariable regions are shaded dark. (From Creighton, 1993)

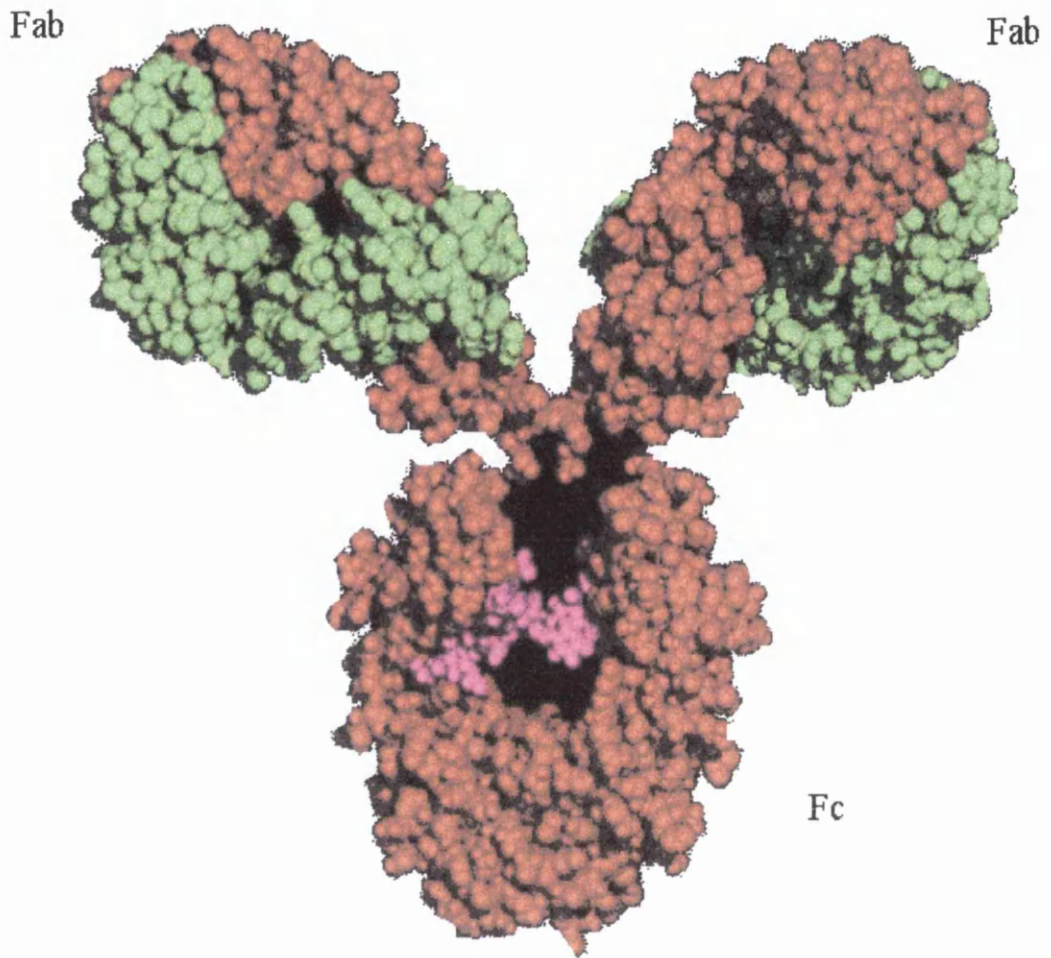


Figure 1.3: Cartoon illustrating the structure of the IgG molecule. The heavy chains are coloured orange and the light chains coloured green. The purple region represents the carbohydrate attached to the heavy chains. The antigen binding regions are labelled Fab and the constant region is labelled Fc.

1.5 What Are Monoclonal Antibodies?

When an antigen provokes an immune response it does so by being recognised by B cells though each B cell which recognises the antigen may bind a different epitope with a different affinity. This diversity of recognition will be carried through to the antibodies which are secreted in the plasma after clonal expansion and differentiation and since many B cells will have undergone clonal expansion, these antibodies will be the product of many clones and are therefore referred to as polyclonal. In polyclonal antibodies, nature has produced a highly effective 'army' to fight invading pathogens, both in terms of sheer quantity of antigen-antibody binding but also in the range of effector functions that can be activated. These properties are not usually required for laboratory reagents though, rather a homogeneous species of constant specificity and affinity which therefore has predictable behaviour is desired. Such a reagent are monoclonal antibodies.

The development of a technique to produce monoclonal antibodies is credited to Gorges Köhler and Cesar Milstein as part of their research into the mechanisms underlying the diversity of antibodies (Köhler and Milstein, 1975). To obtain a monoclonal antibody, it is necessary to isolate and propagate single antibody-secreting B cell clones. This is not directly possible but by combining the nuclei of normal antibody-secreting cells with those of their malignant counterparts, Köhler and Milstein were successful and for their achievements were awarded the Nobel Prize in Physiology and Medicine in 1984.

Put very simply, the essence of the technique involves the selection of a B cell which can produce one specific antibody (but has a lifetime of only a few days in culture) and fusing it with a myeloma cell which although it is no longer viable as an antibody-producing cell, has the property of immortality in culture. The fusion product is a hybridoma cell which is immortal due to mitotic cell division which results in an ever expanding clone of identical cells. A more detailed description of this procedure is contained in Ritter and Ladyman, 1995.

Although this work was the result of basic research into the mechanism of generation of antibody diversity it had revolutionary consequences for biological research and clinical

medicine and resulted in the generation of an industry. It also laid the foundation for other techniques common today, for example the molecular methods which result in the production of 'designer' mAbs after manipulation of the genes encoding the heavy and light chains of the molecule. Such gene manipulation allows for the design and production of humanized mAbs which comprise CDRs of rodent origin genetically grafted into a human mAb framework. This process allows these mAbs to be used *in vivo* without producing an anti-rodent immune response (and subsequent production of human anti-mouse antibody, HAMA) in the patient. Although simple in theory, this approach to mAb production has many pitfalls including a reduction in the final antibody affinity and the technique is very labour intensive and requires specialist expertise in genetic engineering (Borrebaeck, 1992). Despite these drawbacks, the technique remains popular within the pharmaceutical industry as a means of producing mAbs as novel clinical agents. mAbs as clinical agents can be broadly divided into two types: firstly an agent which depends on the antibody binding a specific antigen which is indicated in a particular disease state and secondly the antibody as an agent conjugated to another drug. The former are normally used in the treatment of conditions of the immune system, for example rheumatoid arthritis (Choy, 1998) with the latter being more commonly used as a treatment for cancers (Trail, et al., 1997; Panchal, 1998; Farah, et al., 1998). The three antibodies studied and described within this thesis (Campath-1H, 4162W94 and 1209W95) are all humanized mAbs developed by Glaxo Wellcome and a brief description of each of these pharmaceuticals and their mechanism of action follows.

1.4.1 Campath-1H

Campath-1 is the generic name given to a series of rat mAbs produced by Waldmann, et al for the lysis of normal and malignant cells (Hale, et al., 1983). These antibodies recognise the CD52 antigen (also known as the Campath-1 antigen) which is a small glycosylphosphatidylinositol (GPI) anchored glycopeptide which is abundantly expressed on virtually all human lymphocytes (Hale, et al., 1993; Xia, et al., 1993). This antigen comprises a twelve amino acid sequence (Treumann, et al., 1995; Rowan, et al., 1998) and has recently had its structure, when bound to Campath-1H, solved (Cheetham, et al., 1998).

The unique ability of the Campath-1H antibodies (IgG1 class) to kill lymphocytes by both complement- and cell-mediated lysis led to their extensive development as therapeutic agents. The rat mAb, Campath-1G, was the first agent to be effective therapy *in vivo* but as

it was of rodent origin there was a high possibility that it would elicit an anti-globulin response. To combat this and to produce a therapy which would be more effective in patients, Campath-1H was produced by Riechmann, et al., (1988) using a pioneering humanization technique. This technique involved combining only the CDRs from the original rat mAb and the human IgG framework to produce a humanized mAb which did not elicit an anti-globulin response but retained highly specific and tight binding in addition to providing native human effector functions.

So promising were the preliminary results of clinical trials of Campath-1H, that expression systems were developed in order to produce it in suitable quantities for large scale clinical trials (Page, et al., 1991; Carroll, et al., 1992; Crowe, et al., 1992). Campath-1H has been indicated in the treatment of non-Hodgkin lymphoma (NHL) (Lim, et al., 1993) and rheumatoid arthritis (Isaacs, et al., 1992; Weinblatt, et al., 1995). At the time of writing it had recently been approved by the Federal Drugs Administration (FDA) as a therapy for NHL.

Work carried out on the formulation development of Campath-1H identified an acid labile Asp-Pro bond at residues 274-275 in the heavy chain of the molecule (Wellcome Company Document No: BZGA/91/0018, 1992, private communication) and N-terminal sequencing suggested this acid lability is a general feature which is not unique to Campath-1H but can also be observed in other IgGs. In the case of Campath-1H though, the cleavage could be avoided by minimising exposure to extreme conditions of acid pH and high temperature. Development studies also highlighted another cleavage site within the molecule, this time within the hinge region. The labile Lys₂₂₆-Thr₂₂₇ bond was found to undergo cleavage in the presence of divalent copper ions- a direct effect of the copper ions interacting with amino acid residues within the proximity of this bond (Wellcome Company Document No: BZGA/91/0011, 1991, private communication). These findings, in addition to results from other studies resulted in Campath-1H being formulated as a solution of mAb (10 mg/ml) in pH 7.2 0.01 M phosphate buffered saline, 2 mM EDTA (a chelating agent to bind Cu²⁺ and therefore minimise copper-induced cleavage reactions) with the recommendation that the product be stored at 4 °C out of direct light.

1.4.2 4162W94

4162W94 is the Glaxo Wellcome company name for an investigational drug being studied as immunotherapy for rheumatoid arthritis. Like Campath-1H it is a humanized mAb (IgG1 class) but it recognises the CD4 (cluster differentiation 4) antigen (unlike Campath-1H which has the CD52 molecule as its antigen). CD4 molecules are found on the surface of T cells, which, as described in section 1.2, are molecules crucially involved in the human immune response. It is the T cells that are involved in the initiation and maintenance of auto-immune diseases such as rheumatoid arthritis and therefore to treat these diseases effectively it would be desirable to find a means of controlling these T cells without compromising the rest of the immune system.

4162W94 targets the CD4 molecules and on binding, induces a state of unresponsiveness, or anergy, in the T cells. The ability of the mAb to transiently block the function of the T cells without killing them and render them permanently anergic, while at the same time leaving the rest of the immune response able to respond normally to pathogens, makes it a logical target as a therapy for rheumatoid arthritis.

Formulation studies at the time of development resulted in 4162W94 being formulated as a 10 mg/ml solution in 50 mM citrate buffer, pH 6.0, 0.05 mM EDTA and 0.01% (w/w) polysorbate 80 (Wellcome Company Document, Investigator's Brochure-4162W94, private communication). EDTA was included in the formulation to minimise cleavage at the Cu²⁺ dependent cleavage site identified in the structure of Campath-1H as 4162W94 shares the same IgG framework. The purpose of the polysorbate 80 was to stabilise the mAb by preventing/reducing the formation of insoluble aggregates.

1.4.3 1209W95

Again 1209W95 is a humanized monoclonal antibody (IgG4 class) in development by Glaxo Wellcome as a therapeutic agent. This molecule differs from both Campath-1H and 4162W94 not only in its IgG class but also in the fact that it has been designed as an antibody-bromo-acetyl TMT (terpyridine methylene tetraacid- a metal chelator)-antibody conjugate. TMT allows the chelation of the therapeutic isotopes ⁹⁰Yttrium and ¹⁷⁷Lutetium and, by recognising a 40 kD tumour antigen, directs these radiotherapeutic agents to the

tumour site without causing extensive healthy tissue damage. This mAb is relevant as an oncology therapy in the treatment of advanced prostate and lung cancer.

Work on the development of this molecule has shown it to be 'considerably less stable' than both Campath-1H and 4162W94 (Wellcome Company Document No: DPPP/95/0009, 1995, private communication). Not only is the mAb sensitive to acid pH (below pH 5.5 TMT is cleaved from the molecule) but considerable precipitation is observed by agitation or bubbling with air or nitrogen to the extent that continuous overnight shaking removes 98% of the soluble antibody (Wellcome Company Document No: DPPP/95/0009, 1995, private communication). This inherent propensity to precipitate, which is not a concern with Campath-1H and 4162W94, may be due to the mutations carried out within the IgG framework to allow the site-specific conjugation of the TMT.

To maximise the stability of the molecule in solution, the antibody is formulated as a 15 mg/ml solution in 100 mM tris/HCl buffer, pH 8.0, 0.05 mM EDTA and 0.01% (w/w) polysorbate 80 (Wellcome Company Document No: DPPP/95/0009, 1995, private communication). The additives in this formulation perform the same function as they do in the formulation of 4162W94 i.e. EDTA chelates divalent metal ions and minimises their interaction with the mAb and the polysorbate 80 reduces the formation of insoluble precipitates.

1.5 Stability of Monoclonal Antibodies

It is widely recognised that, as a class of protein pharmaceuticals, mAbs require sensitive handling and storage and, from production through to final formulation, techniques sympathetic to the nature of the proteins must be employed. Despite this recognition, surprisingly little literature is available on the effects of various reagents and techniques on mAbs, a fact which is a little less surprising when one bears in mind that the production of therapeutic mAbs is carried out almost exclusively by the pharmaceutical industry who are notoriously reluctant to divulge the results of their research.

The influence and effects of the production and storage of mAbs on their specificities, as measured by functional assays, has been studied although the mAbs discussed were not

clinical agents but laboratory reagents (Underwood and Bean, 1985). The effects of pH, hydrogen peroxide and temperature on a therapeutic mAb as measured by physical techniques (turbidity measurements, chromatographic techniques and matrix-assisted laser desorption ionization time-of-flight mass spectrometry (MALDI TOF MS)) has also been the subject of published reports (Usami, et al., 1996). Gombotz, et al., (1994), studied the effects of another formulation additive, poly(vinylpyrrolidone), on the stabilization of a therapeutic mAb using a range of techniques including differential scanning calorimetry (DSC) and a functional assay. The use of fluorescence spectroscopic techniques to monitor conformational changes relevant to the stability of mAbs in addition to the use of functional assays has also been reported (Jiskoot, et al., 1990).

The determination of the optimal storage conditions for mAbs, and indeed all protein pharmaceuticals, requires sensitive and reliable assays with which the stability of the mAb to various treatments and additives can be determined. Traditional methods e.g. enzyme-linked immunosorbent assay (ELISA) and even modern surface plasmon resonance (SPR) techniques are used to quantify bioactivity which is the most critical assay of stability but these techniques fail to give any information on the mechanism(s) of inactivation. Such functional assays, especially ELISA can be complex techniques which can be less reproducible than simpler physical techniques. A comparison of the storage stability of a solution of a therapeutic mAb as determined by DSC and two functional assays (ELISA and an affinity chromatographic technique) has been reported (Brouillette, et al., 1996) and concluded that DSC is useful as an 'aid' to protein pharmaceutical formulation.

1.6 DSC and Pharmaceuticals

As mentioned in the preceding section, DSC has been shown to be an aid to protein pharmaceutical development. The maintenance of the native tertiary structure of a protein is required for bioactivity and hence a measure of native structure can be used to determine stability; many modifications of proteins (both chemical and physical) which lead to loss of bioactivity can be detected and quantified by analysing the equilibrium between the folded and unfolded states of the protein as a function of some additive (usually a chaotropic agent e.g. urea) or temperature (Brouillette, et al., 1996). DSC is a technique which lends itself to such an analysis and not only does it provide information on the thermodynamic stability of the

native conformation but it also can be used to quantify the amount of native protein present (Brouillette, et al., 1996).

DSC has proven its value in the field of physical pharmacy but almost exclusively as a tool for analysing the reactions of traditional organic drugs whether it be in solid form or in solution. DSC has been used for studies of the wetting and stability of such compounds and excellent reviews of this area have been published (Buckton and Beezer, 1991; Koenigbauer, 1994). When used to analyse protein pharmaceuticals, DSC is normally used as a means of conveniently studying the effects of various additives on the protein (Ahmad and Bigelow, 1986; Chang et al., 1993; Gombotz et al., 1994; Picó, 1996; Fatouros et al., 1997a; 1997b; Giancola et al., 1997; Remmele et al., 1998) by observing any changes in the T_m of unfolding, that is the peak maximum of the denaturation endotherm. Such observations are made on the basis that an additive expected to stabilise protein should increase the T_m while a destabilizing additive should decrease the T_m . One of the goals of this thesis is to investigate whether the role of DSC in the formulation of protein pharmaceuticals can be taken further than this rather empirical level.

CHAPTER 2

MATERIALS AND METHODS

2.1. Reagents Used

Buffer Reagents

Sodium acetate (anhydrous), sodium dihydrogen orthophosphate dihydrate, potassium chloride and ethylenediamine tetraacetic acid (EDTA) were purchased from BDH Laboratory Supplies, Poole, England. Sodium chloride, citric acid and trisodium citrate were purchased from Fisher Scientific UK Ltd, Loughborough, England. Acetic acid (99.8%) was purchased from Riedel-de Haën, Seelze-Hannover.

Formulation Additives

Pluronic F-68 (Poloxamer 188, Product No.: P 1300), lactitol (4-O- β -D-galactopyranosyl-D-glucitol, Product No.: L 3520), DEAE-dextran (chloride form, Product No.: D9885), L-histidine (Product No.: H 8000) were all purchased from Sigma Chemical Co. N-methylacetamide, hydroxypropyl- β -cyclodextrin (average molar substitution = 0.6, Cat. No.: 33,261-5), methyl- β -cyclodextrin (average molar substitution = 1.8, Cat. No.: 33,261-5) were purchased from Aldrich Chemical Co. Mannitol was purchased from BDH Laboratory Supplies.

Fluorescence Spectroscopy Reagents

Succinimide (Product No.: S 9381) and acrylamide ($\geq 99\%$, electrophoresis reagent, Product No.: A 8887) and L-tryptophan (Product No.: T 8659) were purchased from Sigma Chemical Co. ANS (8-anilino-1-naphthalene-sulphonic acid, Cat. No.: 13,992-0) was purchased from Aldrich Chemical Co. Succinimide was recrystallised from ethanol prior to use.

Circular Dichroism Reagents

Urea (ultrapure grade, Product No.: U-0631) was purchased from Sigma Chemical Co. Guanidine Hydrochloride (ultrapure grade) was purchased from Life Technologies Inc., Paisley, Scotland and the absolute concentrations checked by refractive index measurements (Nozaki, 1972) by Dr Sharon Kelly, University of Stirling.

SDS-PAGE Reagents and Solutions

Coomassie Blue Destain: 25% methanol, 10% acetic acid and 1% glycerol.

Coomassie Blue Stain: 0.1% Coomassie Blue R-250 (Sigma Chemical Co.) in destain.

Chapter 2

Running Buffer: 1440 g glycine (Sigma Chemical Co.), 300 g Tris-base (Sigma Chemical Co.), 50 g SDS (Schwarz/Mann Biotech.) per 10 L.

Sample Buffer: 5 g SDS, 5 ml Tris (1 M, pH 7.5), 100 mM PMSF (phenylmethylsulfonyl fluoride) (Sigma Chemical Co.) in isopropanol, 100 mM EDTA, 10 ml glycerol, 2% bromophenol blue (BDH) made up to 100 ml with distilled H₂O to pH 6.8.

2.2 Differential Scanning Calorimetry

2.2.1 Thermal Stability Studies

The bulk of the stability studies described in this thesis were carried out using the MicroCal MC-2 differential scanning calorimeter fitted with an EM Electronics N2a DC nanovoltmeter. In the latter stages of the project a MicroCal MCS system and a VP-DSC system were also used. All three instruments are PC operated which is also used for data collection. With the exception of experiments to determine kinetic parameters, a nominal scan rate of 60 °C/hr and a “filter” setting of 15 s were applied (the filter setting refers to data acquisition and averaging time e.g. a filter setting of 15 s will record and store averaged energy and temperature data every 15 s).

Sample solutions were prepared by exhaustive dialysis of mAb solutions against the required buffer with the relevant additive then added to both dialysed solution and dialysis buffer to the same exact concentration where necessary. Protein concentrations were typically 2-3 mg/ml for the MC-2 and MCS instruments, 0.5-1 mg/ml for the VP-DSC system. The dialysis buffer was used for reference and baseline scans. Both sample and buffer solutions were degassed before loading into the calorimeter cells (to avoid bubble formation at higher temperatures) by placing the solution under vacuum for two or three minutes using a small desiccator attached to a water aspirator, mounted on a magnetic stirrer.

Both cells of the calorimeter were rinsed thoroughly with buffer prior to filling. Filling of the cells was achieved using a small syringe fitted with a length of narrow gauge Teflon tubing (filling of the VP-DSC cells was achieved using a glass Hamilton syringe and a Teflon filling funnel as supplied by the manufacturer). It is vital that there are no air bubbles either in the cells or in the inlet tube and therefore extreme care was taken to make sure the syringe and tubing were bubble-free. To prevent the cell contents boiling and to suppress bubble formation during DSC, a pressure head of 1-2 atm of nitrogen was maintained (this is unnecessary when using the VP-DSC system as it has a self-pressurising sample chamber). One or more buffer baseline scans were obtained by filling both the reference and sample cells with the appropriate buffer and scanning in the normal manner, as described in the manufacturers instructions.

The protein sample solution was then loaded into the sample cell. The small amount of buffer left in the sample cell prior to filling leads to a slight dilution of the sample, however this is avoided by rinsing the cell with a small quantity of the sample and then discarding. A little of the sample was retained for protein concentration determination using UV/visible spectrophotometry.

2.2.2 DSC Data Analysis

DSC data were analysed using MicroCal Origin software packages (versions 2.90, 4.1 and 5.0 for the MicroCal MC-2, MCS and VP-DSC systems respectively). The software collects differential thermal energy data as a function of time i.e. a typical data file will consist of the time, cell temperature and differential energy input into the cells since the last data point, at intervals determined by the filter setting. Conversion to differential heat capacity requires division by the mean scan rate at each point.

Due to variations in the total heat capacity and heat losses in the instrument, the DSC scan rate can vary over the programmed temperature range. This effect results in a curvature of the DSC trace. Most of the artefacts and nonlinearities arising from instrumental problems such as mismatch of cell volume are eliminated by subtracting a buffer baseline.

It is common practise for the differential heat capacity to be normalized to differential heat capacity per mole of sample by dividing by the total amount of sample in the cell (i.e. conversion of cal/°C to cal/mol/°C). Origin software performs this function and has the cell volumes set as a default and a text box to allow entry of the sample concentration. A non-two state model, based on original work by Sturtevant, Brandts and Privalov (Sturtevant, 1974, 1987; Jackson and Brandts, 1970; Privalov and Potekhin, 1986) was fitted to these normalized experimental data using the facility built into the software package. The model used is based upon the van't Hoff equation:

$$\left(\frac{\delta \ln K}{\delta T} \right)_p = \frac{\Delta H_{vH}}{RT} \quad (2.1)$$

where ΔH_{vH} is the van't Hoff heat change for the reaction which corresponds to the heat change for the cooperative unit which actually participates in the reaction.

Normally it is understood that the protein is composed of a number of structural domains, A, B, C..., each of which is involved independently in a transition between the folded and unfolded forms ($A=A'$, $B=B'$,...). Equilibrium constants are expressed in terms of fractions e.g.

$$K_A = \frac{f_{A'}}{f_A}$$

where K_A is the equilibrium constant for the unfolding of domain A, $f_{A'}$ and f_A are the fractions of the unfolded and folded domain A, respectively. Remembering that $f_{A'}$ and f_A are related simply as follows:

$$f_A = 1 - f_{A'}$$

The total molar enthalpy for the system, H, is given by:

$$H = H_N + f_{A'}\Delta H_A + f_{B'}\Delta H_B + \dots \quad (2.2)$$

where H_N is the total enthalpy of the native state, to which all measurements of ΔH are relative. The total molar heat capacity is the temperature derivative of equation 2.2:

$$C_p = C_{pN} + \left[f_{A'}\Delta C_{pA} + \Delta H_A \left(\frac{\delta f_{A'}}{\delta T} \right) \right] + \dots \quad (2.3)$$

where C_{pN} is the molar heat capacity of the totally folded state. Substituting equilibrium constants in place of fractional concentrations in equation (2.3) and then carrying through the differentiation gives:

$$\left(\frac{\delta f_{A'}}{\delta T} \right) = \left(\frac{K_A}{(1 + K_A)^2} \right) \left(\frac{\delta \ln K_A}{\delta T} \right) \quad (2.4)$$

By substituting equations 2.1 and 2.4 into equation 2.3 gives:

$$C_p = C_{pN} + \left[\frac{K_A \Delta C_{pA}}{1 + K_A} + \frac{K_A \Delta H_{vH} \Delta H_A}{(1 + K_A)^2 RT^2} \right] + \dots \quad (2.5)$$

Equation 2.5 is perfectly general at this point and can be applied to either two-state or non-two-state transitions so long as all parameters are evaluated at the same temperature T.

Model for Independent Two-State Transitions

If we assume each transition is two-state, then the van't Hoff enthalpies (the heat uptake per mole of cooperative unit in the transition which is independent of sample concentration and absolute calorimetric enthalpy, assuming a two-state transition model) become equal to the calorimetric enthalpies (simply the integrated area beneath the peak in the DSC endotherm divided by the total amount of protein in the calorimeter cell). If we also assume that C_{pN} is a linear function of temperature then equation 2.5 gives:

$$C_p(T) = B_0 + B_1 T + \left[\frac{K_A(T) \Delta C_{pA}}{1 + K_A(T)} + \frac{K_A(T) \Delta H_A(T)^2}{(1 + K_A(T))^2 RT^2} \right] + \dots \quad (2.6)$$

where $C_p(T)$, $K_A(T)$ and $\Delta H_A(T)$ are the heat capacity, equilibrium constant and enthalpy change at temperature T, respectively. This can be expressed in terms of the T_m of the transition as follows:

$$\Delta H_A(T) = \Delta H_{mA} + \Delta C_{pA} (T - T_{mA}) \quad (2.7)$$

and then integrating the van't Hoff equation (2.1) from T_{mA} to T gives:

$$K_A(T) = \exp \left\{ \frac{-\Delta H_{mA}}{RT} \left(1 - \frac{T}{T_{mA}} \right) - \frac{\Delta C_{pA}}{RT} \left(T - T_{mA} - T \ln \frac{T}{T_{mA}} \right) \right\} \quad (2.8)$$

By substituting equations 2.7 and 2.8 into equation 2.6, the model to which the DSC data can be fitted, is obtained. To initiate curve fitting with Origin, the operator indicates the

number of transitions needed to fit the experimental DSC heat capacity curve and then inputs guesses of all the T_m values. The software then fits the data to the model by non-linear least-squares until there is no further improvement in fit.

When all heat capacity changes are assumed to be zero, then equations 2.6-2.8 are simplified to:

$$C_p(T) = \frac{K_A(T)\Delta H_A(T)^2}{(1 + K_A(T))^2 RT^2} + \dots \quad (2.9)$$

$$K_A(T) = \exp\left\{\frac{-\Delta H_{mA}}{RT}\left(1 - \frac{T}{T_{mA}}\right)\right\} \quad (2.10)$$

Curve fitting is again by non-linear least-squares regression.

Model for Independent Non-Two-State Transitions

Because of the extra fitting parameters required for the non-two-state model compared with the two-state model, this model is only applied to transitions with no ΔC_p . Before curve fitting with this model, a progress baseline must be subtracted from the experimental data to remove the ΔC_p effects if they are present (the accuracy of this progress baseline is based on an educated guess/good eye of the operator). This also sets C_{pN} to zero at all temperatures. To treat non-two-state transitions we begin with the general equation 2.5 which still includes both van't Hoff and calorimetric heat changes. If the temperature-dependent parameters are indicated, this can be written as:

$$C_p(T) = \frac{K_A(T)\Delta H_{mA}^* \Delta H_{mA}}{(1 + K_A(T))^2 RT^2} + \dots \quad (2.11)$$

In this case, the equilibrium constants will be calculated as in equation 2.10 with the important exception that the van't Hoff enthalpy must be used rather than the calorimetric enthalpy since the two are now no longer equal, i.e.:

$$K_A(T) = \exp\left\{\frac{-\Delta H_{mA}^*}{RT} \left(1 - \frac{T}{T_{mA}}\right)\right\} \quad (2.12)$$

Equations 2.11 and 2.12 are then used for curve fitting again by non-linear least-squares with the operator inputting the number of transitions needed to fit the experimental data and guesses for the corresponding T_m values. It is up to the user to decide whether the fit is successful; if not the procedure is repeated.

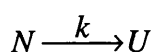
2.2.3 Analysis of Kinetically Controlled Processes

The above analyses of DSC data are only valid if the processes under investigation are thermodynamically controlled. If the processes are kinetically controlled, the above analyses will result in some kind of error and a form of kinetic analysis must be used. Kinetic control is established by the fulfilment of either one (or both) of the two following criteria: rescanning of the protein fails to reproduce the original scan (so-called calorimetric irreversibility) and/or the scans show scan rate dependence (that is, the T_m and/or the trace shape change on changing the scan rate). If the sample meets the above criteria then the process is indeed under kinetic control and the data is interpreted using the method proposed by Sánchez-Ruiz et al., (1988a).

The rate constant, k , characterising a kinetically controlled process, is dependent on temperature. This temperature dependence is governed by the Arrhenius equation:

$$k = A \exp\left(\frac{-E_A}{RT}\right) \quad (2.13)$$

where A is the pre-exponential factor, E_A is the activation energy, R is the gas constant and T is temperature. Consider the case of a two-state irreversible denaturation of a protein (based on Freire et al., 1990). It can be represented by the first-order equation:



where N and U are the native and unfolded form of the protein respectively and k is the first-order rate constant for the process. This can be rewritten as:

$$\frac{-d[N]}{dt} = \frac{d[U]}{dt} = k[N]$$

or, expressing [N] and [U] as mole fractions P_N and P_U where:

$$P_N = \frac{[N]}{P_{Total}} \quad , \quad P_U = \frac{[U]}{P_{Total}}$$

gives:

$$\frac{-dP_N}{dt} = kP_N$$

Temperature dependency is introduced by dividing both sides by the scan rate, v , and substituting the Arrhenius equation for the rate constant giving:

$$\frac{-dP_N}{dT} = \frac{A}{v} \exp\left(\frac{-E_A}{RT}\right) P_N \quad (2.14)$$

Notice the term $-dP_N/dT$ is equivalent to the change in extent of conversion of native to unfolded with temperature.

In kinetics, the Arrhenius parameters are calculated from measurements of the temperature dependence of the rate constant for the process under investigation. The method devised by Sánchez-Ruiz et al. (1988a) allows for the calculation of the rate constant as a function of temperature from experimental DSC data. Using this method, DSC scans at different scan rates (the MC-2 system allows 10, 20, 30, 45, 60 and 90 K/hr scans) are recorded for the protein (and corresponding buffer). A suitable baseline is then fitted to and subsequently subtracted from each scan and each scan normalized to produce a data set of apparent excess molar heat capacity versus temperature. Using Origin software we can then evaluate the calorimetric enthalpy (although it has no thermodynamic significance for a kinetically controlled process it does, however, represent the enthalpy gain or loss for the conversion process).

Values of the rate constant of a reaction at a given temperature, k , are obtained from DSC data using the equation:

$$k = \frac{\nu C_p}{(Q - Q_t)} \quad (2.15)$$

where ν (K/min) represents the scan rate, C_p the excess heat capacity, Q the total heat of the process (proportional to the area below the thermogram) and Q_t the heat evolved at a given temperature (area below the thermogram between an initial temperature and a desired temperature, T). An Arrhenius plot of $\ln k$ versus $1/T$ can then be constructed and the activation energy, E_A , for the process obtained from the slope of the graph. E_A can also be calculated from the slopes of the plots of $\ln[\ln Q/(Q-Q_t)]$ versus $1/T$ according to:

$$\ln \left[\frac{\ln Q}{(Q - Q_t)} \right] = \frac{E_A}{R} \left(\frac{1}{T_m} - \frac{1}{T} \right) \quad (2.16)$$

where T_m is the temperature corresponding to the maximum of the heat capacity curve and $\ln(\nu/T_m^2)$ versus $1/T_m$ according to the following equation:

$$\frac{\nu}{T_m^2} = \left(\frac{AR}{E_A} \right) \exp \left(\frac{-E_A}{RT_m} \right) \quad (2.17)$$

where A is the Arrhenius pre-exponential factor and e is the base of natural logarithms. The activation energy can also be calculated directly from the heat capacity at the maximum of the trace, C_p^{\max} , according to:

$$E_A = \frac{eRT_m^2 C_p^{\max}}{Q_t} \quad (2.18)$$

The above method of DSC data analysis is then applied to data recorded at all six available scan rates for a full data set.

The four methods used to calculate the activation energy (eq. 2.15-2.18) use different experimental information and involve different approximations. Equation 2.18 uses parameters from the maximum of the excess heat capacity curve while equation 2.17 is based on the effect of the scan rate on the T_m and equation 2.16 tests the shape of the traces with changing scan rate. These three functions assume that the Arrhenius equation holds true whereas the method based on equation 2.15 checks that the rate constants calculated from the traces obtained at different scan rates agree and is valid even if the Arrhenius equation does not hold. Agreement between the results obtained by the four different methods is a crucial test of the validity of the proposed kinetic model for the denaturation process.

2.2.4 Extrapolation of DSC Data to Infinite Scan Rates

If the denaturation pathway of a protein is described as the sum of two effects: an endothermic effect comprising the energy involved in the destruction of tertiary structure and an exothermic effect comprising the energy released on aggregation, then we can theoretically analyse each effect separately by extrapolation of the data to infinite scanning rates (La Rosa et al., 1995; Milardi et al., 1998). Such analysis is only valid if the experimental DSC curves obtained at different scanning rates illustrate that the magnitude of the exothermic effect decreases with increasing scan rate (i.e. the exothermic contribution is time dependent) to a greater extent than the endothermic effect. It is this difference in the manner that the changing scan rate affects the exo- and endothermic peaks that allows the reversible and irreversible steps to be considered separately.

Such analysis begins with the calculation of the apparent activation energy for the unfolding process using eq. 2.17. The $C_{p\text{ exc}}$ (specific excess heat calculated according to Privalov and Potekhin, 1986) curve at infinite scanning rate is obtained by means of the following procedure: the cumulative enthalpy functions $\langle \Delta H \rangle$ were calculated from the experimental calorimetric profiles obtained at different scan rates using the following equation:

$$\langle \Delta H \rangle = \int_{T_0}^T C_{p\text{ exc}} dT \quad (2.19)$$

where T_0 is the temperature at which all molecules are in the initial state. For a first-order process, the relationship between $\langle \Delta H \rangle$, $\langle \Delta H \rangle_{\text{rev}}$, T and v is given by the following equation:

$$(\Delta H - \langle \Delta H \rangle) = (\Delta H - \langle \Delta H \rangle_{rev}) \exp\left(-\frac{1}{\nu} \int_{T_0}^T k_{app} dT\right) \quad (2.20)$$

where ΔH is the calorimetric enthalpy calculated at the chosen scan rate, $\langle \Delta H \rangle_{rev}$ is the cumulative enthalpy function containing the information pertinent only to the species that are in equilibrium, and k_{app} is the apparent kinetic constant. Clearly when $\nu \rightarrow \infty$ then $\langle \Delta H \rangle \rightarrow \langle \Delta H \rangle_{rev}$ exponentially.

To obtain the $\langle \Delta H \rangle_{rev}$ function over the entire denaturation range, the numerical values of $\langle \Delta H \rangle$ at each scan rate for a given temperature are plotted against $1/\nu$ and the intercept values with the y-axis give the value of $\langle \Delta H \rangle_{rev}$ at the given temperature. Deriving the $\langle \Delta H \rangle_{rev}$ profile with respect to temperature gives us the $C_{p\ exc}$ profile at infinite scanning rate which allows the calculation of ΔH and a T_m for the process under investigation. (Further mechanical-statistical analysis of the $C_{p\ exc}$ profile via the first derivative of $\langle \Delta H \rangle_{rev}$ with respect to temperature, using the classic deconvolution algorithm of Freire and Biltonen (Freire and Biltonen, 1978; Biltonen and Freire, 1978), allows the path of the folding-unfolding transition to be established. This further method of analysis was not used in this thesis.)

2.3 Protein Analysis

2.3.1 Determination of Protein Concentration

Protein concentrations throughout this thesis were determined spectrophotometrically using a Shimadzu UV160A UV-visible recording spectrophotometer using quartz cells with pathlength 1 cm. Protein concentrations were determined according to the Beer-Lambert law:

$$[c] = \frac{A}{\epsilon \cdot l}$$

where $[c]$ is the protein concentration in mol/L, A is absorbance, l is the pathlength (in cm) and ϵ is the molar extinction coefficient of the absorbing protein. ϵ for each of the three antibodies were obtained by entering the amino acid sequence of each into the ExpASY

ProtParam tool (point browser to <http://www.expasy.ch/tools/protparam.html>) which calculates ϵ from the algebraic sum of contributions from individual tryptophans, tyrosines and disulfides according to the method developed by Gill and Von Hippel (1989). The sequence of Campath-1H is as published (Crowe et al., 1992), the sequences of 4162W94 and 1209W95 were provided by private communication (U.T. Lashmar, 1997). The extinction coefficients of the three mAbs are given in table 2.1 below, the molecular weight of all three mAbs is taken to be 150 kDa. (Due to glycosylation of these molecules, accurate molecular weights derived from sequence data cannot be calculated. Throughout this thesis, all calculations involving protein concentrations used molar concentrations (not mg/ml) and therefore knowledge of the exact molecular weight was unnecessary.)

mAb	$\epsilon_{280\text{nm}}$ ($\text{M}^{-1} \text{cm}^{-1}$)
Campath-1H	132000
4162W94	191000
1209W95	224000

Table 2.1. Summary of extinction coefficients used

2.3.2 SDS-PAGE

The SDS-PAGE gels described in this thesis were cast using a Hoefer Mighty Small™ SE245 Dual Gel Caster (Hoefer Scientific Instruments, San Francisco, U.S.) and were of 0.75 mm width. Proteins were electrophoresed through 10% SDS-polyacrylamide under reducing conditions using a discontinuous buffer system. Lyophilized molecular weight standards (Pharmacia Biotech) were dissolved in 200 μl deionized H_2O . All samples were mixed with equal volumes of sample buffer and heated at 100°C for 4 mins to denature. After loading onto the gel, electrophoresis was carried out at 150 V, 30 mA. Gels were then stained with Coomassie Blue and destained as required.

2.4 Fluorescence Spectroscopy

The process of fluorescence occurs when a substance absorbs light which excites its molecules from a ground state to a higher state only to return to the ground state, reemitting light, usually of a longer wavelength than the exciting light. Substances which normally exhibit fluorescence are those whose structure contains delocalised electrons as part of a conjugated system. The fluorescent compounds of interest when studying biological processes can be separated into two camps: intrinsic or naturally occurring fluorophores such as tryptophan, tyrosine, phenylalanine, and the disulfide chromophore of cysteine, and extrinsic chromophores which include fluorescein and other synthetic probes of which ANS is only one of many. The fluorescence of many fluorophores is extremely sensitive to their surrounding environments, tryptophan residues in proteins are a case in point, and this allows fluorescence to be used as a very sensitive structural probe in many biological systems. The innate sensitivity of the technique allows the study of very small quantities of material, often allowing quantitative studies on the nanomolar scale to be carried out.

In order for any spectroscopic technique to be used to study a conformational transition in a macromolecule, there must be a discernible difference in some signal between the two (or more) macroscopic states. The sensitivity of fluorescence signals to the microenvironment of the fluorophore qualifies the technique for such studies and since we can monitor any of a number of fluorescence signals e.g. fluorescence intensity, quantum yield (ratio of the intensity of the fluorescent light to the intensity of the incident light), emission maximum, fluorescence lifetime, fluorescence anisotropy, to name a few, it is likely that some signal will be sensitive to the conformation of the molecule.

Fluorescence, especially intrinsic tryptophan fluorescence is extremely sensitive to temperature and therefore all experiments were performed with the cuvet holder attached to a thermostatically controlled water bath and circulator to maintain the desired temperature. All measurements were made on a Spex FluoroMax spectrofluorimeter interfaced with a personal computer and using square 1 cm quartz cuvetts. All sides of these cuvetts are optical surfaces to allow detection of fluorescence perpendicular to the incident light. Consideration of sample concentration is vital in fluorescence experiments as high concentrations of sample can lead to inner filter effects. Quite simply this occurs when the sample closest to the source of incident light absorbs light such that the sample further on in the pathlength receives less light and subsequently the intensity of fluorescence may be decreased by either the lowering of the effective intensity of the incident light or by the absorbance of some of the fluorescence. To prevent inner filter effects, experiments were carried out at a protein concentration in the

region of (0.5 μM). When recording fluorescence spectra, buffer baselines were also recorded to ensure not only that the buffer itself was not fluorescent (due to possible contamination) but also to allow subtraction of peaks occurring from light scattering and Raman effects. All buffer solutions were filtered (0.2 μm pore size) to remove any dust and other particulate matter.

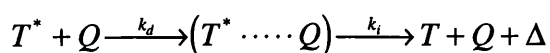
2.4.1 Intrinsic Tryptophan Fluorescence Spectroscopy

All experiments were performed by exciting the sample at 295 nm (both tyrosine and tryptophan absorb maximally at 280 nm although tryptophan has the higher absorbance at its maximum and shows significant absorbance at 295nm whereas tyrosine does not) and collecting emission data in the 300-600 nm wavelength range. Data were collected at 1 nm increments with the software sampling each wavelength for 0.3 s and averaging the fluorescence intensity.

Experiments involving monitoring the fluorescence intensity as a function of temperature required the thermostatically controlled water bath to be adjusted as necessary. A digital thermocouple thermometer was also placed in the sample cuvet to monitor the actual sample temperature. An approximate heating rate of 60 $^{\circ}\text{C}/\text{hr}$ was achieved.

2.4.2 Succinimide quenching

The quenching reaction between the excited state of a tryptophan residue, T^* , and a quenching agent, Q , can be described as follows (Eftink and Ghiron, 1984):



where $(T^* \cdots Q)$ is the complex resulting from the diffusional encounter between T^* and Q with rate constant k_d . Δ is the energy released when the excited state dissipates and k_i is the rate constant for the radiationless deactivation of the complex.

The Stern-Volmer Law (Stern and Volmer, 1919) is a classical relationship often used to analyse data from the collisional process presented above. It relates the drop in fluorescence to the concentration of a collisional quencher, $[Q]$:

$$\frac{F_0}{F} = 1 + K_{sv} [Q] = \frac{\tau_0}{\tau} \quad (2.21)$$

where F_0 and F are fluorescence intensities in the absence and presence of quencher respectively, τ_0 and τ are fluorescence lifetimes in the absence and presence of quencher respectively and K_{sv} is the collisional quenching constant (also known as the Stern-Volmer constant or coefficient). This relationship is valid for quenching processes involving succinimide as the quenching agent as it is a large, relatively inefficient quencher (Eftink and Ghiron, 1981; Eftink and Ghiron, 1984). K_{sv} can be used as a measure of the accessibility of tryptophan residues when compared to the K_{sv} obtained on quenching a solution of L-tryptophan in appropriate buffer.

Experimental determination of K_{sv} involves the following. A 0.5 μM solution of mAb in required buffer is excited at 295 nm and the emission spectrum recorded (a spectrum of buffer alone is also recorded under identical conditions). 20 μl aliquots of succinimide solution (2.5 M in buffer) are then added and the fluorescence intensity at 330nm recorded (Eftink and Ghiron, 1984). A total of 300 μl quencher is added for each experiment and each experiment was repeated to check for reproducibility. Fluorescence intensity data are then corrected for both buffer effects and dilution. F_0/F is then plotted against succinimide concentration, the slope of the graph being equal to K_{sv} in accordance with the Stern-Volmer Law. K_{sv} for free L-tryptophan in identical buffer is also determined by quenching a 2 mM solution in a similar fashion.

2.4.3 Acrylamide Quenching

Acrylamide is a small, organic, uncharged polar quenching agent and is described as being an efficient quencher of tryptophanyl fluorescence and is very discriminating in sensing the degree of exposure of this residue in proteins (Eftink and Ghiron, 1976a) whereas it has been mentioned previously that succinimide is a large and relatively inefficient quencher of tryptophan fluorescence. Because the acrylamide molecule is small, polar and uncharged, the quenching of buried fluorophores can occur as the molecule finds its way into the interior of the protein by making use of dynamic nature of the protein structure.

One major consideration when using tryptophan as a structural probe in proteins is the presence of multiple tryptophan residues causing the fluorescence properties to be heterogeneous in nature as there may be energy transfer between the various tryptophan residues and each fluorescing group may have its own quenching constant. All three mAbs are multi-tryptophan containing proteins but although their quenching data are difficult to analyse precisely, useful qualitative information can still be obtained (Eftink and Ghiron, 1976a).

A complexity which arises when acrylamide is used as a quenching agent is the fact that it quenches indole fluorescence by both a dynamic and a static process. Static quenching involves the formation of a complex between quencher and fluorophore which predates the excitation. Excitation of the fluorophores then results in instantaneous quenching of those that are complexed. This mechanism of static quenching is not explained by the collisional mechanism of Stern and Volmer and leads to positive deviations in Stern-Volmer plots. A modified version of the Stern-Volmer equation that describes quenching data when both dynamic and static quenching occur has been devised (Eftink and Ghiron, 1976b).

$$\frac{F_0}{F e^{V[Q]}} = 1 + K_{sv}[Q] = \frac{\tau_0}{\tau} \quad (2.22)$$

where V is the static quenching constant (taken to be 1.5 M^{-1} for the quenching of tryptophan by acrylamide at $25 \text{ }^\circ\text{C}$, excitation wavelength 295 nm (Eftink and Ghiron, 1976b)). Thus a modified Stern-Volmer plot of $[(F_0/F e^{V[Q]}) - 1]$ against $[Q]$ gives a straight line with gradient K_{sv} .

Acrylamide absorbs light at 295 nm (the excitation wavelength used during quenching experiments) and a correction factor of $\text{antilog } \Delta\text{OD}/2$ (where ΔOD is the incremental increase in optical density at the excitation wavelength as quencher is added, and 0.5 cm is the effective pathlength of the cell) must be applied for the attenuation of the incident light (Eftink and Ghiron, 1976b). This must be determined experimentally. $20 \text{ }\mu\text{L}$ aliquots of 8 M acrylamide (Freskgård and Petersen et al., 1998) in required buffer is added to a 1 cm pathlength quartz cuvet containing a $0.5 \text{ }\mu\text{M}$ solution of protein in identical buffer. The absorbance of the resulting solution at 295 nm is noted after each acrylamide addition over

five additions. The change in absorbance on each aliquot addition should be constant and is taken as ΔOD .

Quenching experiments are carried out by exciting the protein at 295 nm and recording the emission spectrum, then titrating a 0.5 μM protein solution with 20 μl aliquots of 8 M acrylamide until 300 μl is added, recording the emission spectrum after each addition. A 2 mM solution of L-tryptophan is also quenched in the same way to obtain the K_{sv} of fully exposed tryptophan. The fluorescence intensities at 330 nm are then corrected for buffer effects, dilution and acrylamide absorbance and the results plotted as a modified Stern-Volmer plot ($[(F_0/F_e^{V[Q]})-1]$ against $[Q]$) with the gradient of the line equal to K_{sv} .

2.4.4 Extrinsic Fluorescence of ANS

The hydrophobic fluorescent probe ANS (8-anilino-1-naphthalene sulfonic acid) is a powerful tool for monitoring protein unfolding as it can be used to probe the hydrophobicity of a protein surface (Busby and Ingham, 1987). The molecule has a weak fluorescence in aqueous solution but this is markedly increased upon binding to hydrated hydrophobic surfaces on proteins, and a blue shift in the emission maximum occurs (Ptitsyn et al., 1990; Guha and Bhattacharyya, 1995).

For experiments binding ANS to protein, samples were excited at 390 nm and the emission spectrum recorded from 400-700 nm using a 1 cm pathlength quartz cuvet. A stock solution of 2 mM ANS was prepared by dissolving ANS in the relevant buffer. A spectrum of buffer only was obtained for the purpose of subtraction, ANS was then added at a concentration of 20 μM and the spectrum recorded and finally protein was added (0.2 μM) and the final spectrum recorded. All binding experiments, except those involving measuring hydrophobicity as a function of temperature, were carried out at 25 °C. Required temperatures were achieved by means of a thermostatically controlled water bath and circulator.

2.5 Circular Dichroism

Circular dichroism (CD) refers to the differential absorption of the left and right circularly polarised components of plane polarised light and is a widely used technique for

studying peptide and protein conformation (Kelly and Price, 1997). The basis of the technique is that a molecule is optically active if it interacts differently with the left and right circularly polarised light. Optical activity is only observed if the chromophore is chiral either (i) intrinsically, by way of its structure e.g. the peptide bond, or (ii) by being covalently linked to a chiral centre or (iii) via interactions from asymmetrically placed neighbouring groups.

When using CD to analyse protein structure, two types of CD can be distinguished. First, there is CD related to the protein backbone which is derived from amide-amide interactions and second, superimposed on this, there is the CD from the chromophores of the aromatic amino acid, the disulfide bond and prosthetic groups etc which are optically active either by default, i.e. they 'sense' the chirality of the protein backbone, or they may be intrinsically chiral.

Near-UV-CD is a powerful technique that can be used for probing small structural changes (Freskgård and Petersen et al., 1998). The variation of CD in this wavelength region (310-240 nm), for most proteins, is due to the contributions of phenylalanine, tyrosine, tryptophan and the disulfide chromophore of cystine. The near-UV region reflects the tertiary structure of a protein and although it is not readily amenable to detailed interpretation in terms of tertiary structural features, it provides a fingerprint of the native state of a protein.

The far-UV CD spectrum (250-170 nm) is generally used to probe the secondary structure of proteins. It is well known that the different forms of regular secondary structure found in proteins and peptides exhibit distinct far-UV CD spectra and this knowledge has provided a means of taking any observed spectrum and estimating the contributions of the different structural forms. For the purpose of this thesis, the quantitative analysis of such spectra was unnecessary and qualitative data only was extracted.

CD spectra were recorded at the Scottish CD Facility, University of Stirling (run by Prof. N. Price and Dr S. Kelly) on a Jasco J-600 spectropolarimeter fitted with a thermostated cell holder connected to a thermostatically controlled water bath and circulator. A heating rate of 60 °C was achieved. Cell pathlengths of 0.02 and 1.0 cm were used. All buffer and protein solutions were filtered (0.2 µm pore size) prior to use to remove dust and other particles. Protein concentrations were typically 6.7 µM in 0.01M citrate buffer (0.01M Tris was used for 1209W95). Buffer baselines were run under identical conditions for the purpose

of subtraction. Chemical unfolding experiments were carried out at 25 °C, the temperature for thermal unfolding experiments was increased by means of the waterbath/circulator and the sample temperature monitored using a thermocouple thermometer probe inserted directly in to the cell.

2.6 Induced Aggregation Experiments

Experiments to monitor the effect of preformed aggregate on the rate of thermal aggregation of Campath-1H took two forms. Firstly the rate of aggregation was studied by using UV/visible spectrophotometry to measure the absorbance of protein solutions at 280 nm (and hence measure protein concentration (see section 2.3.1)) and the turbidity of the solutions at both 320 and 400 nm, and secondly, activation energies and rate constants for the process of thermal denaturation in the presence of preformed aggregate were calculated using the method described in section 2.2.3 and compared to the values in the absence of preformed aggregate presented in table 4.7.

The first type of experiments were performed as follows. 1 ml aliquots of a 0.009 mM solution of Campath-1H (pH 6 CBS) were incubated over a period of days in a thermostatically controlled waterbath at certain temperature at which the folded form of the protein was deemed unstable (i.e. below the T_m of main transition endotherm as observed by DSC). 60, 65, and 70 °C were used in separate trials. Half the samples contained either 5, 10 or 20 μ l of a dispersed solution of aggregated Campath-1H (prepared by heating an aliquot of Campath-1H (0.009 mM, pH 6 CBS) to 85 °C). At specific time intervals, nominally every 24 hours, 200 μ l was removed from each sample, centrifuged for 5 mins at 13 000 r.p.m. and the absorbance of the supernatant at 280 nm recorded. The absorbance was then plotted against time for each of the controls and the samples with 5, 10 and 20 μ l of added aggregate.

Experiments involving the measurement of solution turbidity were performed in a similar manner: Samples of a Campath-1H solution (0.009 mM, pH 6 CBS) were incubated at a range of temperatures between 65 and 75 °C. A number of these samples were 'seeded' by the addition of either 0.5, 1, 5 or 10% (v/v) of a solution of preformed aggregate. Over a period of 500 minutes, the turbidity of the solutions were recorded by measuring the

absorbance of the solutions at 320 and 400 nm. The absorbance was then plotted against time.

The second type of experiments, those in which the activation energies and rate constants for the denaturation process are calculated were performed as described in section 2.2.3 the only difference being the sample in the calorimeter cell contained an amount of preformed aggregate. Results were obtained for Campath-1H in pH 4 ABS with 0.2% (v/v) of preformed aggregate solution added and for Campath-1H in pH 5 CBS with 0.6, 1.0, 1.4 and 2.0% (v/v) of preformed aggregate solution added (only very small amounts of preformed aggregate were added as the presence of insoluble particulate matter in the DSC cell results in baseline noise).

2.7 Long-Term Storage Sample Preparation

Long-term storage samples were prepared by dialysing the protein into the desired buffer/additive formulation. The bulk filling solutions were then passed through a 0.22 μm sterilising grade filter and 1 ml (nominal volume) aliquots collected in sterile neutral glass vials and stoppered with sterile latex caps and then finally sealed with sterile crimped aluminium seals. The complete filling procedure was carried out within a laminar flow cabinet. Vials were then labelled and stored at 4 °C in darkness for 2 years.

2.8 Isothermal Calorimetry

The VP-DSC has two basic modes of operation; scanning (conventional DSC) and isothermal. A description of the DSC mode is given in sections 2.1.1 and 2.2.2. In isothermal mode, constant temperature is maintained for relatively long periods of time while measuring differential power between the reference and sample cells (the duration of the experiment is limited only by PC disc space). All measurements were carried out for a duration of 24 hours with a filter setting of 60 s.

Sample preparation and filling is identical to the DSC mode with the exception that relatively high protein concentrations are necessary (in the region of 0.03-0.10 mM) and

Chapter 2

buffer baseline experiments are still performed. Again the data are analysed using MicroCal Origin 5.0 software.

CHAPTER 3

THERMAL UNFOLDING OF MONOCLONAL ANTIBODIES

3.1 Introduction

The thermal unfolding of mAbs is of great interest to the pharmaceutical industry due to their interest in developing them as possible therapeutic targets. mAb functionality is directly linked to their antigen binding abilities which are determined by their structural features. DSC has been used in the past to monitor thermal events occurring when these polyglobular glycoproteins unfold (Tischenko et al., 1982; Loseva, 1986; Kravchuk, 1998) and deconvolution of DSC data to obtain information about individual domain events has been attempted (Tischenko et al., 1982) and comparisons to data obtained from electron microscopy data made (Ryazantsev et al., 1990). Other studies of thermal stability have utilised CD and capillary electrophoresis (Kats et al., 1995), micellar electrokinetic capillary chromatography (Kats et al., 1997), capillary isoelectric focusing (Dai et al., 1998), and matrix-assisted laser desorption/ionization mass spectrometry (Alexander and Hughes, 1995).

A common problem in previous work, which leads to some disagreement between publications from different groups, is the assignment of multiple calorimetric endotherms (or rather many sharper endotherms representing two-state transitions which have been arrived at via deconvolution of one or two broad endotherms from the experimental DSC profile), to the unfolding of individual IgG domains. Tischenko et al., (1982) fit DSC data to seven cooperative transitions in an IgG molecule with twelve domains whereas Kravchuk et al., (1998) fit DSC data to six or five simple two-state transitions. In this chapter, such controversial fitting (and deconvolution) of DSC data is avoided. The purpose of the work presented in this chapter is to present a comprehensive analysis of the thermal unfolding of the three mAbs; Campath-1H, 4162W94 and 1209W95, using data obtained from DSC, CD and fluorescence spectroscopy experiments. The work is an attempt to understand the effects of elevated temperatures on these proteins and to investigate how unfolding information gained using different techniques is related.

3.2 Results

3.2.1 DSC Data

The pH dependence of the thermal stability was investigated by obtaining the DSC profiles of the three mAbs at a range of pHs (scans were all carried out at a nominal scan rate of 60 °C/hr unless stated otherwise). In the case of Campath-1H scans in, 0.1 M CBS pH 3, 4, 5 and 6, ABS pH 4, and PBS pH 7.1 were recorded. No difference was observed in trial scans if pH4 ABS was replaced with pH4 CBS so pH4 ABS was normally used throughout. Figure 3.1a shows the effect of pH on the DSC profiles of Campath-1H with the corresponding T_m values presented in table 3.1. Initial experiments were repeated several times, however results were very consistent (typical errors on the T_m values were ± 0.1 °C). Figure 3.1b shows a plot of T_m versus pH and the resultant curves are typical of the titration of carboxylate residues. DSC scans were always repeated to check for any calorimetric reversibility but none was observed (unless otherwise stated). Above pH 6, Campath-1H produced a single asymmetric endotherm, the asymmetry being caused by a sharp exothermic peak on the high temperature side of the main endotherm and a shoulder on the low temperature side. As pH is decreased, the T_m of both the main endotherm and the shoulder decrease in such a manner that the shoulder becomes a discrete small endotherm and also the exothermic peak is not observed at pH 4 and below. If the exothermic peak is present on the DSC profile, when removed from the instrument, the sample had invariably aggregated (this aggregation is also the cause of noisy posttransition baselines as the precipitated protein is involved in erratic convection effects within the calorimeter cell) and therefore it was decided to carry out thermal unfolding experiments using CD and fluorescence spectroscopy at pH 3.5 to prevent aggregation of the molecule at elevated temperatures.

DSC profiles of 4162W94 were recorded at pH 3-6 and results are shown in figure 3.2 with corresponding T_m values in table 3.2. The DSC profile of 4162W94 at pH 6 is very similar in shape to those of Campath-1H at pH ≥ 6 , though if the buffer is made more acidic, the exothermic peak is no longer observed and two more small endotherms appear on the high temperature side of the main endotherm. Again, the exothermic peak was indicative of gross thermal aggregation of the sample and further investigations into thermal unfolding were carried out at pH 3 so that gross aggregation would not occur.

In the case of 1209W95, DSC scans were recorded at pH 6.6 and 8 (protein visibly aggregated outside this pH range), DSC scans and T_m values are presented in figure 3.3 and table 3.3 respectively. DSC profiles of 1209W95 throughout this pH range consisted of one large asymmetric endotherm, foreshortened its high temperature side by a sharp exothermic peak consistent with aggregation of the sample.

DSC transitions were also analysed using a successive annealing technique which checks the reversibility of individual endotherms and exposes any small endotherm hidden 'beneath' larger endotherms (Shnyrov and Mateo, 1993, Kreimer et al., 1995, Shnyrov et al., 1996). The results of this technique for Campath-1H, 4162W94 are presented in figures 3.4 and 3.5 respectively (1209W95 was also investigated using this technique but the sample invariably aggregated before any relevant data could be collected). The first endotherm of Campath-1H is reversible at pH 3.5 (as long as the temperature is not raised above that of the T_m of the second endotherm) and the fourth endotherm of 4162W94 (pH 3) is reversible though the degree of reversibility decreases with successive heating cycles, as shown in figure 3.6.

3.2.2 CD Data

In order to assist with the interpretation of the structural events occurring on heating, which are evident from DSC profiles, both near- and far-UV CD spectra for each mAb were collected at a range of temperatures. These CD spectra were used qualitatively to monitor structural changes. To avoid thermal aggregation occurring while CD spectra were being recorded at elevated temperatures, buffer pH was chosen to prevent such aggregation based on results from low pH DSC experiments. To minimise buffer absorbance, dilute buffers (10 mM) were used to maintain pH and buffer components which contain chloride ions were omitted as Cl^- ions absorb strongly below 195 nm (Kelly and Price, 1997). 'Blank' CD spectra of buffer only were also run to ensure buffer components did not lead to excessive noise or other artefacts in the spectra.

CD spectra of Campath-1H (pH 3.5), 4162W94 (pH 3) and 1209W95 (pH 8) were recorded over a temperature range of 25-65 °C (waterbath/circulator set-up could not reach and maintain higher temperatures). The results of these experiments are shown in figures 3.7,

3.8 and 3.9 for Campath-1H, 4162W94 and 1209W95 respectively. Spectra recorded at every temperature are not plotted, only a sample of relevant recorded spectra are presented.

As can be seen from figure 3.7a (near-UV CD spectra), monitoring changes in the molar ellipticity at 295 nm (a wavelength at which the CD of most proteins is sensitive to changes in tertiary structure) reveals a small but significant change in tertiary structure between 25 and 50 °C followed by a collapse of tertiary structure between 50 and 65 °C. Monitoring the molar ellipticity at 225 nm as shown in figure 3.7b (far-UV CD spectra) reveals changes within the secondary structure of the molecule i.e. changes in the strong β -sheet signal typical of IgGs (Kats et al., 1995). It shows no change in the secondary structure of the molecule below 50 °C though above this temperature there is a major change where in fact all secondary structure is lost.

Similar changes are observed with 4162W94. The near-UV CD spectrum (fig. 3.8a) as monitored at 295 nm reveals an initial change in tertiary structure at approximately 48 °C followed by another change above 60 °C which results in loss of all tertiary structure. The far-UV CD spectrum (fig. 3.8b) as monitored at 225 nm reveals no change in secondary structure below 45 °C but at higher temperatures there is a major change which results in loss of secondary structure.

The near-UV CD spectrum of 1209W95 (fig. 3.9a) reveals changes in tertiary structure at approximately 55 °C with loss of tertiary structure occurring by 60 °C. The far-UV CD spectrum (fig. 3.9b) reveals secondary structural changes coincident with these tertiary structure changes. By 60 °C, the sample of 1209W95 used for CD measurements had visibly aggregated.

3.2.3 Fluorescence Spectroscopy

3.2.3.1 Intrinsic Tryptophan Fluorescence

Using intrinsic tryptophan fluorescence as a probe to monitor structural changes, fluorescence emission spectra of the three mAbs as a function of temperature were recorded. Again we attempted to carry out experiments with proteins buffered at pHs which prevented gross thermal aggregation as such aggregation and the resultant turbidity of the solution

would prevent measurement of the spectra. Therefore Campath-1H was buffered at pH 3.5, 4162W94 at pH 3 and 1209W95 at pH 8 and the spectra recorded from 25-70 °C. The fluorescence intensity at 350 nm (excitation λ was 295 nm) was then plotted as a function of temperature and figures 3.10 and 3.11 show data for Campath-1H and 4162W94 respectively. (1209W95 repeatedly aggregated before any relevant data could be obtained therefore no data are shown). The fluorescence spectrum of a solution of free tryptophan in relevant buffer as a function of temperature was used as a control experiment.

Figure 3.10 shows two points inflection arrowed at approximately 41 °C and 63 °C indicating changes in the polarity of the environment of Campath-1H tryptophan residues at these temperatures. Figure 3.11 shows three points of inflection at 38 °C, 48 °C and 60 °C again representing changes in the polarity of the environment of the tryptophan residues within 4162W94. All chosen points of inflection are positive. The fluorescence intensity decreases at high temperatures probably due to photobleaching and/or a reduction in quantum yield caused by increased thermal energy.

Measurements of intrinsic tryptophan fluorescence were also recorded before and after DSC scans. The emission spectrum (excitation λ was 295 nm) of Campath-1H (pH 4) has a maximum emission intensity at 335 nm but after heating to 100 °C in the DSC cell this maximum becomes red shifted to 347 nm, similarly there is a red shift from 339 nm to 348 nm with 4162W94 (pH 3). Again the aggregation of 1209W95 during DSC scans precluded such experiments.

3.2.3.2 Extrinsic Fluorescence of ANS Binding

In a similar fashion to the intrinsic tryptophan fluorescence experiments described in section 3.2.3.1, the binding of ANS to the three mAbs, as a function of temperature was recorded by monitoring the fluorescence emission of ANS. The binding of ANS to free tryptophan, in solution in the relevant buffer, as a function of temperature was used as a control experiment. These data revealed the temperature-induced changes in the hydrophobicity of the protein surface. Data were plotted as graphs of fluorescence intensity at 480 nm (excitation λ was 390 nm) as a function of temperature. The results pertaining to Campath-1H, 4162W94 and 1209W95 are presented as figures 3.12a, 3.12b and 3.12c respectively.

Figure 3.12a shows two transitions in ANS binding to Campath-1H at approximately 50 °C and 70 °C. ANS binding to 4162W94 reveals a transition with a midpoint at approximately 48 °C as shown in figure 3.12b. Such ANS binding also indicates the irreversibility of thermal denaturation as on cooling the sample of 4162W94 back to room temperature, the fluorescence intensity returns to a much higher value. This is consistent with the irreversible nature of the transition (Ingham et al., 1993). The denaturation curve produced when ANS binds to 1209W95 has a midpoint at approximately 60 °C, as illustrated in figure 3.12c, though the sample did aggregate before the experiment was completed.

The ability of Campath-1H and 4162W94 to bind ANS was measured before and after DSC scans. When excited at 390 nm, ANS in the presence of Campath-1H (pH 3.5) has an emission maximum at 490 nm whereas in the presence of Campath-1H which has been heated to 100 °C in the DSC cell, ANS has an emission maximum of 479 nm with a corresponding increase in fluorescence intensity. Similarly the emission maximum of ANS in the presence of 4162W94 is blue shifted from 488 nm to 476 nm on heating the protein to 100 °C.

3.3 Discussion

Despite previous reports suggesting that mAbs thermally unfold by sequential domain unfolding (Tischenko et al., 1982) the results presented in this chapter indicate that this may not be the case. DSC experiments have shown that when Campath-1H is heated there are two main thermal events, both endothermic; a small 'pre-transition' endotherm and a larger endotherm at a higher temperature whereas 4162W94 produces four endotherms in total but again the largest main endotherm is preceded by a smaller 'pre-transition' endotherm (1209W95 will be discussed separately at the end of this section). DSC has also demonstrated that the first transition of Campath-1H is calorimetrically reversible (at pH 3.5) as long as heating cycles do not involve temperatures higher than the T_m of the main transition and similarly the fourth endotherm of 4162W94 shows a degree of calorimetric reversibility which decreases with successive heating cycles. The reversibility of this particular transition is interesting in that the T_m of the endotherm apparently decreases with each cycle.

Both intrinsic tryptophan fluorescence spectroscopy and monitoring the hydrophobicity of the proteins using ANS, as a function of temperature correlate with the DSC data in so much as they reveal changes to the proteins occurring at temperatures in the same regions of the T_m s of the endotherms gained from DSC experiments. Intrinsic tryptophan fluorescence experiments reveal that for both Campath-1H and 4162W94, the 'pre-transition' peak and main endotherm represent events which involve subtle changes in the environments of the tryptophan residues within the molecules. ANS binding experiments with Campath-1H reveal two maxima of binding again in the region of the T_m s of the transition evident from DSC experiments and also at comparable temperatures to those which induce changes in the tryptophan environment as revealed by intrinsic tryptophan fluorescence results. 4162W94 and 1209W95 have only one ANS binding maximum at temperatures which again correlate with the main transition from their respective DSC traces.

CD spectra of all three mAbs are most informative when we ask the question of what structural changes are occurring at these relevant temperatures. Using CD we can show that there are crucial similarities in the manner that the three molecules react to thermal treatment. Campath-1H and 4162W94 have very similar behaviour; both undergo a small change in tertiary structure, probably some domain rearrangement, followed by a major change in both tertiary and secondary structure which results in all loss of tertiary and secondary structure.

The possibility of the first transition representing some domain rearrangement is in agreement with work by Privalov (1982) which suggested that the first transition observed when the Fab fragment of an immunoglobulin unfolds is either due to the disruption of the contact between nonequivalent domains or one of the two types of the domains in the Fab fragment has a subdomainial structure as in Bence-Jones protein. 1209W95 differs in that its structural changes are not discrete events. It undergoes gradual changes in tertiary structure on heating which are eventually superimposed on changes in secondary structure at higher temperatures. These changes eventually lead to aggregation of the protein.

It is clear from the CD spectra of 4162W94 that at temperatures above that of the T_m of the second transition there is no recognisable tertiary or secondary structure, yet, it is evident from the DSC traces that there are a further two endothermic thermal events occurring, one of which shows some degree of reversibility. Both intrinsic tryptophan fluorescence and the extrinsic fluorescence of ANS binding fail to provide any useful data pertaining to these events. We have also shown that none of the four endotherms show any concentration dependence (see Chapter 4) which suggests that the peaks are not the result of the dissociation of dimers or other oligomeric aggregates. Clearly this apparent discrepancy between results gained by DSC and those from CD requires further investigation to shed more light on the subject.

In conclusion, CD, intrinsic tryptophan fluorescence and the binding of ANS have shown that the first endotherm in the case of Campath-1H and 4162W94 is due to some small change in the tertiary structure of the molecule, we propose some form of domain rearrangement. The second (main) endotherm has been shown to represent the loss of both the tertiary and secondary structure of the molecules. This was achieved by using intrinsic tryptophan fluorescence spectroscopy to probe the changes occurring in the environment of the tryptophan residues of the mAbs as temperature is increased and by monitoring changes in the hydrophobicity of the molecules as temperature increased using ANS as a hydrophobic fluorescent probe. CD was used as a synergistic technique to reveal the temperature induced structural changes in more detail. Near-UV CD spectra provided information on the tertiary structure of the proteins while far-UV CD spectra completed the unfolding picture by providing information on the changes in secondary structure. Discrete thermal transitions were distinguishable by both techniques.

1209W95 proved to behave slightly differently from the other two antibodies. CD did reveal that, when heated, the molecule did undergo changes in tertiary structure followed by major changes in tertiary and secondary structure but unlike Campath-1H and 4162W94, this process was continuous with no real distinction between the temperatures at which these processes commenced and finished. The DSC too revealed only one endotherm within the pH range that was investigated. It is not unreasonable to suggest that at lower pHs the processes may become discrete in a similar fashion to Campath-1H on going from pH 7.1 to pH 3.5 but the aggregation propensity of the molecule outside the pH 6.6-8.0 range precluded experimental proof of this theory.

pH	T _{m1} (°C)	T _{m2} (°C)
3.0	-(^a)	48.6
3.5	40.9	63.1
4.0	52.6	71.4
5.0	63.4	77.1
6.0	69.4	78.2
7.1	70.6	77.2
8.0	71.6	77.1

Table 3.1: T_m values for Campath-1H over the 3.0-8.0 pH range. (^a) Only one large endotherm (T_m= 48.6 °C) was apparent from the DSC trace. All DSC scans were performed at 60 °C/hr. Errors on T_m values were typically ±0.1 °C.

pH	T _{m1} (°C)	T _{m2} (°C)	T _{m3} (°C)	T _{m4} (°C)
3.0	46.0	48.6	60.7	72.8
4.0	50.2	65.6	(-)	(-)
5.0	63.1	75.1	(-)	(-)
6.0	71.3	77.1	(-)	(-)

Table 3.2: T_m values for 4162W94 over the 3.0-6.0 pH range. (-) indicates exothermic aggregation at temperatures above T_{m2}. All DSC scans were performed at 60 °C/hr. Errors on T_m values were typically ±0.1 °C.

pH	T _m (°C)
6.6	60.0
8.0	61.3

Table 3.3: T_m values for 1209W95 at pH 6.6 and 8.0. All DSC scans were performed at 60 °C/hr. Errors on T_m values were typically ±0.1 °C.

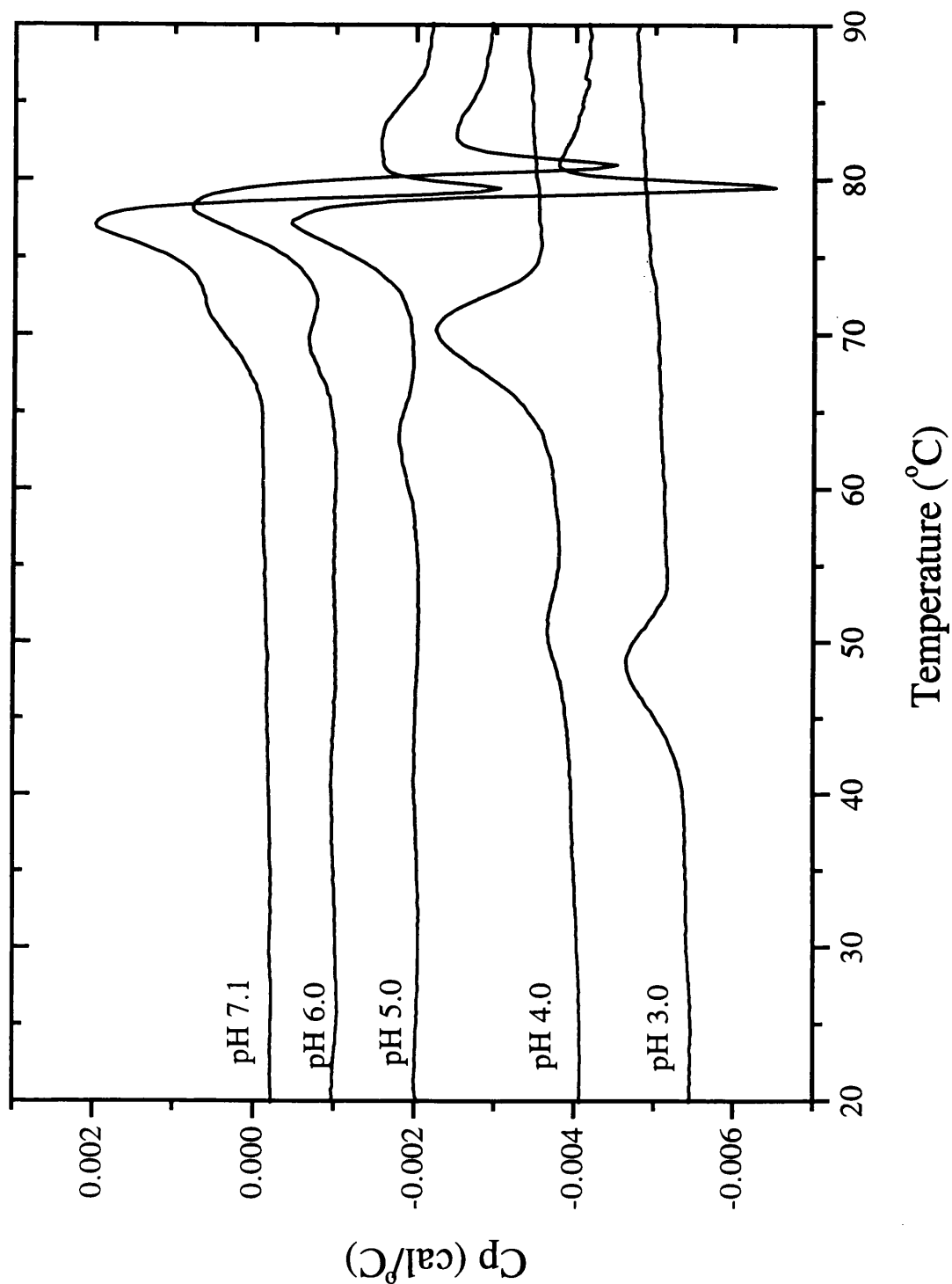


Figure 3.1a: Raw DSC data for Campath-1H (0.013 mM) in a range of pH conditions (pH 3.0-7.1) scanned at a nominal scan rate of 60 °C/hr. Buffer baseline scans have been subtracted and scans are y-offset for clarity.

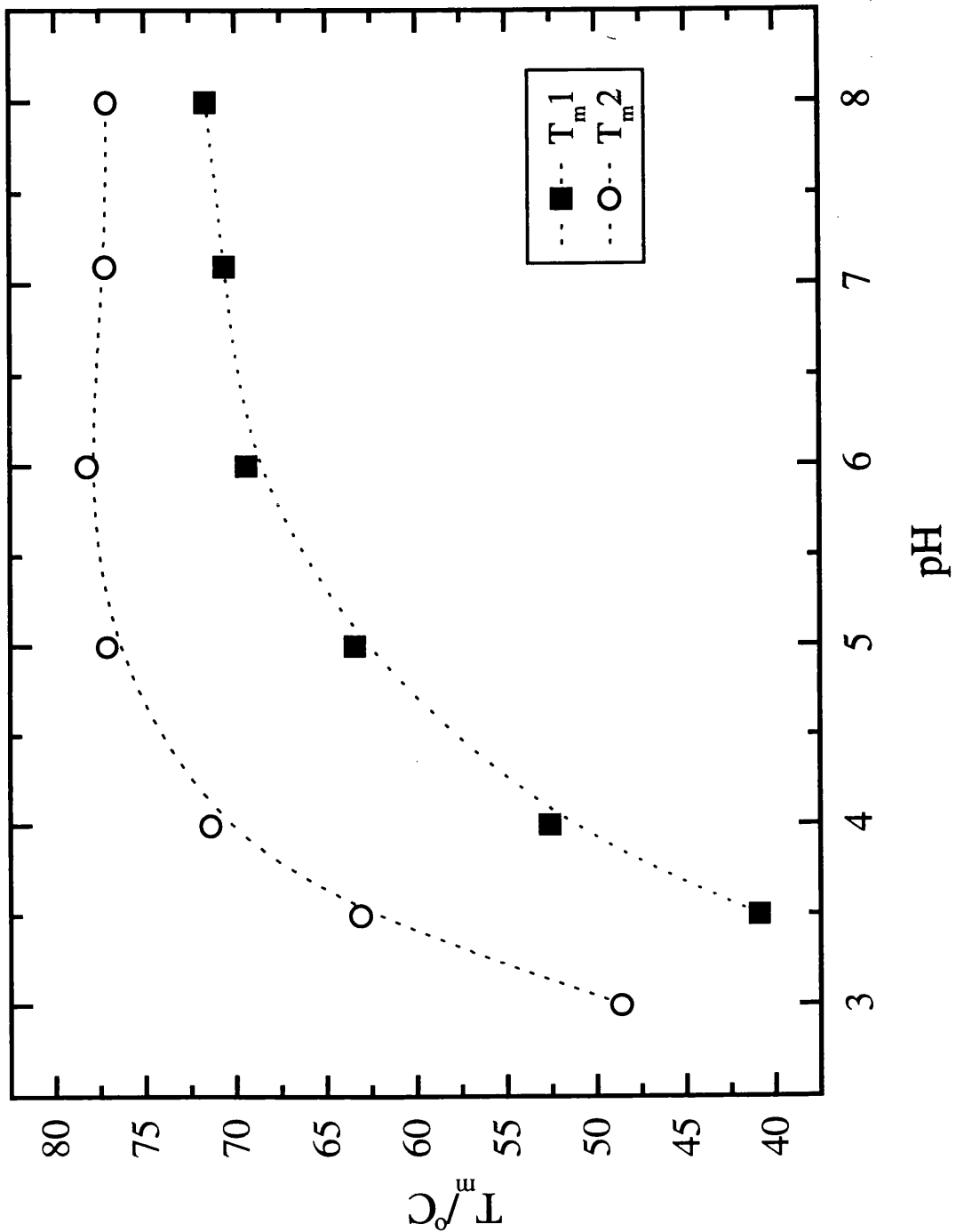


Figure 3.1b: Plots showing the variation of T_m with pH for Campath-1H (0.013 mM). T_{m1} and T_{m2} are the midpoints of the lower and higher temperature endotherms respectively as observed in the DSC scans presented in Figure 3.1a.

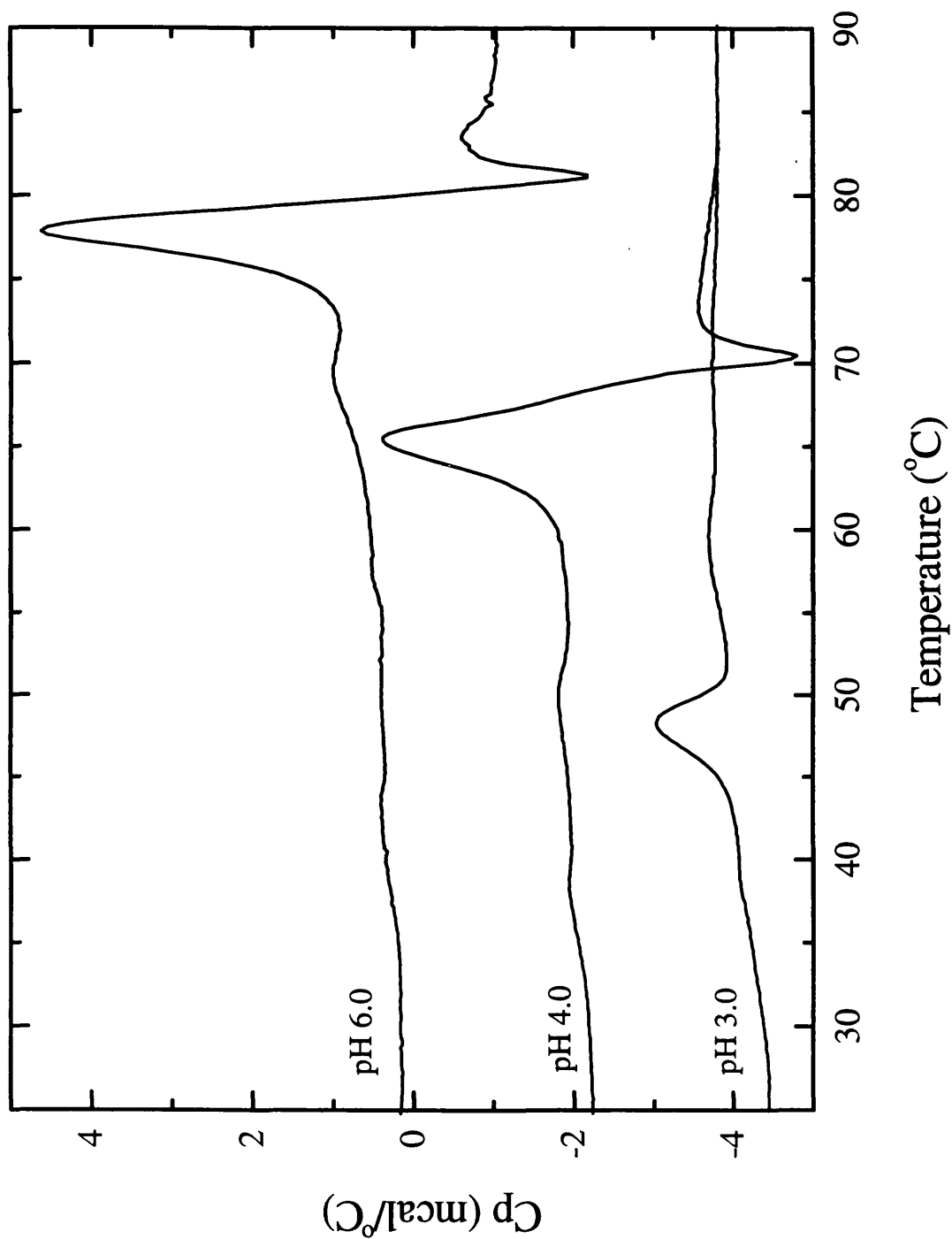


Figure 3.2: Raw DSC data for 4162W94 (0.013 mM) in a range of pH conditions (pH 3.0-6.0) scanned at a nominal scan rate of 60 °C/hr. Buffer baseline scans have been subtracted and scans are y-offset for clarity.

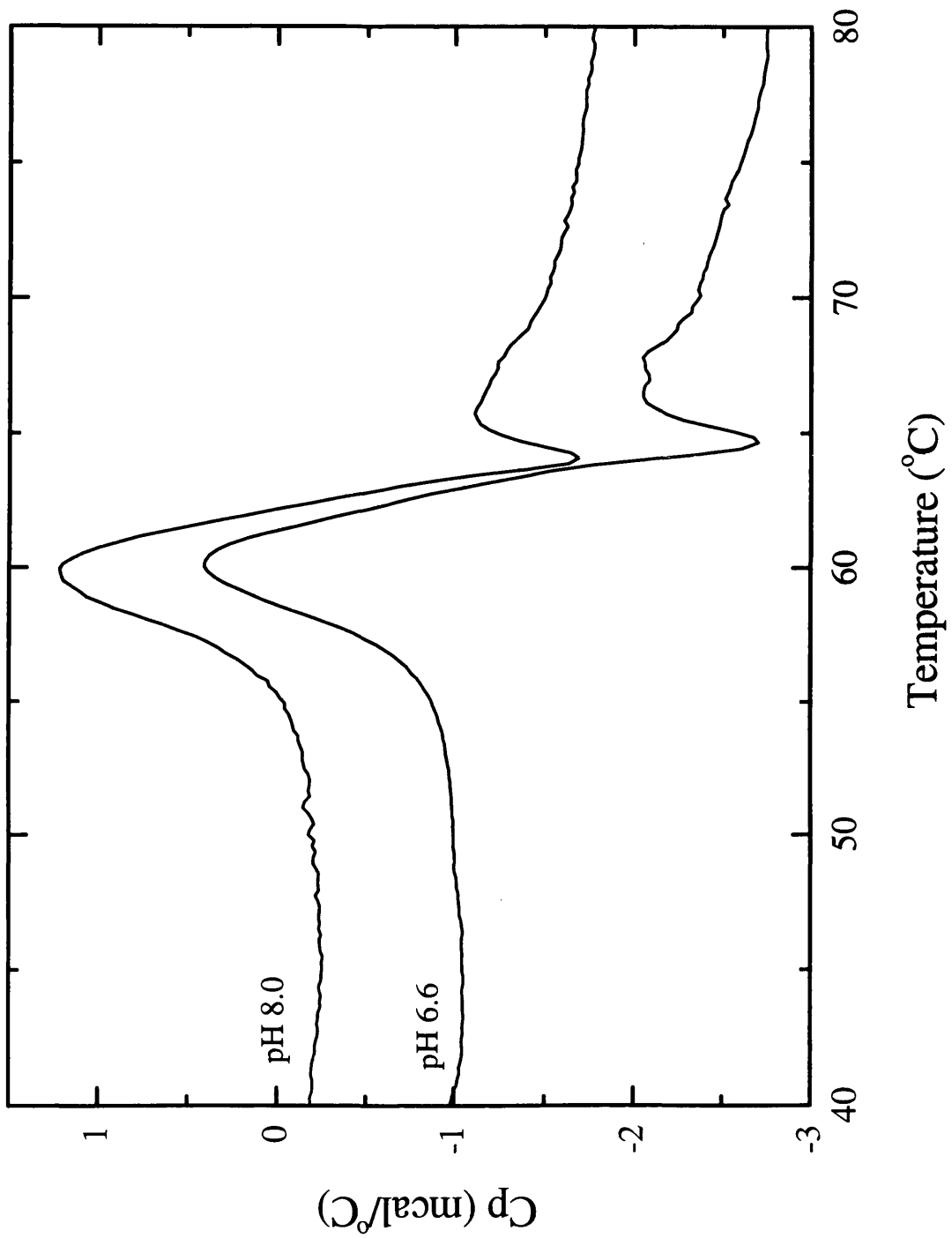


Figure 3.3: Raw DSC data for 1209W95 (0.013 mM) in two pH conditions (pH 6.6 and 8.0) scanned at a nominal scan rate of 60 °C/hr. Buffer baseline scans have been subtracted and scans are y-offset for clarity.

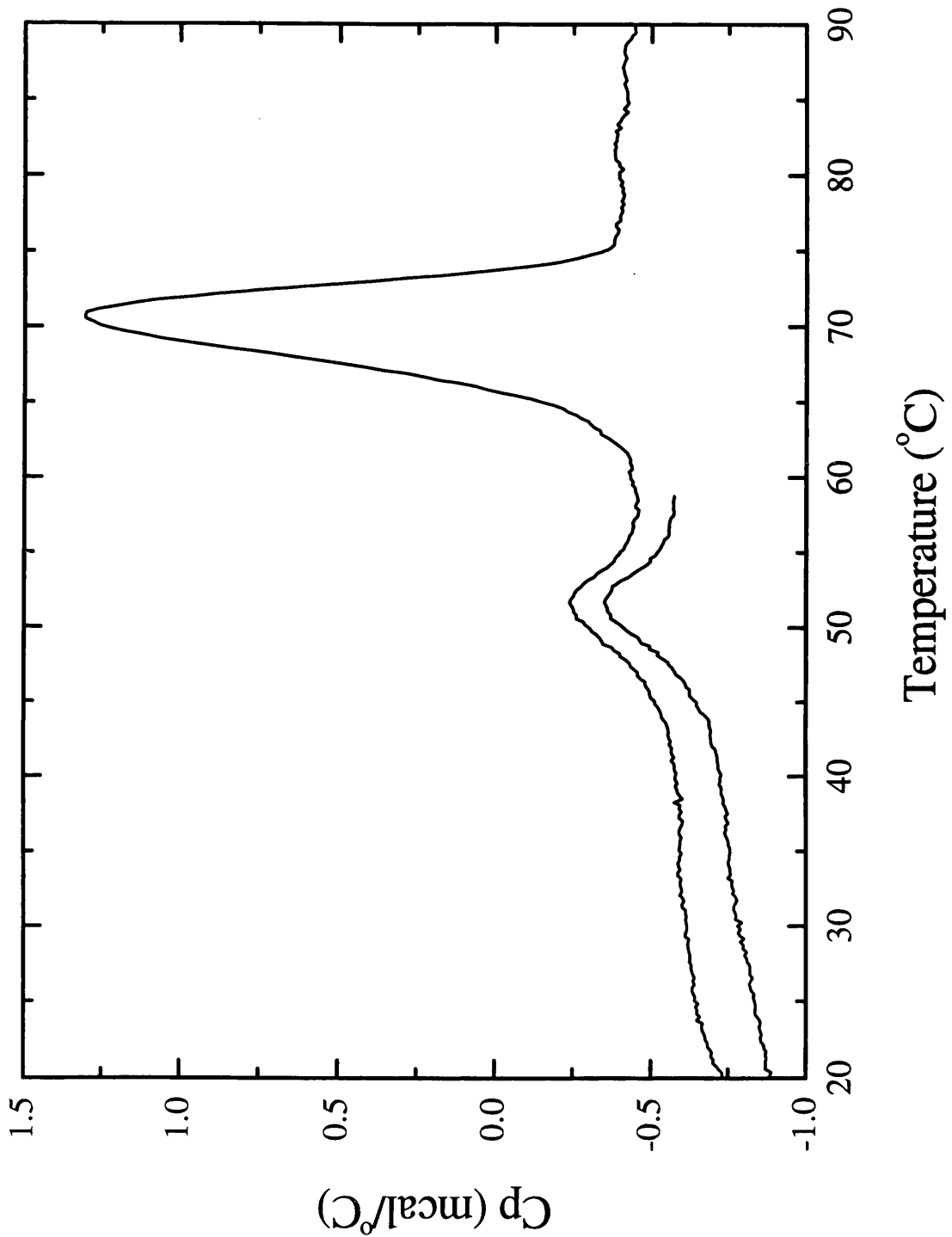


Figure 3.4: Raw DSC results of successive annealing of Campath-1H (0.013 mM, pH 3.5) showing calorimetric reversibility of first endotherm. Scans were performed at a nominal scan rate of 60 $^\circ\text{C}/\text{hr}$, buffer baseline scans have been subtracted and scans are y-offset for clarity.

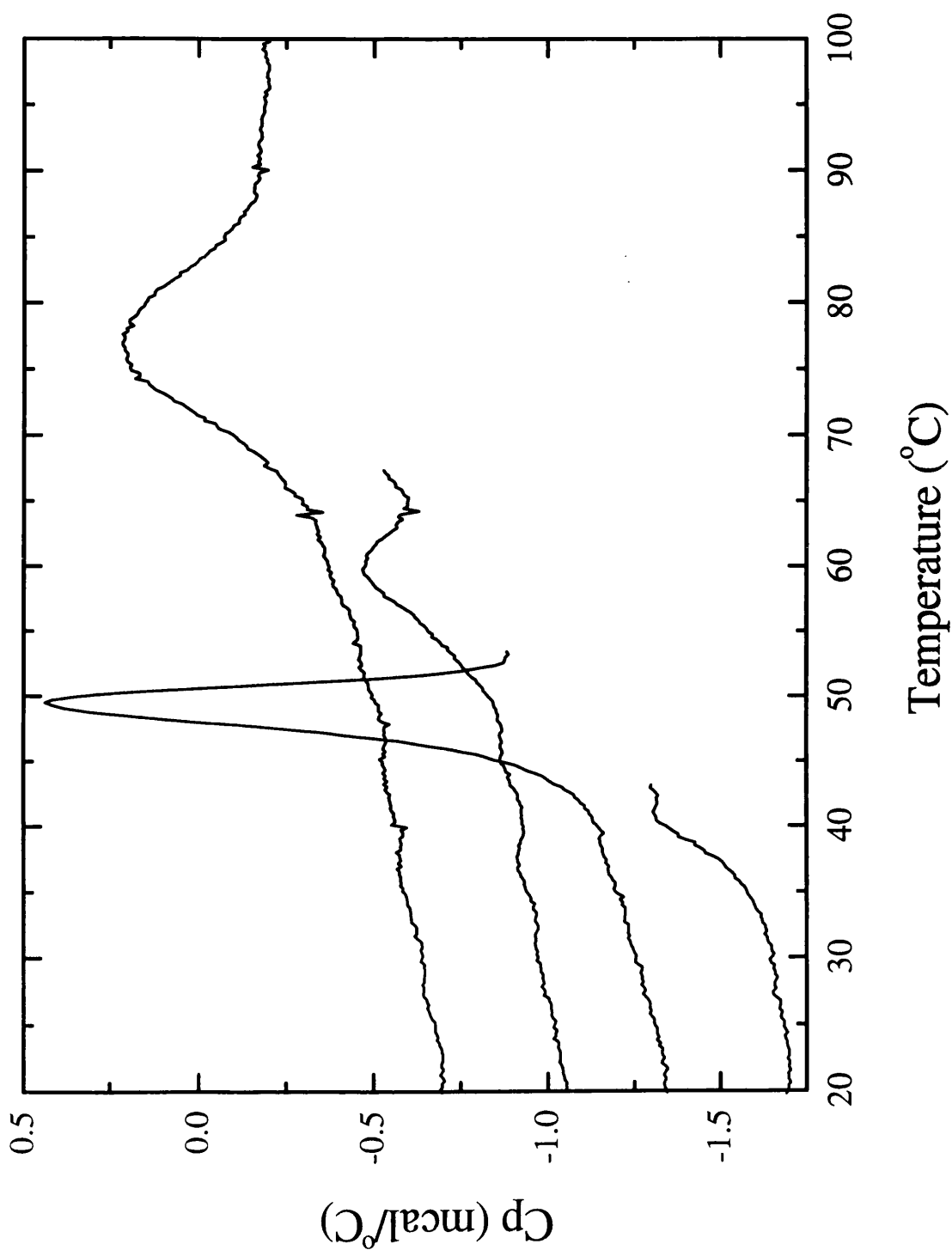


Figure 3.5: Raw DSC results of successive annealing of 4162W94 (0.015 mM, pH 3). Scans were performed at a nominal scan rate of 60 °C/hr and scans are y-offset for clarity. Buffer baseline scans have been subtracted.

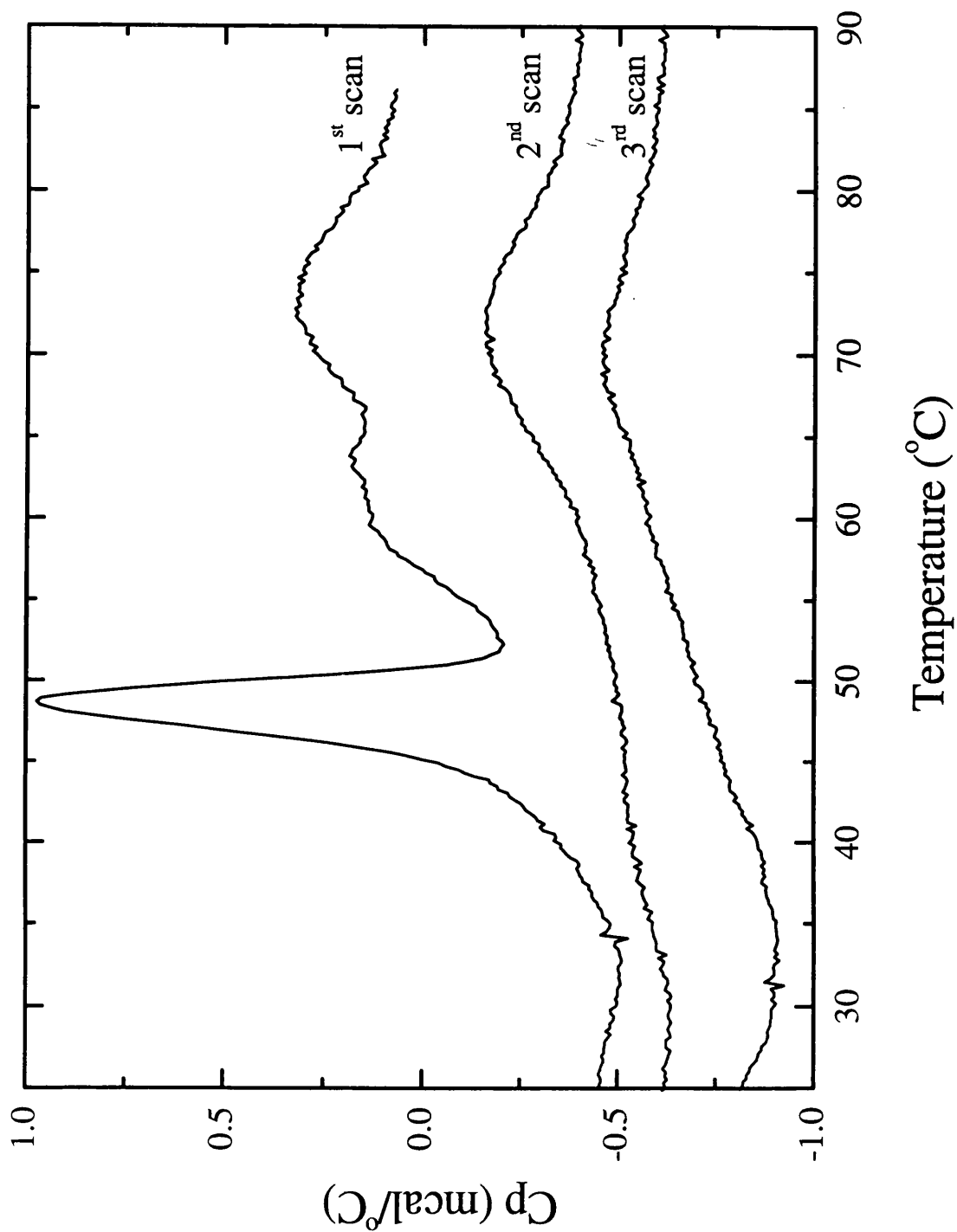


Figure 3.6: Raw DSC data showing three successive scans of 4162W94 (0.015 mM, pH 3) revealing partial calorimetric reversibility of the fourth endotherm. Scans were performed at a nominal scan rate of 60 °C/hr, are y-offset for clarity and are shown after baseline subtraction.

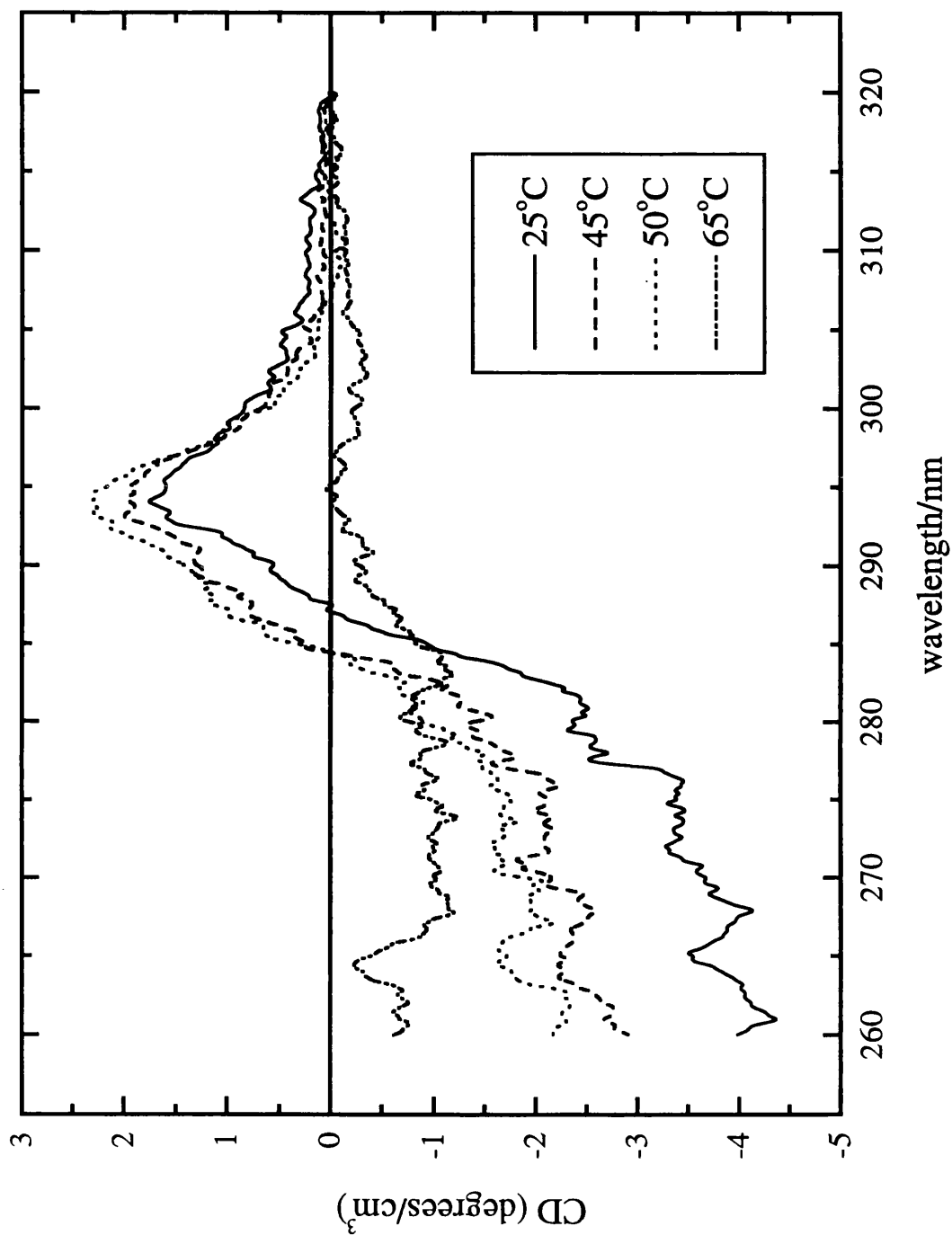


Figure 3.7a: Near-UV CD spectra of Campath-1H (6.7 μ M, pH 3.5) recorded at a range of temperatures (25-65 $^{\circ}$ C).

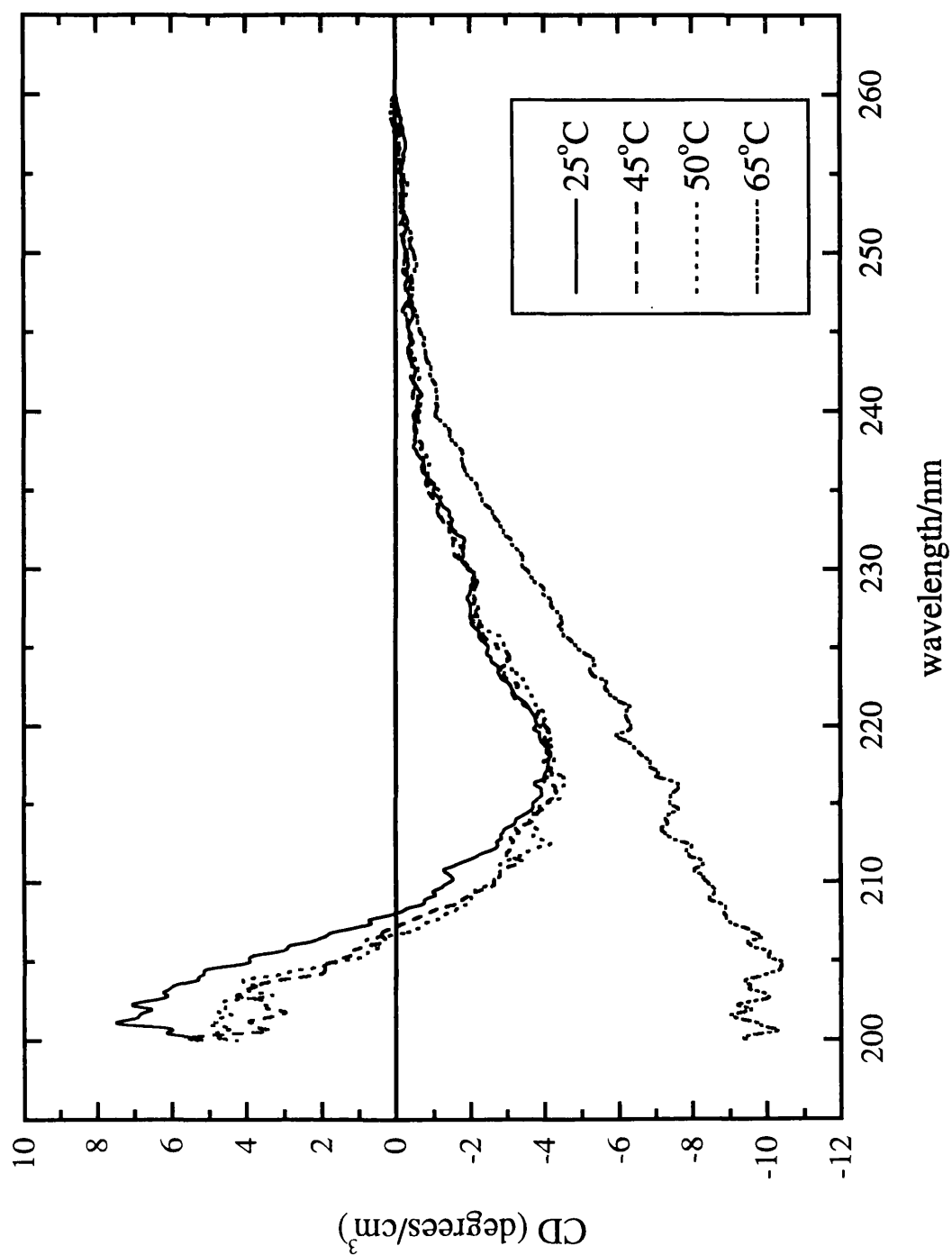


Figure 3.7b: Far-UV CD spectra of Campath-1H (6.7 μ M, pH 3.5) recorded at a range of temperatures (25-65 $^{\circ}$ C).

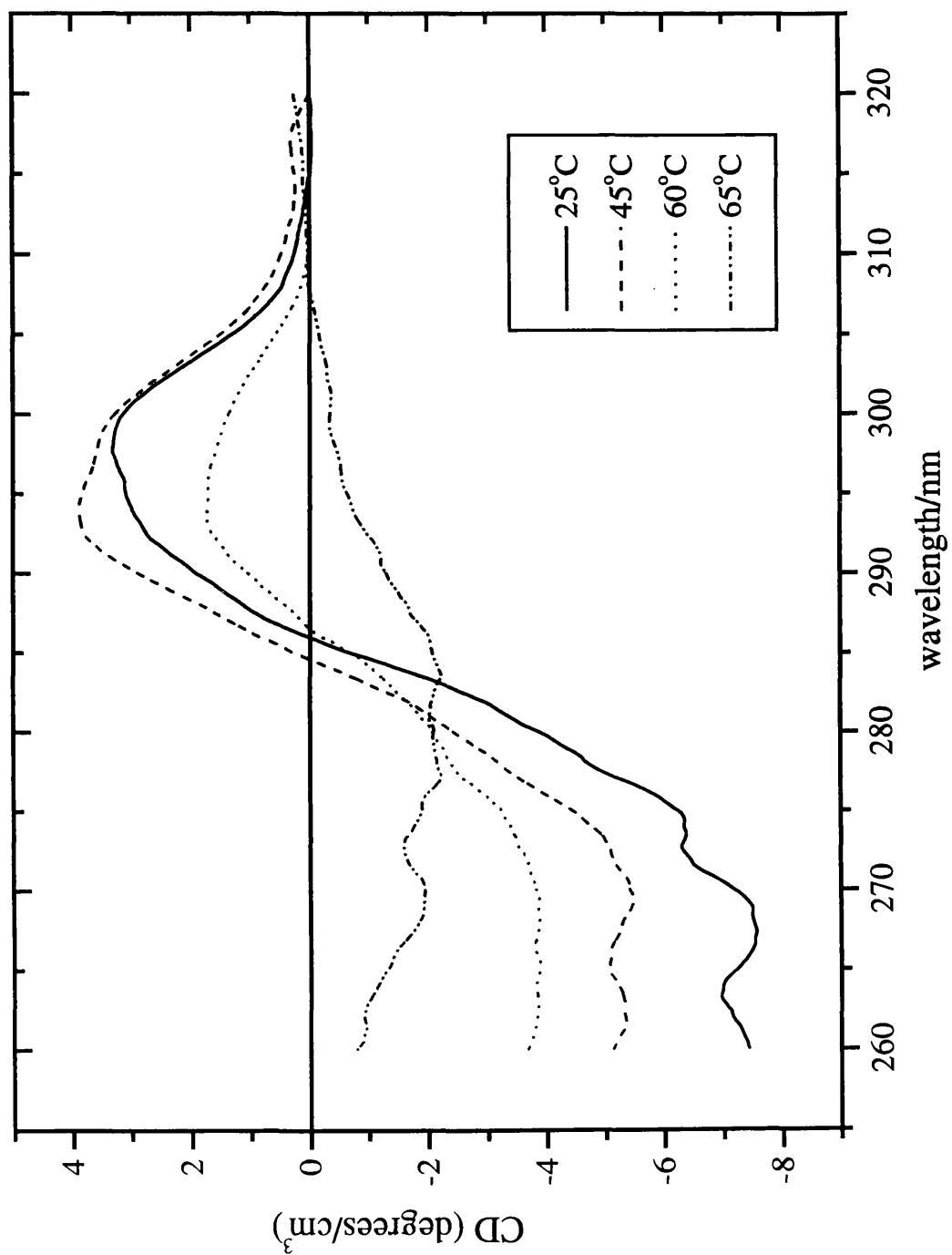


Figure 3.8a: Near-UV CD spectra of 4162W94 (6.7 μ M, pH 3) recorded at a range of temperatures (25-65 $^{\circ}$ C).

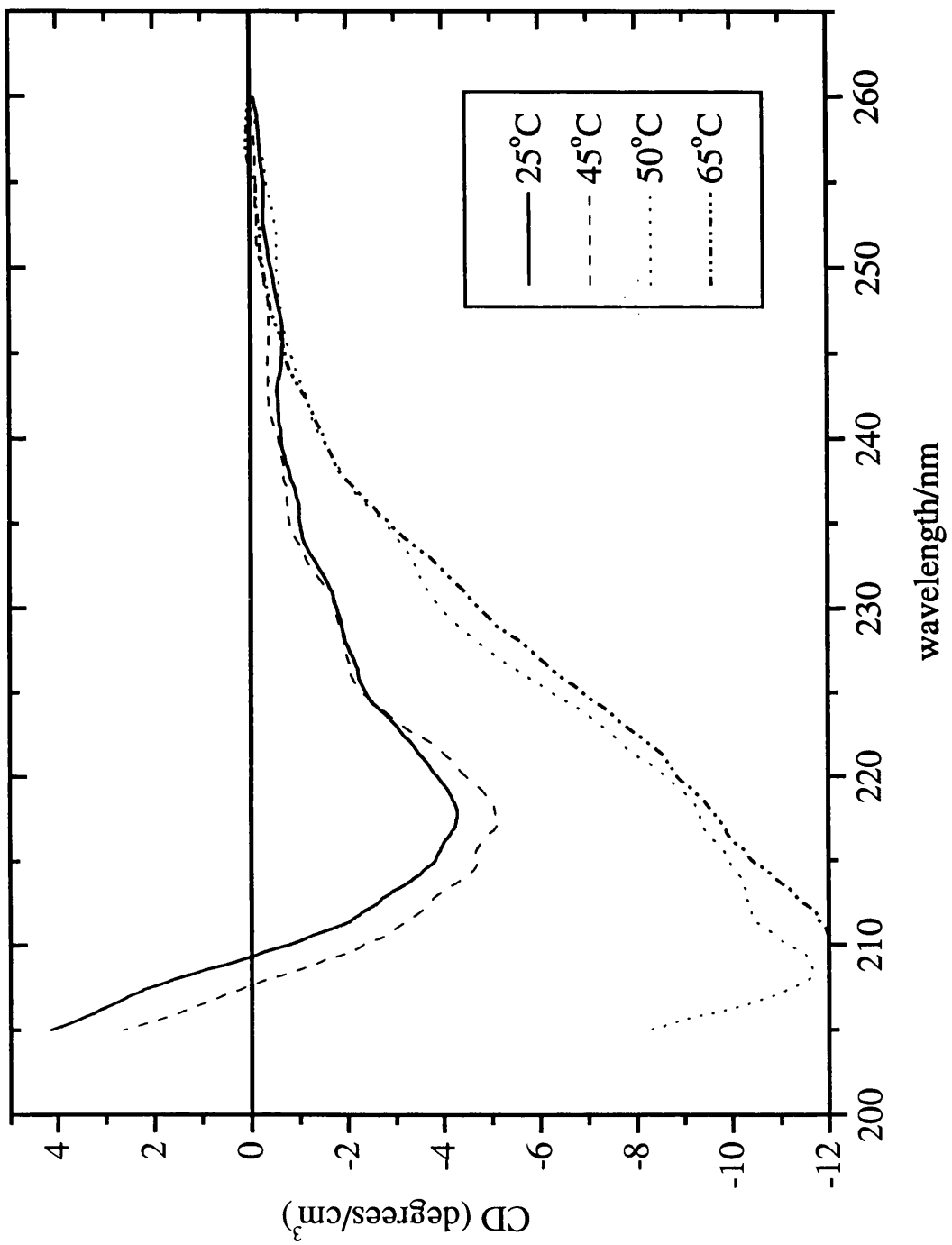


Figure 3.8b: Far-UV CD spectra of 4162W94 (6.7 μM , pH 3) recorded at a range of temperatures (25-65 $^{\circ}\text{C}$).

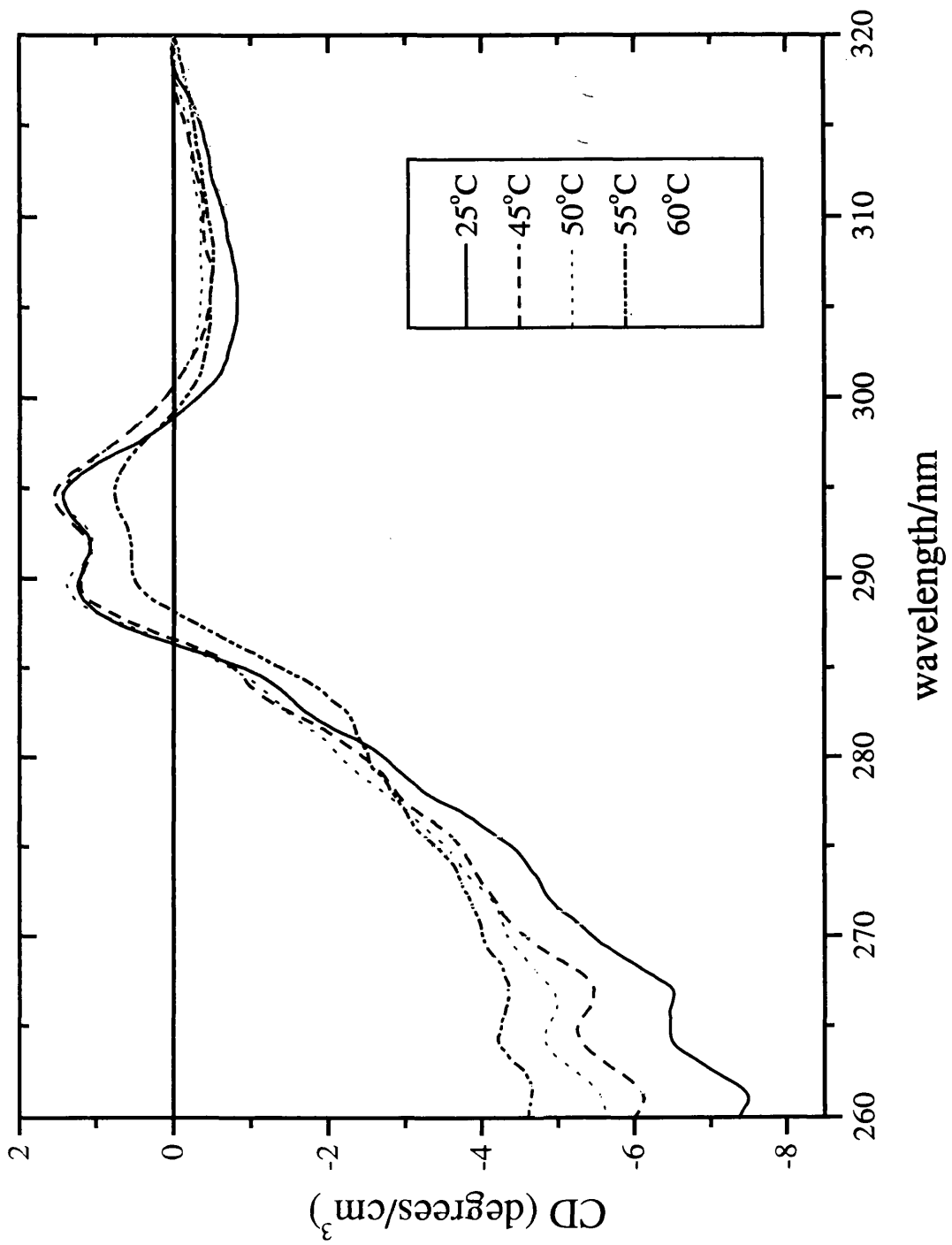


Figure 3.9a: Near-UV CD spectra of 1209W95 (6.7 μ M, pH 8) recorded at a range of temperatures (25-60 $^{\circ}$ C).

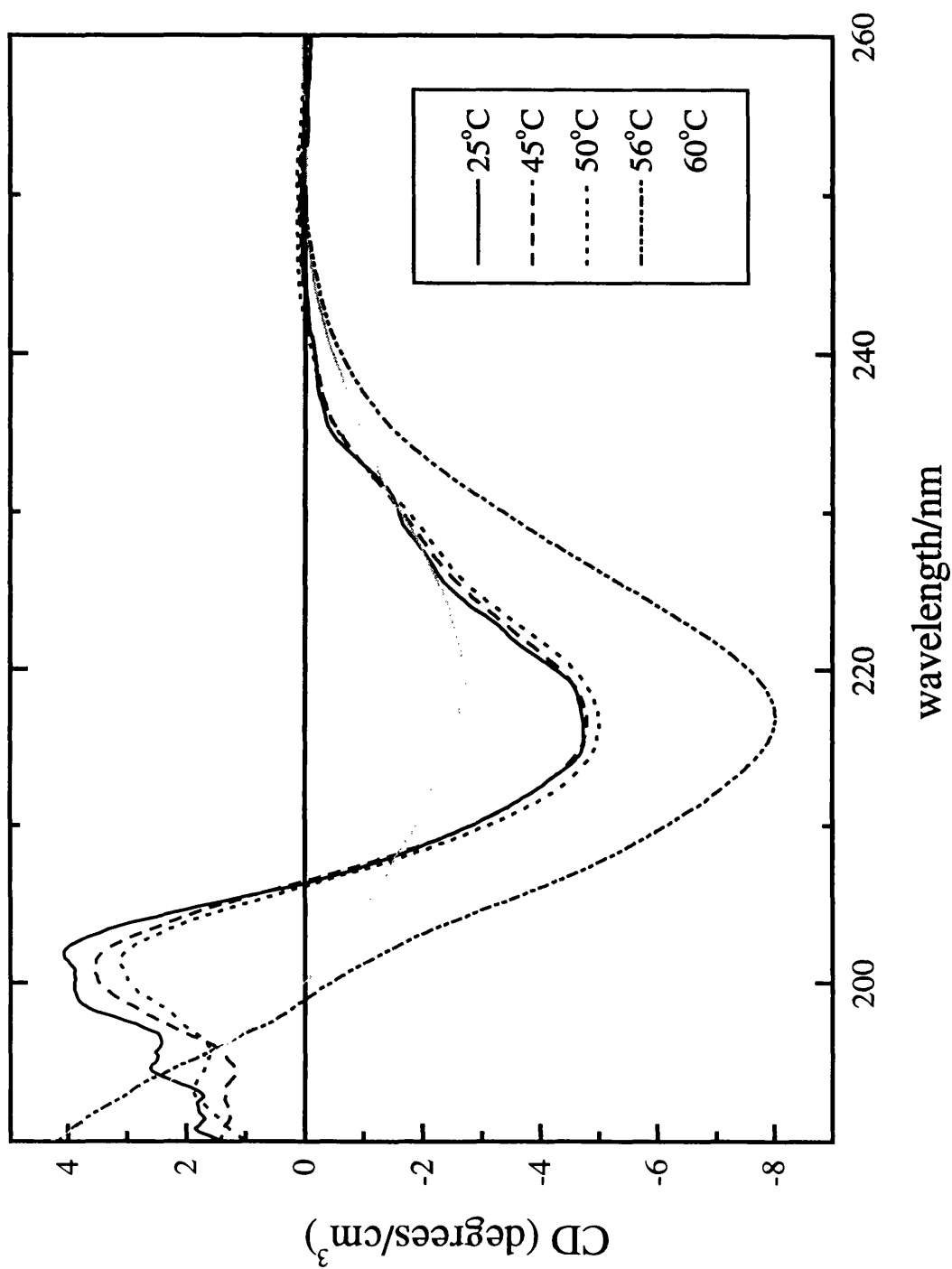


Figure 3.9b: Far-UV CD spectra of 1209W95 (6.7 μ M, pH 8) recorded at a range of temperatures (25-60 $^{\circ}$ C).

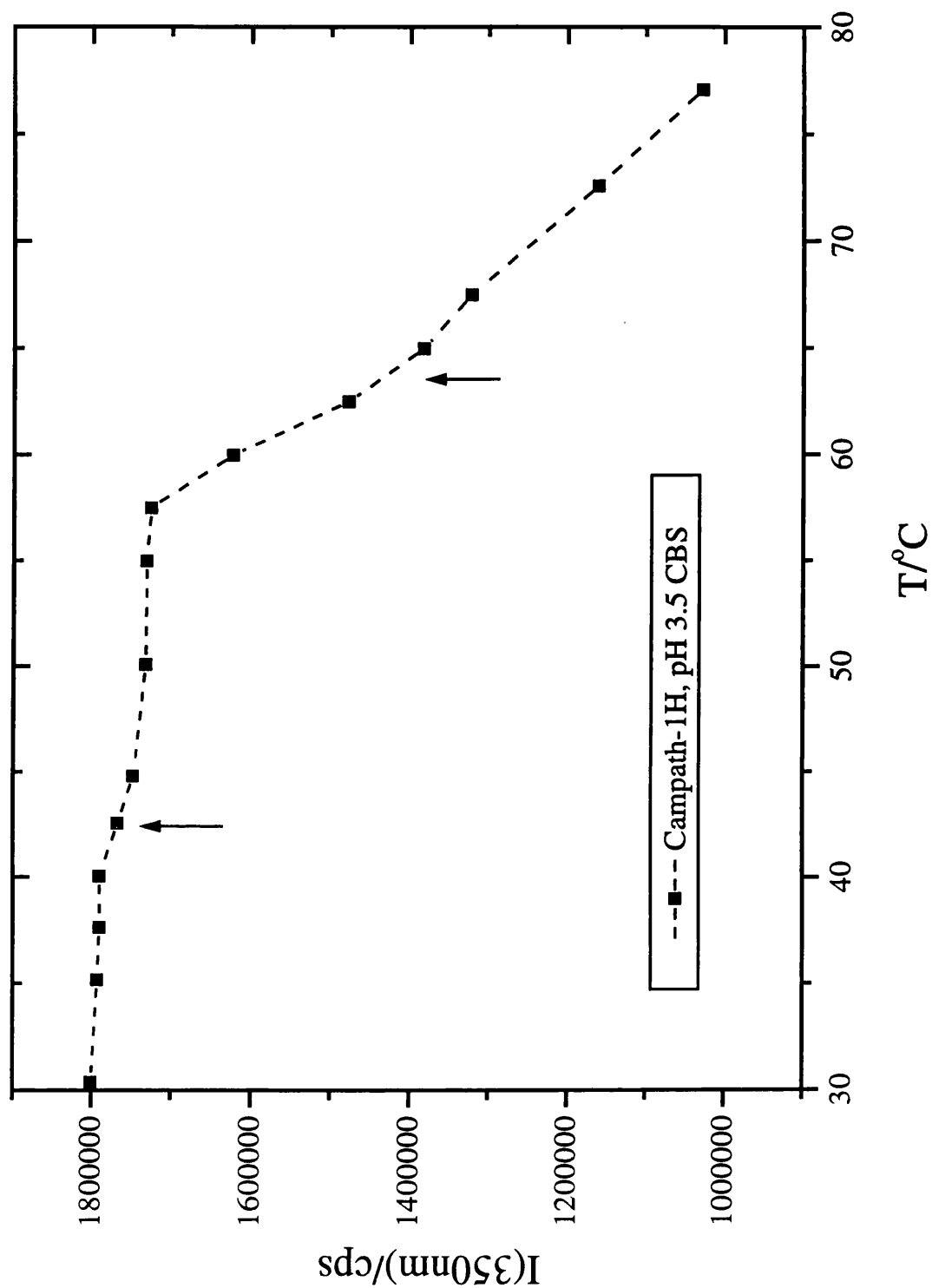


Figure 3.10: Fluorescence intensity, I , (as measured in counts per second (cps) at 350 nm) of Campath-1H (0.5 μM , pH 3.5) plotted as a function of temperature. Excitation wavelength is 295 nm. Graph shows two points of inflection (arrowed) at 41 and 63 $^{\circ}\text{C}$.

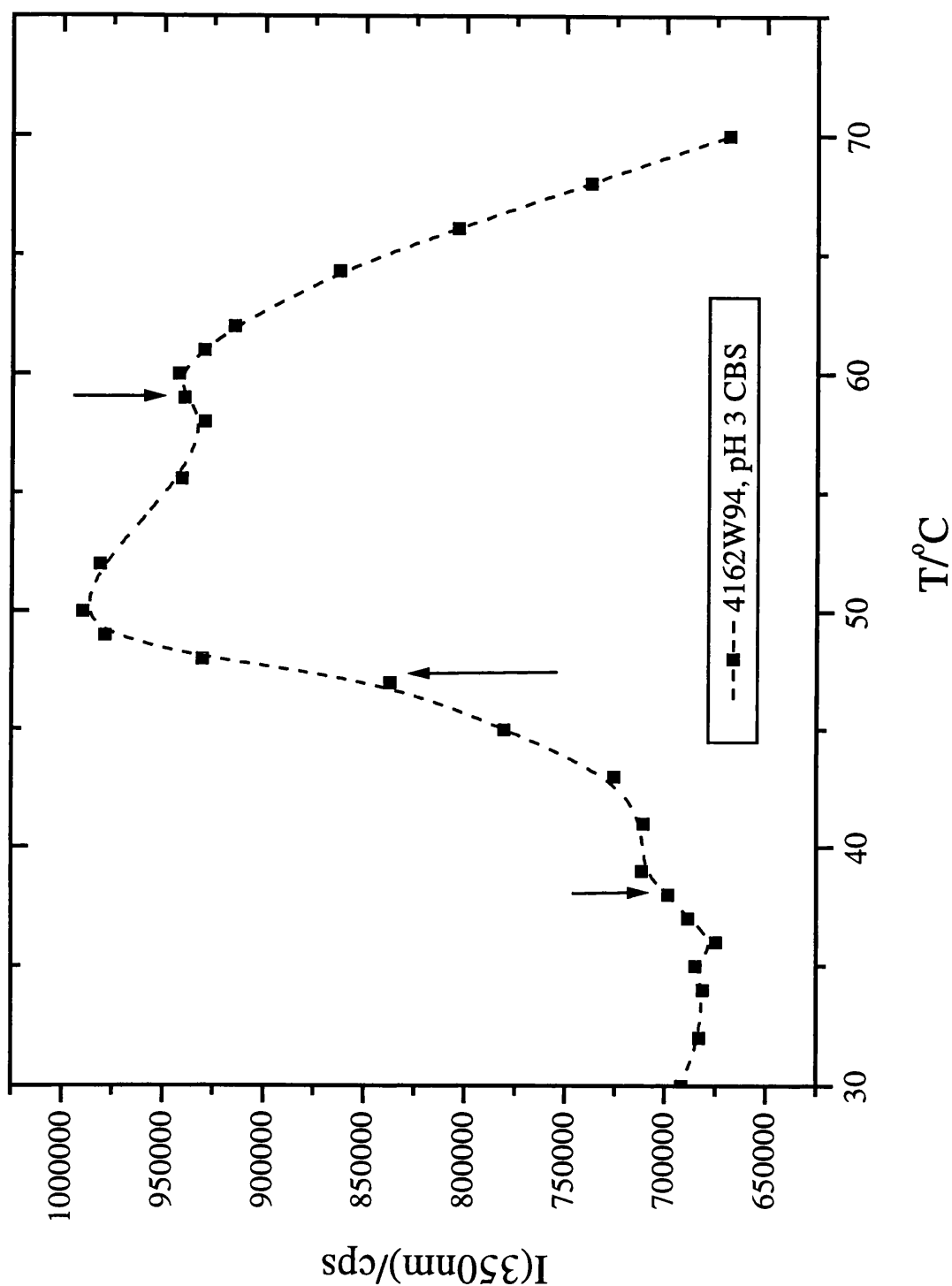


Figure 3.11: Fluorescence intensity, I , (as measured in counts per second (cps) at 350 nm) of 4162W94 (0.5 μM , pH 3) plotted as a function of temperature. Excitation wavelength is 295 nm. Graph shows three points of inflection (arrowed) at 38, 48 and 60 °C.

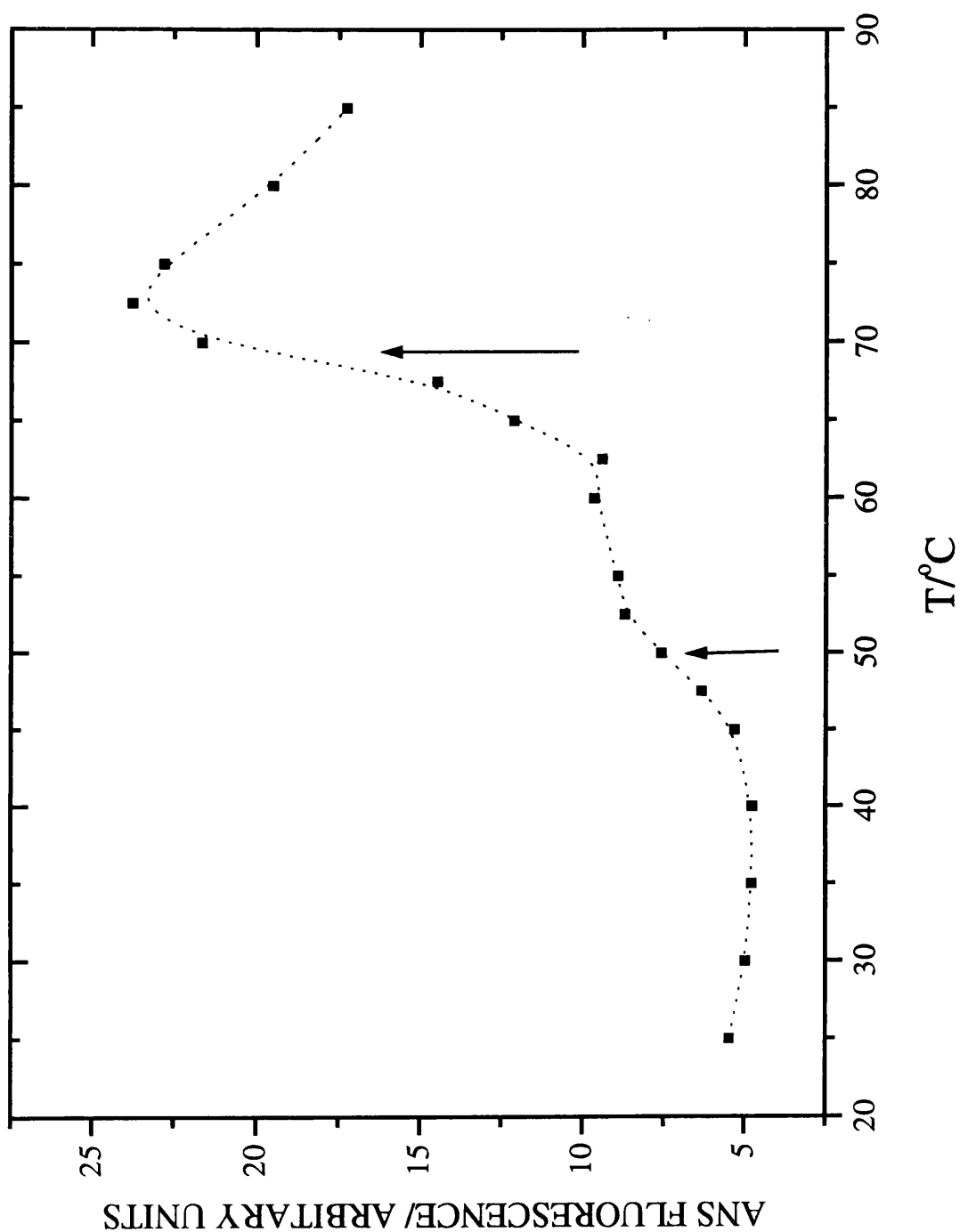


Figure 3.12a: Effect of thermal denaturation of Campath-1H on fluorescence of ANS. Measurements were made at a protein concentration of 0.2 μM in 0.1 M acetate buffer, pH 4, 0.051 M NaCl containing 20 μM ANS. The fluorescence emission at 480 nm was monitored as a function of continuously increasing temperature with excitation at 390 nm. The arrows at 50 $^{\circ}\text{C}$ and 70 $^{\circ}\text{C}$ designate the midpoints of the denaturation curves.

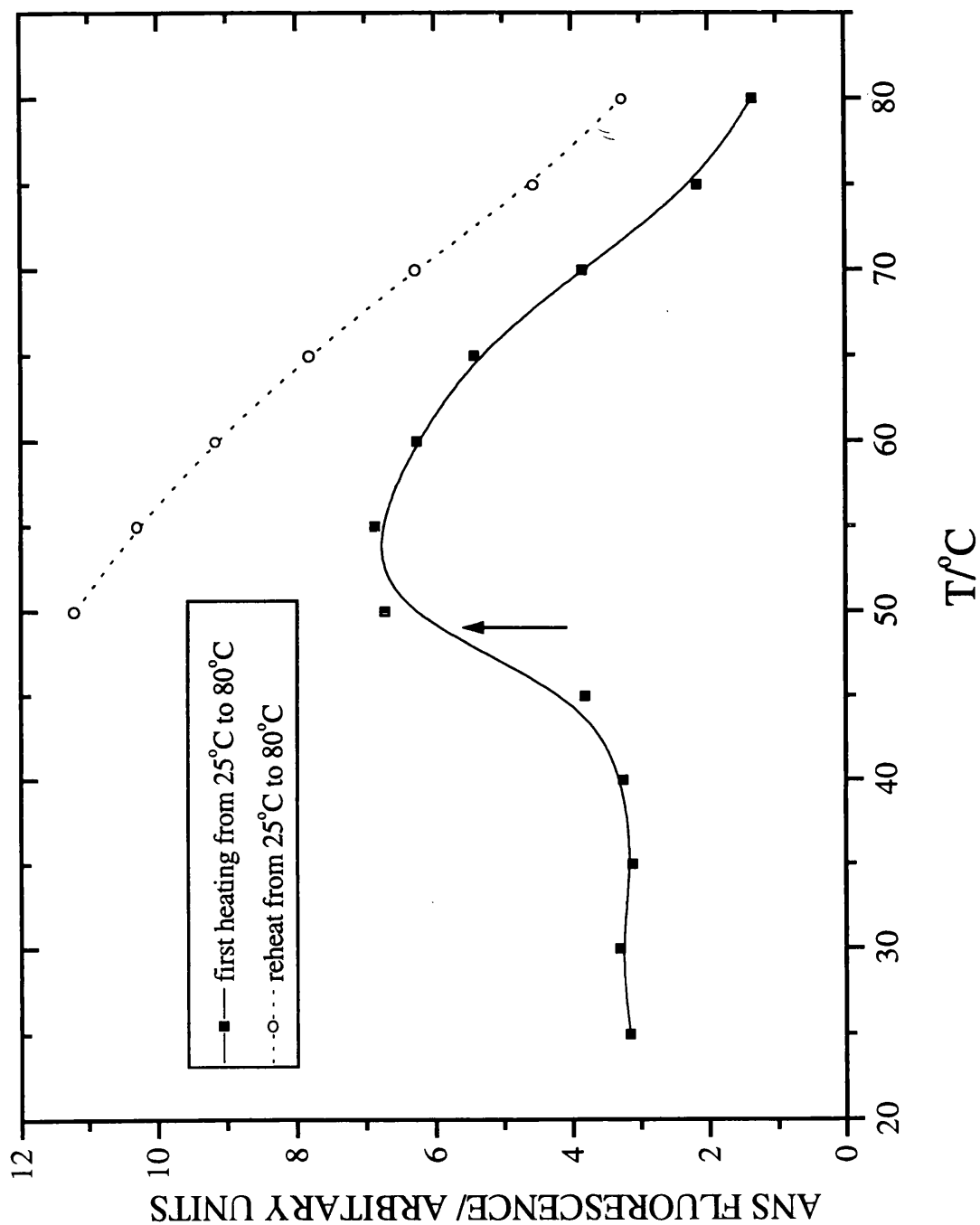


Figure 3.12b: Effect of thermal denaturation of 4162W94 on fluorescence of ANS. Measurements were made at a protein concentration of 0.2 μM in 0.1 M citrate buffer, pH 3, 0.051 M NaCl containing 20 μM ANS. The fluorescence emission at 480 nm was monitored as a function of continuously increasing temperature with excitation at 390 nm. The arrow at 48 $^{\circ}\text{C}$ designates the midpoint of the denaturation curve. O represents data obtained after cooling to 25 $^{\circ}\text{C}$ and then reheating to 80 $^{\circ}\text{C}$.

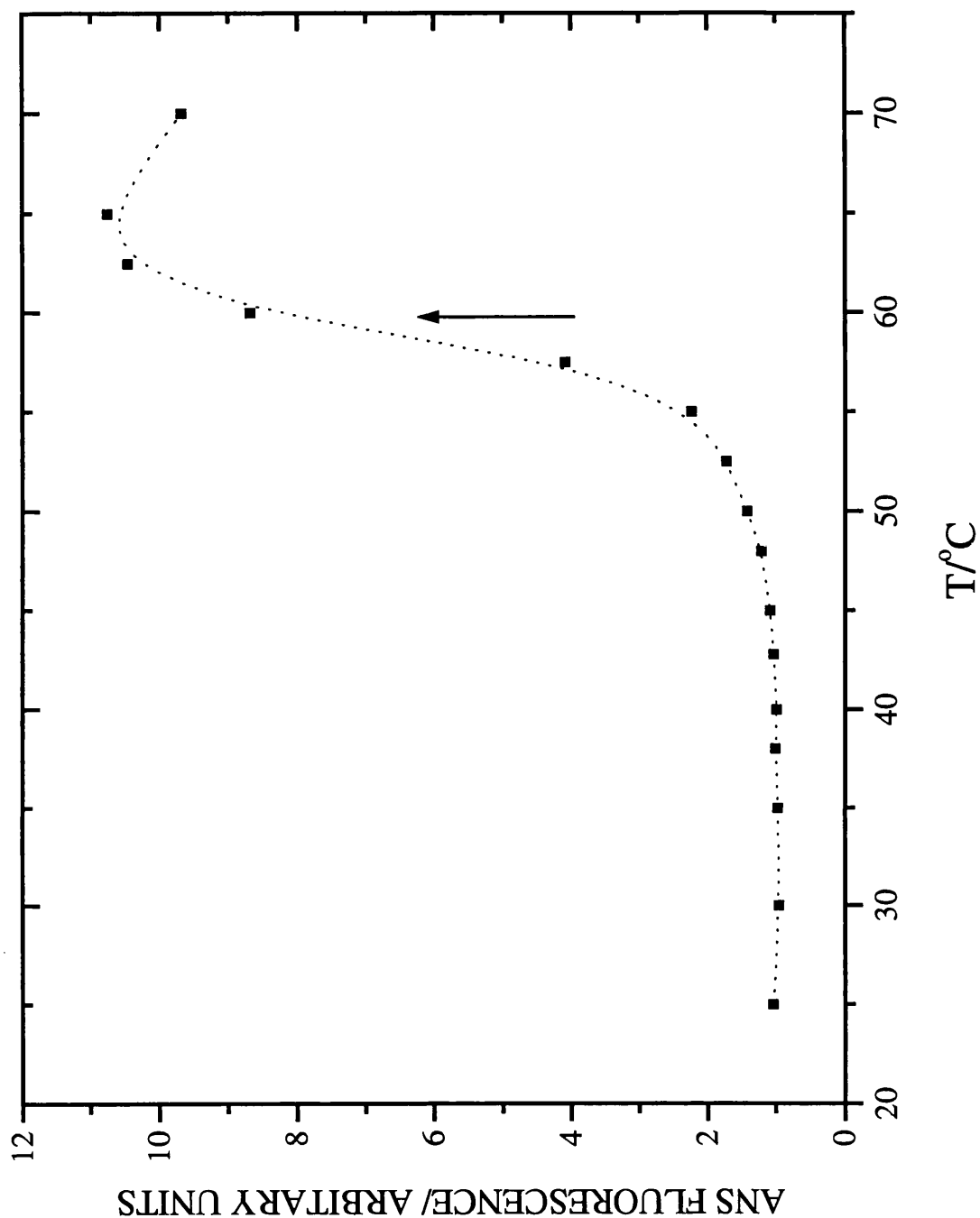


Figure 3.12c: Effect of thermal denaturation of 1209W95 on fluorescence of ANS. Measurements were made at a protein concentration of 0.2 μM in 0.1 M Tris buffer, pH 8, 0.051 M NaCl containing 20 μM ANS. The fluorescence emission at 480 nm was monitored as a function of continuously increasing temperature with excitation at 390 nm. The arrow at 60 $^{\circ}\text{C}$ designates the midpoint of the denaturation curve. Sample aggregated during the experiment.

CHAPTER 4

KINETIC ANALYSIS OF UNFOLDING

4.1 Introduction

Traditional analysis of DSC data to obtain a complete energetic characterisation of the stability of a protein molecule, including the overall thermodynamic parameters such as transition enthalpies, entropies and temperatures, requires that the system under study should be in thermodynamic equilibrium (Privalov, 1974; Privalov and Khechinashvili, 1974; Sturtevant, 1974; Shnyrov et al., 1997). The equilibrium criterion usually applied is the reproducibility of the original DSC trace on a second heating of the sample, the so-called calorimetric reversibility. Irreversibility in protein denaturation is usually attributed to some form of alteration that locks the protein in a final state that is unable to fold back to the native structure, for example, autolysis or aggregation (Shnyrov et al., 1997). These irreversible alterations are fundamentally kinetically controlled processes which must be described by rate equations. It was previously thought that such alterations were slow enough on the timescale of a DSC experiment to allow equilibrium thermodynamic analysis of irreversible DSC transitions (Sturtevant, 1987; Baker and Agard, 1994; Manly et al., 1985; Sánchez-Ruiz, 1992; Lepock et al., 1990). However experimental work has shown that many irreversible DSC transitions are subject to distortion by the kinetics of the irreversible alterations illustrated by obvious scanning rate effects (Sánchez-Ruiz et al., 1988a; Sánchez-Ruiz et al., 1988b; Morin et al., 1990; Galisteo et al., 1991; Conejero-Lara et al., 1991a; Conejero-Lara et al., 1991b; Galisteo and Sánchez-Ruiz, 1993; Le Bihan and Gicquaud, 1993; Garda-Salas et al., 1996; Davoodi et al., 1998) and possibly exothermic effects caused by aggregation. Kinetic analysis of these DSC transitions can be carried out according to the methods devised by Sánchez-Ruiz et al. (1988a).

It is clear from the data presented in chapter three that the thermal unfolding of the three mAbs proceeds via an irreversible process (exothermic aggregation peaks on the DSC traces and calorimetric irreversibility as illustrated by successive annealing, results presented in this chapter will also demonstrate the high scan rate dependence of the scans) and therefore the data have been analysed by the aforementioned method developed by Sánchez-Ruiz et al (1988a). Such analysis allows the calculation of activation energies and rate constants for the process under investigation at a given temperature in addition to the calorimetric and van't Hoff enthalpies determined by fitting the experimental DSC data to non-two state transitions.

If the rate constants for a particular process over a range of temperatures are available, the calculation of half life ($t_{1/2}$) is a simple process ($t_{1/2} = \ln 2/k$, if k is a first order rate constant) and theoretically, the availability of such kinetic parameters would allow for the quantitative extrapolation of thermal stability results to untested conditions (or conditions which give data unsuitable for analysis e.g. pHs which result in DSC traces heavily distorted by aggregation phenomena) which is data unattainable from functional assays (Brouillette et al., 1996). Such a method of predicting half lives would be of benefit to the pharmaceutical industry as it would allow the effective shelf life of any protein pharmaceutical in any formulation to be calculated in advance of long-term storage studies.

In this chapter we have also attempted to analyse the DSC data from Campath-1H (for this analysis we view this mAb as a model system simply due to its predictable behaviour, ease of handling and availability) by viewing the denaturation process as separate reversible and irreversible processes. This is achieved by mathematical extrapolation of the data to infinite scanning rate and allows the calculation of kinetic and thermodynamic parameters associated with the denaturation steps (La Rosa et al., 1995; Milardi et al., 1998).

The results of these methods of analysis of the DSC data of the mAbs will be discussed and the accuracy and relevance of the methods to these mAbs which are large, complex molecules will be considered.

(Note: Although the calorie is not an SI unit, it is still current in much of the literature pertinent to the subject of DSC analysis- especially from the USA. MicroCal instruments and software are calibrated in calories and so the majority of the results presented in this chapter are in kcal mol^{-1} . Some theoretical analysis within this chapter yield results in kJ mol^{-1} but where this occurs, the equivalent value in kcal mol^{-1} is given in parentheses to avoid potential confusion. $1 \text{ cal} = 4.184 \text{ J}$.)

4.2 Results

In order to carry out a full kinetic analysis of unfolding, it must be shown that the system under study is indeed irreversible and subject to kinetic control. In addition to data presented in chapter 3 revealing calorimetric irreversibility of protein unfolding (as shown by successive annealing) and obvious irreversible aggregation effects, kinetic control can also be revealed if the DSC transitions show strong scanning rate effects (Sánchez-Ruiz et al., 1988a; Galisteo et al., 1992). Figure 4.1 shows the DSC profiles of Campath-1H (pH 3) at six different scanning rates ranging from 10.7 to 72.3 °C/hr. It is evident that the temperature corresponding to the heat capacity maximum, T_m , is highly scan rate dependent (this high scan rate dependence is a common feature of all three mAbs and the effect of scan rate on the unfolding of 4162W94 and 1209W95 can be observed by looking at the variation of T_m with scan rate as tabulated in table 4.4 for 4162W94 and table 4.5 for 1209W95) and this suggests that the final denaturation process is rate-limited.

A prerequisite to kinetic analysis of the denaturation process as described in section 2.2.3, is a large quantity of experimental DSC data. The method devised by Sánchez-Ruiz et al (1988a) requires that the T_m , calorimetric enthalpy (ΔH_{cal}), exact scan rate and the heat evolved at any given temperature be known for the process under study. The T_m and ΔH_{cal} are determined by non-two state curve fitting using Origin software (ΔH_{vH} , the van't Hoff enthalpy is also calculated by this process) (Note: if precipitation occurs in the course of a scan, the post-transition baseline tends to be very noisy due to erratic convection effects within the calorimeter cell. This phenomenon invalidates post-transition experimental DSC data when curve fitting is attempted.) and the results for: Campath-1H in pH 3, 4 and 5 are presented in tables 4.1, 4.2 and 4.3 respectively, 4162W94 (pH 3) are presented in table 4.4, and 1209W95 (pH 6.6) are presented in table 4.5. These tables also contain the enthalpy ratio $\Delta H_{vH}/\Delta H_{cal}$ which, under reversible conditions, is an index of the cooperativity of the transition. The kinetic model upon which this method is based is unimolecular and therefore is independent of concentration. DSC scans were recorded for sequential dilutions of Campath-1H (pH 6) to investigate the presence of any concentration dependence of thermal aggregation. Data was recorded for 0.026, 0.006, 0.002, and 0.001 mM samples using a scan rate of 39.8 °C/hr. Gross thermal aggregation occurred at a similar temperature at all concentrations and the apparent T_m stayed constant (approx. 77 °C) as shown in figure 4.2, proving the process is independent of concentration. A similar analysis was carried out on the

first endotherm of Campath-1H in pH 4 ABS. DSC scans of 0.018, 0.007, and 0.004 mM solutions of Campath-1H in pH 4 ABS were recorded, the data normalised and fitted to a non-two state transition and the corresponding T_m s, calorimetric and van't Hoff enthalpies are presented in table 4.6. These data show the process which produces this endotherm is concentration independent.

Activation energies and rate constants are calculated using equations 2.15-2.18. Graphs produced using equations 2.15-2.17 for Campath-1H (pH 3) are shown in figure 4.3 as an example of the data produced. Similar graphs must be plotted for each transition undergoing analysis though these data are not shown. The calculated activation energies for each transition, calculated using each of the four equations (equation 2.15-2.18) analysed are presented in table 4.7.

In the process of deriving E_A using equation 2.15, the rate constant (k) for the process under investigation is calculated at a range of temperatures. Assuming that the denaturation process is a first order process, the extrapolated half-life of the molecule can then be calculated at any given temperature using the relationship, $t_{1/2} = \ln 2/k$. Figure 4.4 consists of graph plotted as the extrapolated half-life of Campath-1H at 20 °C against pH. The actual numerical values of the extrapolated half-lives plotted are 615, 7.5×10^7 and 3.0×10^{12} days in pH 3, 4 and 5 respectively.

The denaturation of Campath-1H (pH 3) was then analysed by extrapolating the data contained in table 4.1 to infinite scanning rate according to the method described by La Rosa et al., 1995 and Milardi et al., 1998. The first step in the process is the calculation of the cumulative enthalpies $\langle \Delta H \rangle$ at different scanning rates using equation 2.19. A graph of these cumulative enthalpies as a function of temperature is shown in figure 4.5a. Exponential plots of the cumulative enthalpies of denaturation versus $1/v$ (v represents the scan rate) are then plotted (figure 4.5b) and the intercept values with the y-axis give the desired value of $\langle \Delta H \rangle_{rev}$ at a given temperature. Deriving the $\langle \Delta H \rangle_{rev}$ profile with respect to temperature, the $\langle \Delta H \rangle_{rev}$ profile at infinite scanning rate is obtained and is shown in figure 4.6. This plot is sigmoidal, the midpoint of the transition representing the theoretical T_m of the transition at infinite scanning rate is 52.0 ± 1 °C and the y-axis value at which the curve plateau's represents the

enthalpy of the theoretical, reversible unfolding transition, in this case a value of $958 \pm 8\%$ kJmol^{-1} ($= 229 \pm 2\%$ kcal mol^{-1}).

It is possible to establish the path of the folding-unfolding transition in simple terms using a mechanical-statistical analysis of the thermodynamic $C_{p \text{ exc}}$ profile, obtained from the first derivative of $\langle \Delta H \rangle_{\text{rev}}$, with respect to temperature (La Rosa et al., 1995). The $C_{p \text{ exc}}$ profile for Campath-1H is shown in figure 4.7. It is clear that the curve comprises at least two components and if we treat this curve as though it was an experimental DSC profile, the main 'transition' ($T_m \approx 51 \text{ }^\circ\text{C}$) has $\Delta H_{\text{cal}} = 975 \pm 10\%$ kJmol^{-1} ($233 \pm 3\%$ kcal mol^{-1}) and $\Delta H_{\text{vH}} = 529 \pm 7\%$ kJmol^{-1} ($126 \pm 2\%$ kcal mol^{-1}) (in this case, since the data are not experimental DSC data, Origin software cannot be used to calculate the calorimetric and van't Hoff enthalpies). ΔH_{cal} is taken to simply equal the area under the curve and ΔH_{vH} is calculated using the equation below (Sturtevant, 1974; Privalov, 1980):

$$\Delta H_{\text{vH}} = \frac{4RT_m^2 \langle C_p \rangle_{\text{max}}}{\Delta H}$$

The ratio of these calorimetric and effective enthalpies (i.e. $\Delta H_{\text{vH}}/\Delta H_{\text{cal}}$) is 0.54 which suggests that the reversible step involves at least one significantly populated intermediate phase (Sturtevant, 1987).

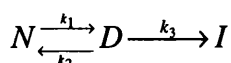
4.3 Discussion

By demonstrating the calorimetric irreversibility of the DSC scans of each of the mAbs using a successive annealing technique (Shnyrov and Mateo, 1993; Kreimer et al., 1995; Shnyrov et al., 1996) and the fact that the T_m of the 'main' transition of all three mAbs increases on increasing the scan rate, we have shown that the denaturation process is, at least to some extent, kinetically controlled (Sánchez-Ruiz, 1992). In doing so we have precluded the interpretation of the calorimetric data in terms of equilibrium thermodynamics (Freire et al., 1990). Irreversible, scan rate dependent calorimetric transitions have been successfully analysed in terms of a two-state kinetic model originally developed by Sánchez-Ruiz et al. (1988a) in many examples (Sánchez-Ruiz et al., 1988b; Arriaga et al., 1992; Galisteo et al., 1992; Galisteo and Sánchez-Ruiz, 1993; La Rosa et al., 1995; Zhadan and Shnyrov, 1994; Kreimer et al., 1995; Garda-Salas et al., 1996; Shnyrov et al., 1996; Vogl et al., 1997; Milardi et al., 1998; Davoodi et al., 1998). The model, one particular case of the Lumry and Eyring model (Lumry and Eyring, 1953), assumes that a calorimetric transition can be represented as $N \rightarrow D$, where N is the native state, D the unfolded (or final) state formed with the first-order kinetic rate constant of k . This model has the mathematical form given in equations 2.15-2.17.

Analysis of the DSC traces of all three mAbs, according to the method described by Sánchez-Ruiz et al. (1988a) was carried out and the results presented in table 4.7. The validity of equations 2.15-2.17 requires the linear dependence of $\ln k$ and $\ln[\ln(Q_f/(Q_f-Q))]$ versus $1/T$ and $\ln(v/T_m^2)$ versus $1/T_m$ and that the activation energies calculated using equations 2.15-2.18 are all in agreement. All the plots for each of the three mAbs fulfil this linearity criterion (figure 4.3 is an example) but it is obvious from table 4.7 that the activation energies calculated using equations 2.15-2.18 differ significantly. From this we can conclude that the two-state irreversible model does not accurately represent the DSC data from these mAbs. Despite this there is some merit in this method of analysing the DSC traces of the mAbs as although it may not give a definite value for the activation energy, the values obtained from equations 2.15-2.18 are in the same region and can be used empirically to judge the stability of the protein. For example, we have shown in table 4.7 that the average activation energy for the thermal denaturation of Campath-1H increases over the pH range 3-5, this is in agreement with the increase in the T_m (the most empirical indication of stability) of the main thermal transition over this pH range. We can therefore state that Campath-1H is

more stable in pH 5 than in pH 3 both in terms of the temperature that it will start to unfold and in terms of the actual amount of energy required to carry out thermal denaturation. This is possibly due to hydrogen ion (H^+) interacting with the residues on the unfolded form of the protein and thus destabilising the folded form. Utilising activation energies in this manner as a measure of stability will be used again in chapter 5 to monitor the effects of formulation additives on the stability of the mAbs. It is interesting to note that the activation energy of $366 \text{ kJ mol}^{-1} \pm 15\%$ calculated for Campath-1H (pH 3) is larger than the denaturation enthalpy per mole ($\Delta H = 254 \text{ kJ mol}^{-1} \pm 5\%$) and this may suggest a transition state made up of more than one molecule of Campath-1H and would be consistent with a mechanism in which the irreversible step is preceded by the cooperative (and non-dissociative) unfolding of a dimer (or other aggregate) (Galisteo and Sánchez-Ruiz, 1993). A similar difference in activation energy and denaturation enthalpy is observed for all the mAb transitions studied.

Calculation of the activation energy of a two-state kinetic process using equation 2.15 requires the calculation of the first-order rate constant at a range of temperatures and these rate constants are easily converted to half-lives. We have calculated the half-life of Campath-1H (pH 3) at 20°C to be 615 days which is a realistic value but on increasing the pH to 4 and then 5 yields half-life predictions of 7.5×10^7 and 3.0×10^{12} days respectively. These values at pH 4 and 5 are clearly unrealistic (10^{12} days is a literally astronomical number) for a protein which has a pharmaceutical shelf-life of two years and suggests the system is more complex than can be represented by a simple two-state model (the complexity of the unfolding has already been indicated by the $\Delta H_{\text{vH}}/\Delta H_{\text{cal}}$ ratios for the DSC transitions presented in tables 4.1-4.5. Consistently $\Delta H_{\text{vH}} < \Delta H_{\text{cal}}$ which, in the case of reversible systems, usually reflects a breakdown of the simple two-state model assumption, indicating that the unfolding of Campath-1H involves several steps with at least one significantly populated intermediate phase (Sturtevant, 1987)). Although this model is indeed simple, other more complex models may come back to a first-order kinetic process (Sánchez-Ruiz et al., 1988a). For instance, a more realistic representation of the irreversible thermal denaturation of these mAbs might be (Lumry and Eyring, 1954)



where I is a final state irreversibly arrived at from the unfolded state, D . This model still applies even if the reversible unfolding step involves one or more significantly populated

intermediate states (Freire et al., 1990; Sánchez-Ruiz, 1992). If it assumed that all three processes are first-order and that $k_3 \gg k_2$ at any moment, most of the D molecules will be converted to I rather than returning to N through the process $D \rightarrow N$. As a result the equilibrium between N and D will not be established as the concentration of D will always be low and the denaturation may be considered as an irreversible process, $N \rightarrow I$, kinetically controlled by the rate-determining N to D conversion step, i.e. $N \xrightarrow{k_1} I$, which leads to the same kinetic equations describing the original model $N \rightarrow D$ (Sánchez-Ruiz et al., 1988a). This leads to the question of how to devise a model of suitable complexity to represent mAb thermal unfolding which cannot be simplified to this same original model. It must be made clear at this stage that any model devised with the purpose of half-life predictions should take into account denaturation processes other than thermal unfolding which affect the mAbs. For example, Campath-1H is known to be subject to acid cleavage and copper ion (Cu^{2+}) induced cleavage in addition to the more universal oxidative processes which affect proteins. It is these processes rather than thermal unfolding which are likely to dictate the half-life of a mAb at ambient temperatures. It is possible therefore that the half-lives calculated for Campath-1H (pH 3, 20 °C) are accurate but are relevant only if thermal unfolding is the single process leading to denaturation of the mAb.

DSC data pertaining to the denaturation of Campath-1H at pH 3 was successfully extrapolated to infinite scanning rate using in an attempt to separate the reversible and irreversible steps of the denaturation process (Freire et al., 1990; La Rosa et al., 1995; Milardi et al., 1998). This analysis yielded information pertinent only to the species that are in thermodynamic equilibrium and a T_m of 52 ± 1 °C (comparable to the experimental T_m observed at a scan rate of 72.3 °C/hr reported in table 4.1) was calculated for the reversible transition with a corresponding ΔH of $229 \pm 2\%$ kcal mol⁻¹. Analysis of the time independent C_p exc profile (obtained from the first derivative of $\langle \Delta H \rangle_{\text{rev}}$, with respect to temperature) allowed the calculation of a ΔH_{cal} of $233 \pm 3\%$ kcal mol⁻¹ and a ΔH_{vH} of $126 \pm 2\%$ kcal mol⁻¹, leading to a $\Delta H_{\text{vH}}/\Delta H_{\text{cal}}$ value of 0.54 which again suggests that the reversible step involves at least one significantly populated intermediate phase (Sturtevant, 1987). Note: where $\Delta H_{\text{vH}}/\Delta H_{\text{cal}} > 1$, no explanation can be given but such a result suggests that the cooperative unit consists of more than one molecule.

Scan Rate /°C hr ⁻¹	T _m /°C	ΔH _{cal} /kcal mol ⁻¹	ΔH _{vH} /kcal mol ⁻¹	ΔH _{vH} /ΔH _{cal}
10.7	47.4 ±0.04	307 ±4	126 ±2	0.41 ±0.03
17.9	48.7 ±0.02	266 ±2	138 ±1	0.52 ±0.01
26.8	49.7 ±0.02	209 ±2	153 ±2	0.73 ±0.02
39.8	50.8 ±0.02	208 ±2	154 ±2	0.74 ±0.02
51.0	51.2 ±0.02	249 ±2	146 ±2	0.58 ±0.02
72.3	52.5 ±0.01	286 ±1	131 ±1	0.46 ±0.01

Table 4.1: Curve fitting data for Campath-1H (pH 3 CBS). Data are fitted to one non-two state curve, all data are scan rate and concentration normalised. ΔH_{cal} and ΔH_{vH} denote the apparent calorimetric and van't Hoff enthalpies respectively.

Scan Rate /°C hr ⁻¹	T _{m1} /°C	ΔH _{cal1} /kcal mol ⁻¹	ΔH _{vH1} /kcal mol ⁻¹	ΔH _{vH1} /ΔH _{cal1}	T _{m2} /°C	ΔH _{cal2} /kcal mol ⁻¹	ΔH _{vH2} /kcal mol ⁻¹	ΔH _{vH2} /ΔH _{cal2}
10.7	50.6 ±0.2	36 ±3	139 ±14	3.85 ±0.18	66.8 ±0.02	395 ±3	150 ±1	0.38 ±0.01
18.0	50.8 ±0.2	82 ±4	101 ±7	1.23 ±0.12	68.0 ±0.03	418 ±4	144 ±2	0.34 ±0.02
26.6	51.1 ±0.2	56 ±3	120 ±9	2.13 ±0.13	68.8 ±0.02	393 ±3	146 ±2	0.37 ±0.02
39.4	50.9 ±0.2	57 ±5	131 ±13	2.27 ±0.19	69.4 ±0.03	386 ±5	153 ±2	0.40 ±0.02
50.9	51.3 ±0.2	57 ±4	127 ±10	2.22 ±0.15	70.3 ±0.03	370 ±4	152 ±2	0.41 ±0.03
72.5	51.5 ±0.2	77 ±5	104 ±8	1.35 ±0.14	70.8 ±0.03	405 ±4	148 ±2	0.36 ±0.02

Table 4.2: Curve fitting data for Campath-1H (pH 4 ABS). Data are fitted to two non-two state curves, all data are scan rate and concentration normalised. ΔH_{cal} and ΔH_{vH} denote the apparent calorimetric and van't Hoff enthalpies respectively.

Scan Rate /°C hr ⁻¹	T _{m1} /°C	ΔH _{cal1} /kcal mol ⁻¹	ΔH _{vH1} /kcal mol ⁻¹	ΔH _{vH1} /ΔH _{cal1}	T _{m2} /°C	ΔH _{cal2} /kcal mol ⁻¹	ΔH _{vH2} /kcal mol ⁻¹	ΔH _{vH2} /ΔH _{cal2}
10.6	-	(-)	(-)	(-)	73.6 ± 0.06	506 ± 13	185 ± 6	0.36 ± 0.06
17.8	65.6 ± 0.2	252 ± 9	77 ± 4	0.31 ± 0.09	74.7 ± 0.02	469 ± 7	206 ± 3	0.44 ± 0.03
26.5	69.0 ± 0.3	459 ± 21	59 ± 2	0.13 ± 0.08	75.4 ± 0.03	418 ± 14	238 ± 6	0.57 ± 0.06

Table 4.3: Curve fitting data for Campath-1H (pH 5 CBS). Data are fitted to two non-two state curves, all data are scan rate and concentration normalised. (-) indicates that the DSC scan had a high noise content (due to slow scan rate) which prevented fitting of first transition. ΔH_{cal} and ΔH_{vH} denote the apparent calorimetric and van't Hoff enthalpies respectively.

Scan Rate /°C hr ⁻¹	T _m 2 /°C	ΔH _{cal} 2 /kcal mol ⁻¹	ΔH _{vH} 2 /kcal mol ⁻¹	ΔH _{vH} 2/ΔH _{cal} 2	T _m 3 /°C	ΔH _{cal} 3 /kcal mol ⁻¹	ΔH _{vH} 3 /kcal mol ⁻¹	ΔH _{vH} 3/ΔH _{cal} 3
10.8	45.7 ±0.02	276 ±4	200 ±3	0.72 ±0.03	54.9 ±0.1	123 ±5	119 ±6	0.97 ±0.09
18.2	46.8 ±0.02	229 ±17	245 ±9	1.08 ±0.11	55.3 ±0.1	56 ±4	167 ±14	2.94 ±0.16
26.4	47.2 ±0.02	225 ±12	247 ±7	1.10 ±0.08	56.7 ±0.1	63 ±3	145 ±9	2.33 ±0.11
39.2	47.7 ±0.02	249 ±12	236 ±7	0.94 ±0.08	57.9 ±0.2	61 ±4	149 ±11	2.44 ±0.14
50.6	48.0 ±0.02	266 ±8	222 ±5	0.83 ±0.05	59.6 ±0.2	100 ±5	105 ±6	1.05 ±0.11
71.9	48.4 ±0.02	303 ±3	199 ±2	0.66 ±0.02	60.2 ±0.1	114 ±4	114 ±5	1.00 ±0.08

Table 4.4: Curve fitting data for 4162W94 (pH 3 CBS). Data are fitted to two non-two state curves, all data are scan rate and concentration normalised. ΔH_{cal} and ΔH_{vH} denote the apparent calorimetric and van't Hoff enthalpies respectively.

Scan Rate /°C hr ⁻¹	T _m /°C	ΔH _{cal} /kcal mol ⁻¹	ΔH _{vH} /kcal mol ⁻¹	ΔH _{vH} /ΔH _{cal}
10.8	58.0 ±0.05	569 ±14	160 ±5	0.28 ±0.06
18.0	58.7 ±0.09	447 ±21	180 ±9	0.40 ±0.09
26.1	59.4 ±0.25	412 ±42	159 ±20	0.39 ±0.23

Table 4.5: Curve fitting data for 1209W95 (pH 6.6 ABS). Data are fitted to one non-two state curve, all data are scan rate and concentration normalised. ΔH_{cal} and ΔH_{vH} denote the apparent calorimetric and van't Hoff enthalpies respectively.

Concentration /mM	T _m /°C	ΔH _{cal} /kcal mol ⁻¹	ΔH _{vH} /kcal mol ⁻¹
0.018	50.8 ±0.04	49 ±3	153 ±8
0.007	50.7 ±0.02	51 ±3	153 ±7
0.004	50.5 ±0.09	88 ±8	135 ±14

Table 4.6: Concentration dependence. Curve fitting data for first endotherm of Campath-1H (pH 6 CBS) scanned at a nominal scan rate of 60 °C/hr showing thermodynamic parameters are independent of concentration. Data are fitted to one non-two state curve, all data are scan rate and concentration normalised. ΔH_{cal} and ΔH_{vH} denote the apparent calorimetric and van't Hoff enthalpies respectively.

mAb (pH)	E_A /kJ mol ⁻¹ Eq. 2.15	E_A /kJ mol ⁻¹ Eq. 2.16	E_A /kJ mol ⁻¹ Eq. 2.17	E_A /kJ mol ⁻¹ Eq. 2.18	Average E_A /kJ mol ⁻¹
Campath-1H (pH 3)	319 ±4%	324 ±3%	422 ±10%	400 ±11%	366 ±15%
Campath-1H (pH 4), 2 nd transition.	406 ±7%	452 ±12%	486.2 ±11%	414 ±13%	439 ±11%
Campath-1H (pH 5), 2 nd transition.	531 ±9%	612 ±10%	490 ±7%	582 ±11%	554 ±10%
4162W94 (pH 3), 2 nd transition.	549 ±8%	633 ±6	597 ±9%	636 ±12%	604 ±9
4162W94 (pH 3), 3 rd transition.	241 ±5%	394 ±8	275 ±8%	378 ±9%	321.9 ±16%
1209W95 (pH 6.6)	381 ±10%	483 ±11	556 ±13%	465 ±13%	471 ±19%

Table 4.7: Activation energies (E_A) calculated using equations 2.15-2.18 for Campath-1H (pH 3, 4, 5), 4162W94 (pH 3) and 1209W95 (pH 6.6).

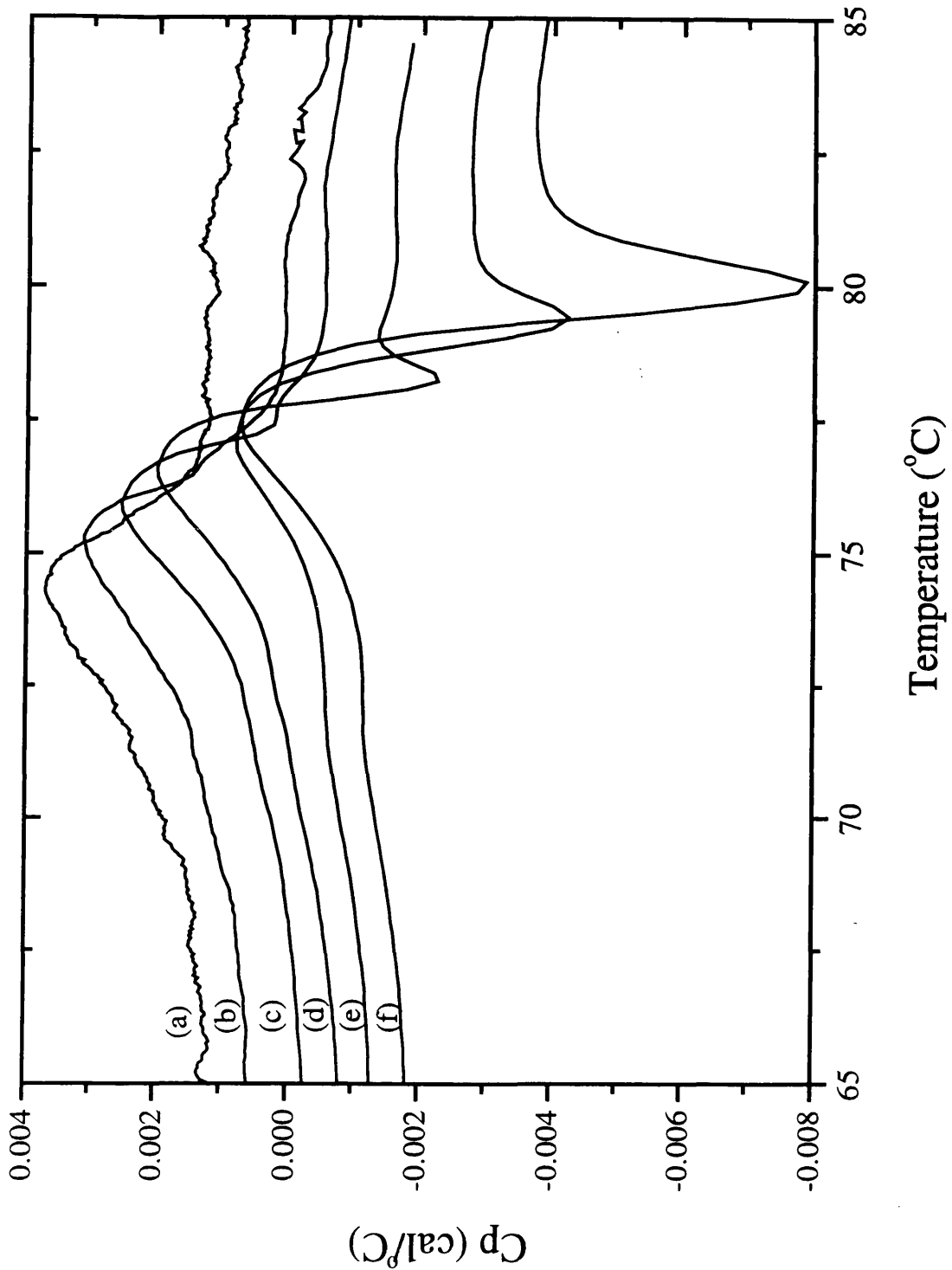


Figure 4.1: Effect of scan rate on the DSC trace of Campath-1H (pH 3 CBS). Graph shows raw data produced on scanning at six different scan rates: (a) 10.7, (b) 17.9, (c) 26.8, (d) 39.8, (e) 51.0 and (f) 72.3 °C/hr. Buffer baselines have been subtracted and scans are y-offset for clarity.

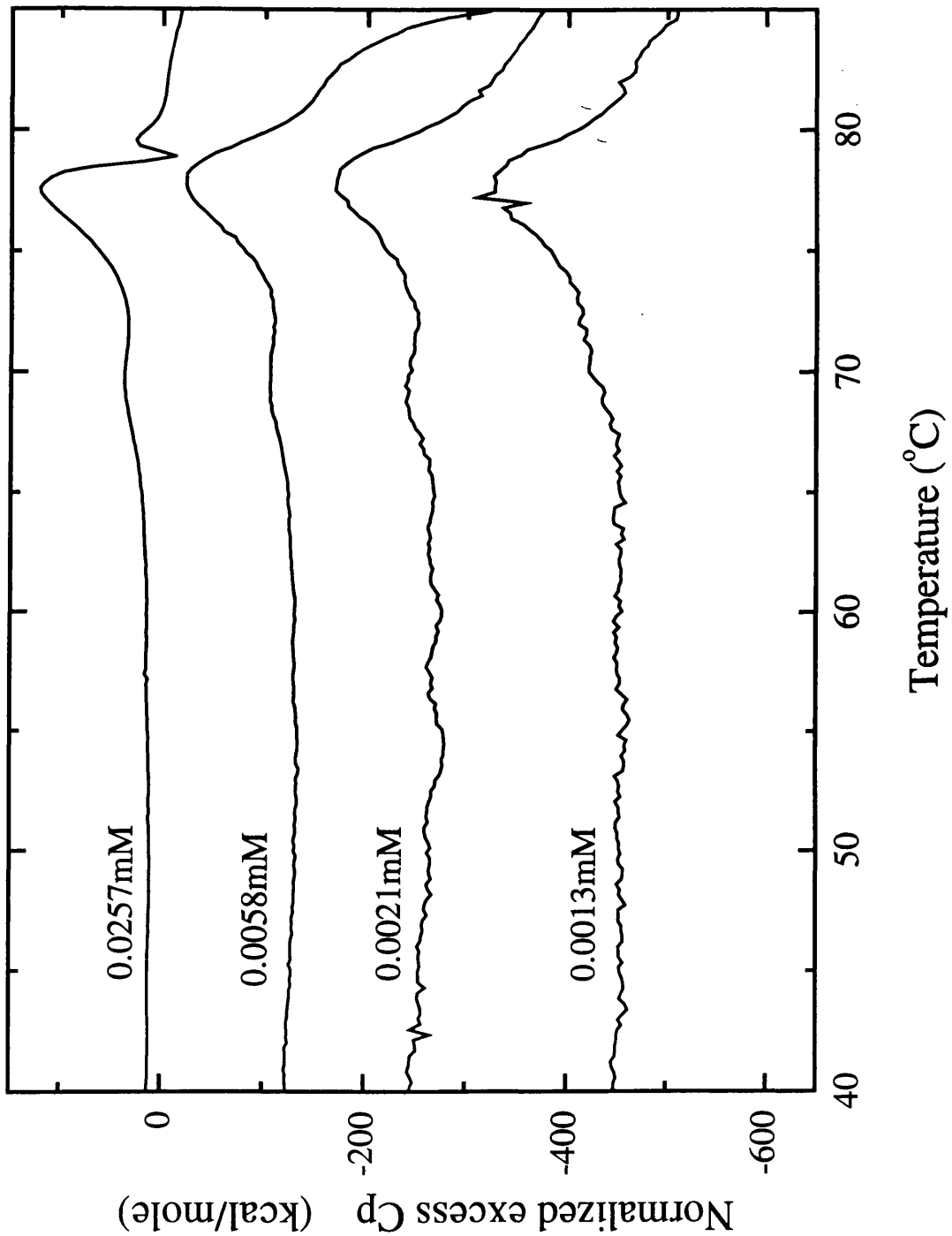


Figure 4.2: Effect of concentration on the thermal unfolding of Campath-1H (pH 6 CBS). All scans were performed at a scan rate of 39.8 °C/hr using protein concentrations in the range 0.001 mM to 0.026 mM. The graph shows data after baseline subtraction and concentration normalization. Scans are y-offset for clarity.

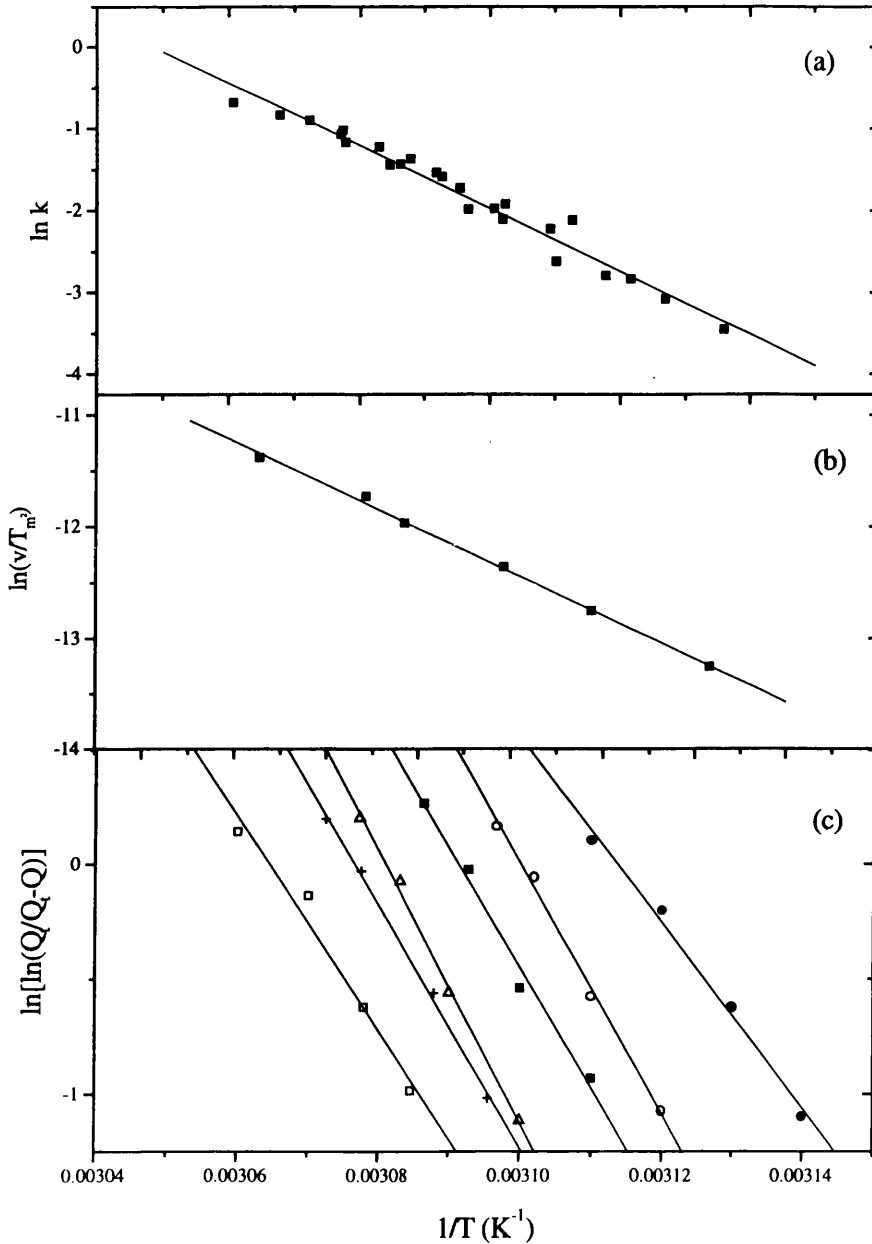


Figure 4.3: Plots corresponding to equations 2.15-2.17 for Campath-1H (pH 3 CBS). (a): Arrhenius plot. ■, k values calculated from equation 2.15 for each of the six scan rates used. (b): Plot of $\ln(v/T_m^2)$ versus $1/T_m$. Here the $1/T$ coordinate represents $1/T_m$. Each data point corresponds to one of the six scan rates used. (c): Values of $\ln[\ln(Q/(Q-Q_i))]$ plotted versus $1/T$. Each set of symbols represents a different scan rate: □, 10.7, +, 17.9, △, 26.8, ■, 39.8, ○, 51.0 and ●, 72.3 °C/hr.

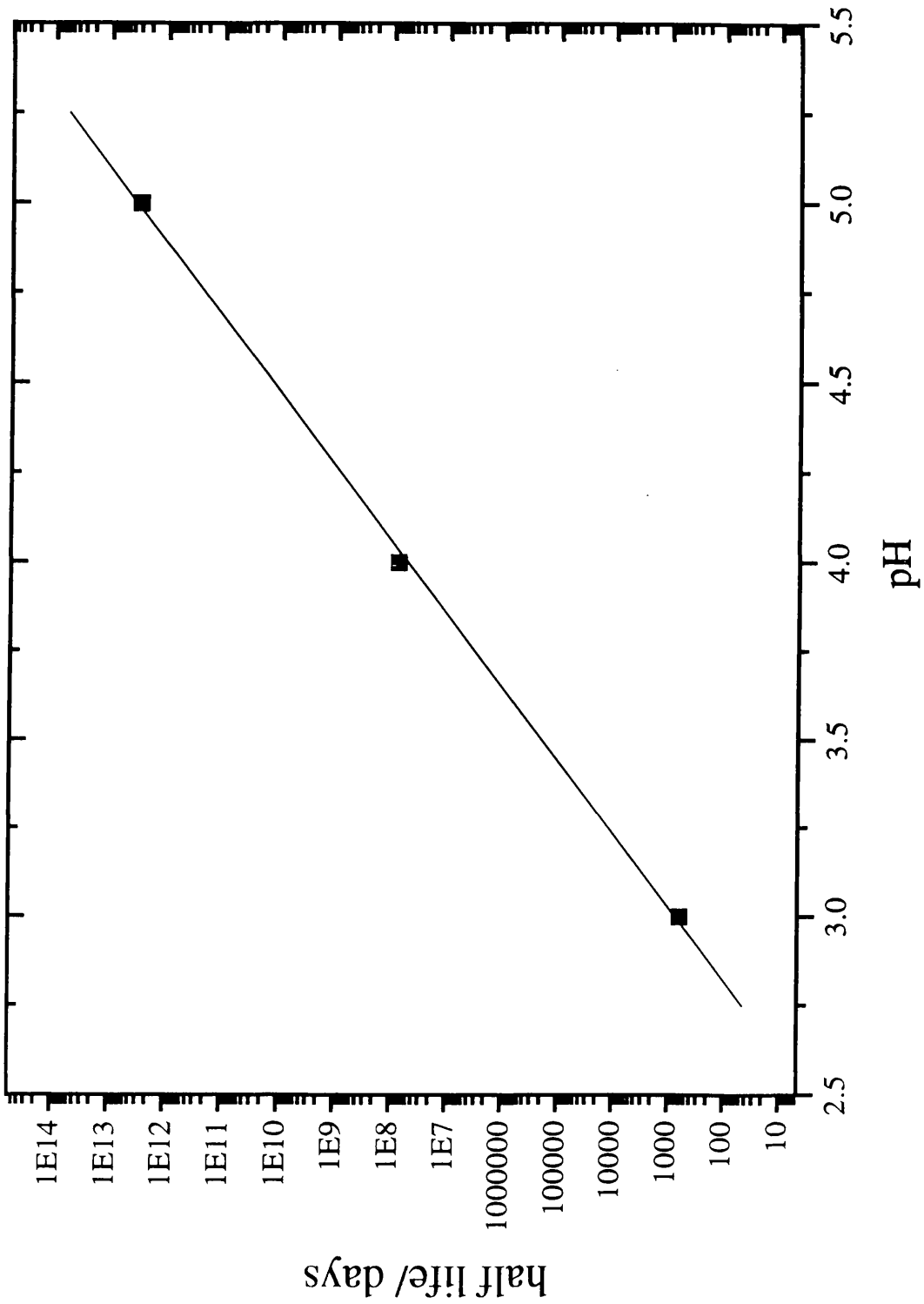


Figure 4.4: Plot of extrapolated half life (in days) versus pH for Campath-1H at 20 °C. The graph is plotted as a logarithmic plot. Each data point represents the half life calculated at a particular pH

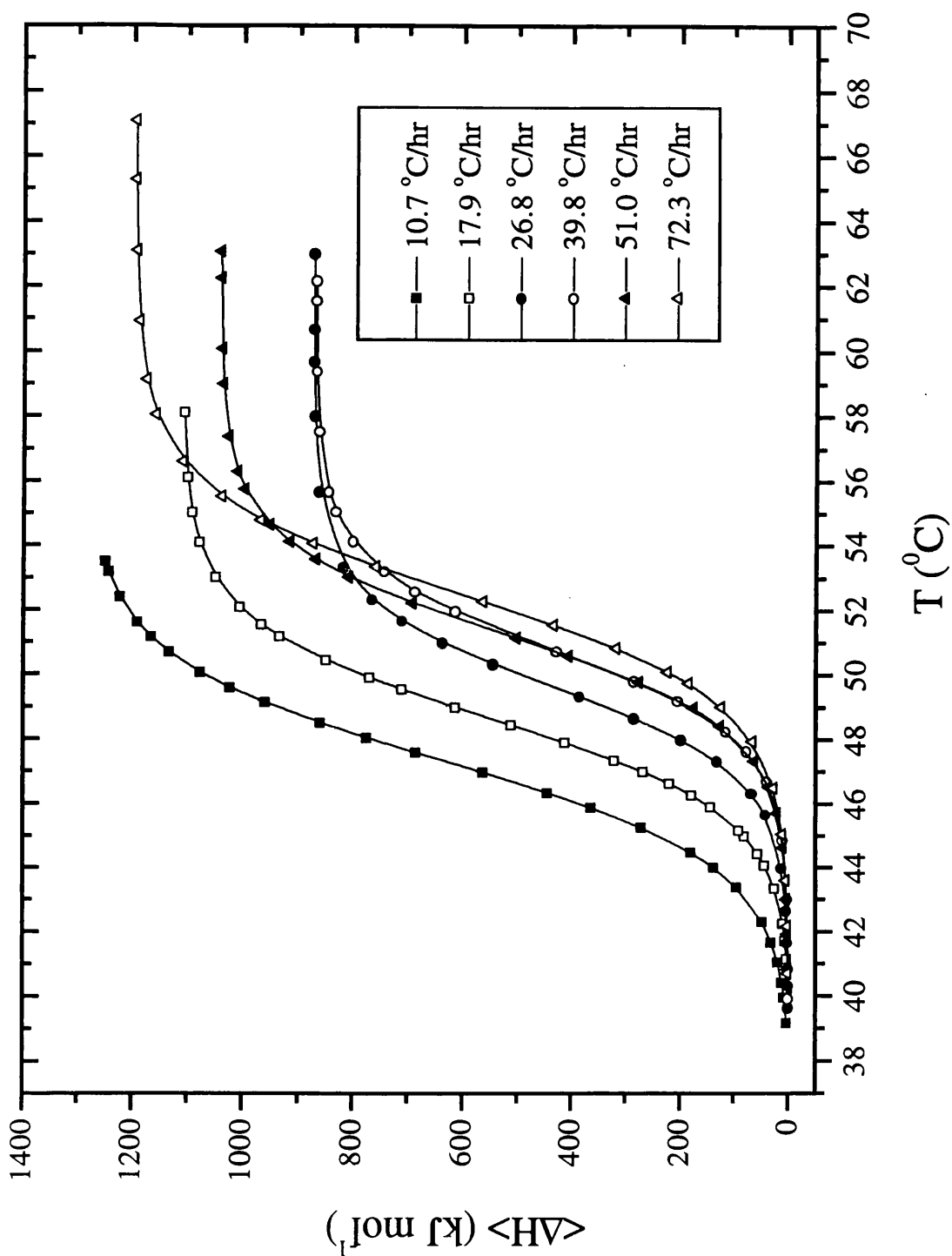


Figure 4.5a: Plot of the cumulative enthalpies, $\langle \Delta H \rangle$, calculated for Campath-1H (pH 3 CBS), at six different scan rates as a function of temperature. $\langle \Delta H \rangle$ is calculated using equation 2.19 in accordance with the method described by La Rosa et al., (1995) and Milardi et al., (1998). Each data point represents the thermodynamic cumulative enthalpy over all the temperatures within the denaturation range.

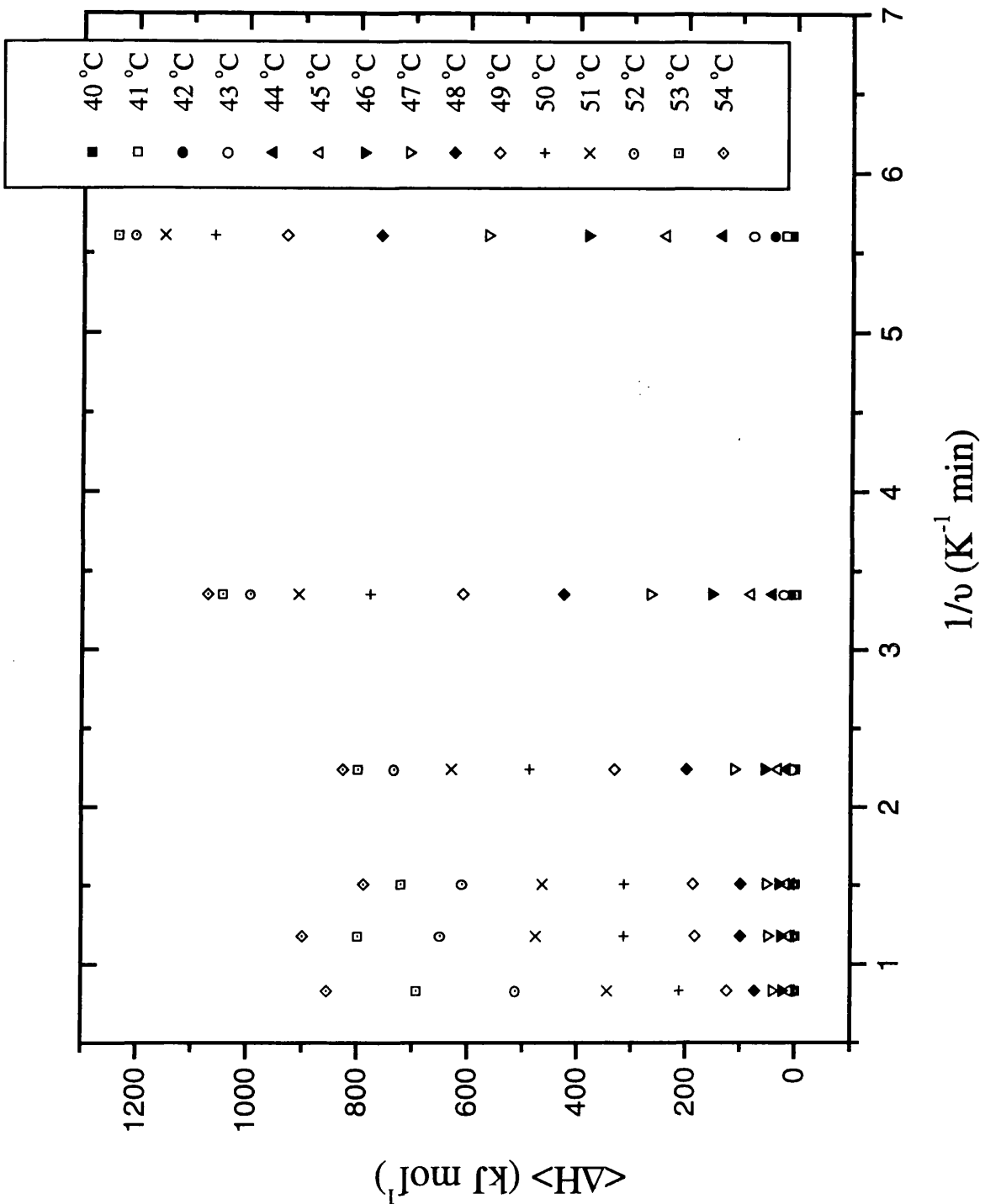


Figure 4.5b: Exponential plots of the cumulative enthalpies of denaturation $\langle \Delta H \rangle$ versus $1/v$ (v represents the scan rate) obtained at a range of temperatures over the entire denaturation range (40-54 °C). The intercept values with the y-axis give the desired value of $\langle \Delta H \rangle_{\text{rev}}$ at a given temperature ($\langle \Delta H \rangle_{\text{rev}}$ represents the cumulative enthalpy function containing information pertinent only to the species in thermodynamic equilibrium as described by La Rosa et al., (1995)).

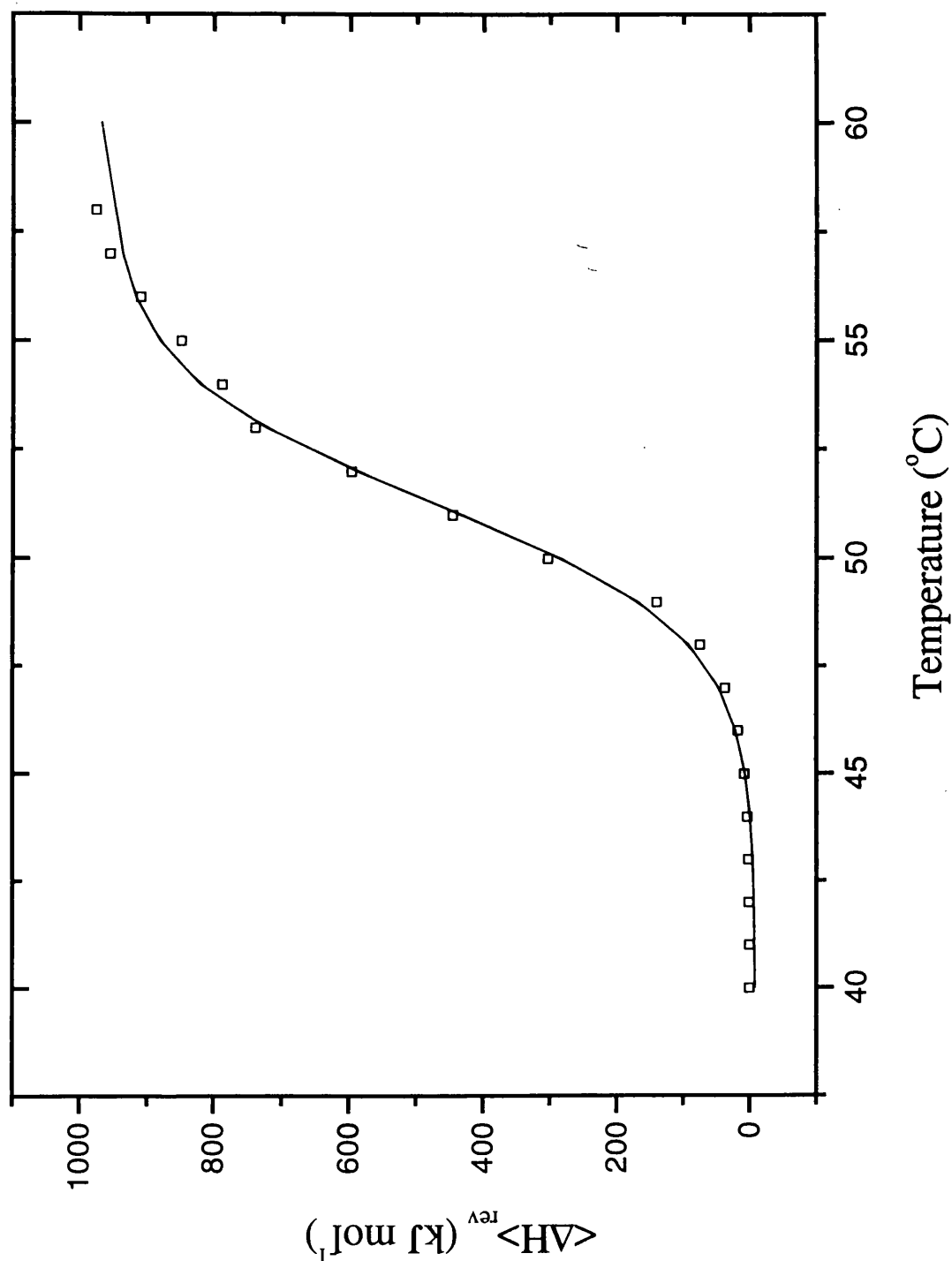


Figure 4.6: Plot of $\langle \Delta H \rangle_{\text{rev}}$ with respect to temperature for Campath-1H (pH 3 CBS). $\langle \Delta H \rangle_{\text{rev}}$ represents the cumulative enthalpy function containing the information pertinent only to the species that are in thermodynamic equilibrium. The data plotted represents the thermodynamic cumulative enthalpy of the denaturation process extrapolated at infinite scanning rate. The midpoint of the sigmoidal plot, 52.0 ± 1 $^{\circ}\text{C}$, represents the T_m of the transition at infinite scanning rate, and its maximum of $958 \pm 8\%$ kJmol^{-1} ($229 \pm 2\%$ kcal mol^{-1}) represents the enthalpy of the transition.

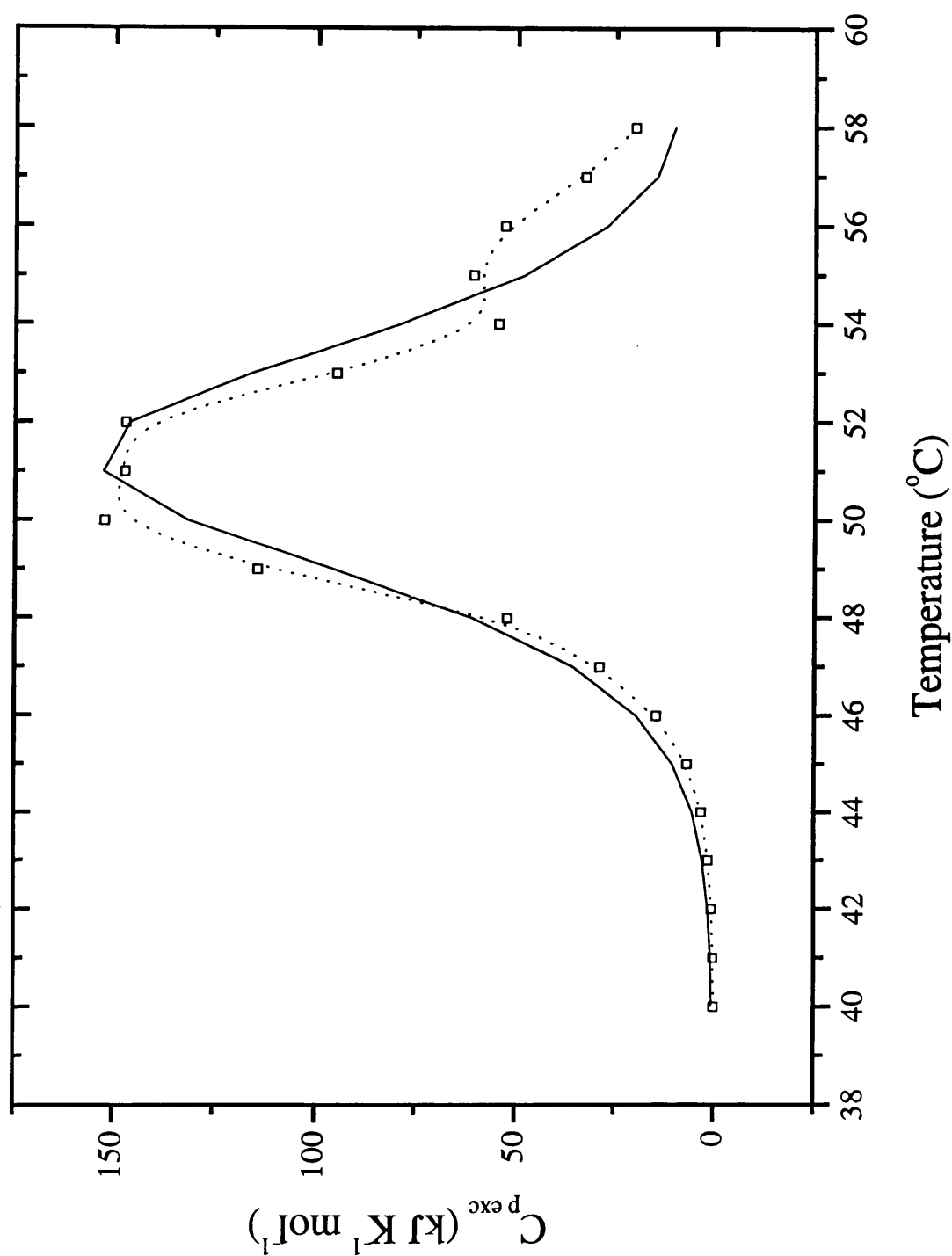


Figure 4.7: $C_{p,exc}$ profile of Campath-1H (pH 3 CBS) at infinite scanning rate obtained from the first derivative of $\langle \Delta H \rangle_{rev}$ with respect to temperature (dashed line). The solid line represents best fit curve of the data using Origin software and represents a transition with a T_m of 51 $^{\circ}\text{C}$ and a calorimetric enthalpy of $975 \pm 10\% \text{ kJmol}^{-1}$ ($233 \pm 3\% \text{ kcal mol}^{-1}$).

CHAPTER 5

**FORMULATION AND THE EFFECT OF ADDITIVES AND
ADJUVANTS**

5.1 Introduction

When studying any aspect of a protein, one of the most important considerations is the formulation of that protein. If the species under investigation is lyophilized, it may contain cryoprotectants e.g. sucrose or dextran (Chang et al., 1993), buffer salts or other additives. When dealing with proteins in solution, the picture becomes somewhat more complex with the consideration of pH, buffer components, ionic strength, protein concentration, preservatives, and when studying proteins of pharmaceutical interest further complexity is introduced when toxicity and suitability for parenteral dosage must be determined (Wang and Hanson, 1988; Manning et al., 1989).

Solution pH plays a critical role in the stability of a protein or peptide and proper selection of pH may be considered as the key to a successful formulation. A basic rule of thumb is to identify the pH at which overall degradation reactions are minimal. Many peptides are formulated at a slightly acidic pH: the pH of oxytocin injection (9 amino acid peptide, Mol. Wt. 1007) is in the range of 2.5-4.5; that of desmopressin injection is 3.5; and nafrelin is most stable at pH 5 (Johnson et al., 1986). At low pH, degradation reactions include the deamidation of asparagine and glutamine and the general hydrolysis of the peptide backbone and glycosides; whereas at high pH, oxidation of cysteine, transpeptidation of aspartic and glutamic acids, deamidation of asparagine and glutamine, and the racemization of amino acids with an electron withdrawing side chain, e.g. proline, are potential degradation mechanisms. In the case of more complex proteins where the stabilization of the native conformation (necessary for bioactivity) is the main concern, the pH is often set at the isoelectric point (point at which the net charge on the protein is zero) presumably to maximise interactions between salt bridges and reduce interactions between neighbouring protein molecules (Wang and Hanson, 1988). In a pharmaceutical context, the pH of globulin products (i.e. antibodies and related proteins) is close to neutrality; 7.4 for Orthoclone OKT® 3 and 6.6 for Sandoglobulin®. However an exception to this is the immunoglobulin Gamimune® N, which for reasons of stability, is formulated at pH 4.25 for intravenous use (Tenold, 1983).

Campath-1H in addition to other IgG molecules is sensitive to acidic conditions. Cleavage occurs at the acid labile Asp-Pro bond at residues 274-275 in the heavy chain at pH 3 (Wellcome Company Document No: BZGA/91/0018, 1992, private communication). The

acid degradation of Asp-Pro peptides is well documented (Landon, 1977; Inglis, 1983). The results of acid induced cleavage of Campath-1H, and indeed other IgG molecules can be examined by reducing SDS-PAGE (Laemmli, 1970). To avoid complications caused by acid induced cleavage, Campath-1H was only studied in acidic pH when absolutely necessary (in reality for most experiments) and care was taken to ensure that samples were freshly prepared and stored cold.

In this thesis, the effect of pH, additives such as L-histidine and n-methylacetamide (known as osmolytes), sugars (mannitol and lactitol), cyclodextrins (methyl- β -cyclodextrin and hydroxypropyl- β -cyclodextrin), surfactants (Poloxamer 188 (Pluronic F68) and polysorbate 80), and polyelectrolytes (DEAE-dextran), and combinations of the above on the thermal stability of all three mAbs has been studied both in the short term and, in the case of Campath-1H and 1209W95, long-term (2 years at 4 °C in formulation containing additive(s)). The long-term effects of additives on 4162W94 has not been studied as its stability is thought to be comparable to Campath-1H which we consider to be a stable model mAb. The effect of these additives has been determined using a combination of biophysical techniques namely DSC and fluorescence spectroscopy (both fluorescence quenching experiments and the use of the extrinsic fluorescent probe ANS).

DSC has been used in previous studies as a means of conveniently and qualitatively studying the effects of a wide range of additives (Ahmad and Bigelow, 1986; Chang et al., 1993; Gombotz et al., 1994; Picó, 1996; Fatouros et al., 1997a; 1997b; Giancola et al., 1997; Remmele et al., 1998) by observing any changes in the T_m of unfolding, that is the peak maximum of the denaturation endotherm, on the basis that an additive expected to stabilise protein should increase the T_m while a destabilizing additive should decrease the T_m . Presented in this chapter, in addition to additive induced changes in T_m , are the effects of cyclodextrins on the activation energies of denaturation calculated by the method reported by Sánchez-Ruiz et al., (1988a). Fluorescence too has been used previously to assess the formulation of proteins. Busby and Ingham (1984) used ANS to probe the effect of various sugar compounds on the thermal stability of antithrombin III and this method, in addition to fluorescence quenching, is useful when studying the structural effects of pH.

In many instances the mechanisms by which additives exert their effects have been the subject of much work. The stabilising effects of neutral salts has been explained by Ahmad

and Bigelow (1986) and Picó (1996) as a combination of several factors including the strengthening of hydrophobic interactions within the protein, and the effects are often discussed in terms of the preferential interactions between the protein and solutes (Timasheff and Arakawa, 1989). Polyalcohol materials such as mannitol and other sugars are well known to stabilize proteins with respect to denaturation through selective solvation of the protein (Lee and Timasheff, 1981), that is, at low additive concentrations, more water molecules pack around the protein in order to exclude the additive.

Many organisms which have adapted to environmental stress such as high temperatures or desiccation accumulate low concentrations of low molecular weight compounds called osmolytes which are believed to confer protection to enzyme and other macromolecular systems against such denaturing stresses (Lin and Timasheff, 1994). These osmolytes can include urea, amino acids, methylamines and sugars. For the purpose of this thesis we have taken L-histidine and n-methylacetamide as representative osmolytes. Osmolytes in general are thought exert their stabilizing effect through selective solvation of the protein in a similar manner to the mechanism described above for polyalcohol materials (Santoro et al., 1992; Plaza del Pino and Sánchez-Ruiz, 1995).

Cyclodextrins and their effects on proteins are probably the least studied though probably best understood of the additives which were chosen for study in this thesis. They are cyclic oligomers of glucose produced by the enzymatic degradation of starch by cyclodextrin transglycosylase (CTG) and are classified by the number of α -1,4-linked glucose units which comprise their structure. α -cyclodextrin has six such units, β -cyclodextrin has seven and γ -cyclodextrin, eight. The molecules themselves are toroidal in shape comprising a hydrophilic outer surface with an apolar cavity which in the case of β -cyclodextrin has a diameter of 6.0-6.5 Å (Li and Purdy, 1992). This cavity allows the cyclodextrins to form inclusion complexes with small nonpolar molecules and therefore bind to exposed aromatic groups on unfolded proteins (Cooper, 1992; Cooper, 1996). For the purpose of this thesis, the cyclodextrins studied were methyl- β -cyclodextrin (MCD) and hydroxypropyl- β -cyclodextrin (HPCD) which in actual fact are not true cyclodextrins but cyclodextrin derivatives which have been created from β -cyclodextrin to improve its solubility. Only β -cyclodextrin derivatives were studied as β -cyclodextrin represents at least 95% of all produced and consumed cyclodextrins and hence benefits from low cost and wide availability. The potential use of cyclodextrins in parenteral formulations has been reviewed by Brewster et al., (1989) with HPCD emerging as the most

promising due to its high solubility and low intravenous toxicity (Brewster et al., 1990) and its ability to increase the solubility and stability of several protein drugs (Brewster et al., 1991; Szejtli, 1991).

The surfactants Poloxamer 188 and polysorbate 80 have been chosen as additives to study as they are both surfactants which are available for use in the parenteral formulation of drugs. Orthoclone OKT® 3, a therapeutic mAb approved by the Federal Drugs Administration (FDA) formulated with 0.02% polysorbate 80 as a stabilizer, is just one example. Surfactants have the ability to cause denaturation of protein both by charge group separation and hydrophobic disruption and therefore for the purpose of drug formulation they are used at extremely low concentrations (<0.04%). At these low concentrations they are able to prevent denaturation of proteins at air/liquid or liquid/liquid interfaces. Protein has a tendency to denature at these interfaces due to the fact that their combination of polar and nonpolar side chains creates a tendency for them to concentrate at these interfaces. Once the protein has concentrated at the interface, a monolayer of protein can form at the surface of the protein solution which will not dissolve due to irreversible unfolding when the surface area is increased (Adamson, 1960; MacRitchie, 1978). The addition of surfactant reduces this problem by reducing the interfacial tension and therefore reducing the propensity for unfolding or by solubilizing the protein to reduce the amount of protein at the interface. If, even at low concentrations surfactants cause some degree of denaturation, it should be noted that for an injectable formula, surfactant concentration can be greatly reduced by dilution in intravenous bags prior to injection.

Inspired by data presented at The First International Conference on Protein Stabilization (Leeds, U.K., 28 June-1 July 1998) by Dr T. Gibson (Applied Enzyme Technology (Ltd.) which suggested that protein stability may be increased by a combination of low concentrations of DEAE-dextran (polyelectrolyte) and lactitol (polyalcohol), the effect of these additives on Campath-1H has been investigated. This chapter contains details of how these additives affect both the calorimetric reversibility of unfolding and the T_m of the main transition. Dr T. Gibson has proposed that the DEAE-dextran bound to protein surface charges to form a cage-like structure which protected and supported the native form of the protein (no relevant publications are available at time of writing).

5.2 Results

5.2.1 Determination of Optimal pH

The effect of pH on the DSC scans of the three mAbs has been discussed in chapter 3 with the effect of pH on T_m presented in tables 3.1, 3.2 and 3.3 for Campath-1H, 4162W94 and 1209W95 respectively. With a view to studying long-term stability and the effect of additives on the mAbs, the pH and buffer type which resulted in the highest T_m and therefore greatest thermal stability was chosen. For Campath-1H and 4162W94 pH 6 CBS was selected and pH 8 TBS was selected for 1209W95.

The effect of pH on the structure of the mAbs was also studied using fluorescence quenching techniques to probe the accessibility of the tryptophan residues within each of the proteins. Succinimide quenching of Campath-1H was carried out at pH 3.5, 4, 5, 6 and 7.4. All results were corrected for buffer effects and dilution of protein sample on addition of aliquots of quencher (a 2.5 M solution of succinimide was used throughout) and plotted as Stern-Volmer plots as described in chapter 2: Materials and Methods. The gradient of the line, K_{sv} (the Stern-Volmer constant) was then calculated using Origin software and used as a measure of the accessibility and hence compactness of the protein structure, with a large K_{sv} indicating greater tryptophan accessibility (and hence less compactness of structure) and a smaller K_{sv} indicating the opposite (Eftink and Ghiron, 1976a; 1976b; 1984). The Stern-Volmer plot obtained on quenching Campath-1H (pH 6 CBS) with succinimide is shown in figure 5.1 as an example of the high quality of results obtained (inset plot shows slight negative deviation of line). K_{sv} values for Campath-1H, 4162W94 and 1209W95 obtained under other pH conditions are presented in table 5.1. Succinimide quenching studies were also carried out on samples of Campath-1H (pH 4 ABS) which had been scanned at 10 °C/hr to 100 °C. These samples had not visibly aggregated during the scan but quenching gave a K_{sv} of $4.1 \pm 0.5 \text{ M}^{-1}$ (compared to a pre-scan value of $0.7 \pm 0.2 \text{ M}^{-1}$) which is indicative of increased tryptophan exposure conducive to unfolding.

The quenching data plotted in the inset plot of figure 5.1 are identical to the data presented in the main plot but the scale is chosen to illustrate the fact that what appears to be a linear relationship in the main plot, has in fact a slight negative deviation, that is, a downward curve. Similar quenching patterns have been observed by Lehrer (1971), and

Teale and Badley (1970) and are the result of the ability of certain tryptophans in a protein to be selectively quenched before others (Eftink and Ghiron, 1976a). It is an effect only observed for multi-tryptophan proteins. At a low concentration of quencher, the slope of the Stern-Volmer plot reflects the quenching of the more accessible residue(s) whereas at higher quencher concentrations, the tryptophans having lower quenching constants become dominant as the easily quenched fluorescence has become greatly depleted. This type of selective quenching can only be detected if the quenching constants for each fraction of the fluorescence are quite different as if they do not differ sufficiently the results are apparently linear plots.

In an attempt to compliment the data obtained from quenching experiments it was decided to move from succinimide quenching to acrylamide quenching. Acrylamide is a small organic uncharged quenching probe that is very sensitive to the degree of exposure of tryptophans in proteins (Eftink and Ghiron, 1976a). It also quenches with a larger rate constant than succinimide (Eftink and Ghiron, 1984). It was hoped that using acrylamide as a quencher would produce more significant differences in K_{sv} on changing the pH conditions of the proteins. The results from a typical acrylamide quenching experiment are shown in figure 5.2a. This figure shows the data obtained by quenching Campath-1H (pH 6 CBS) with acrylamide in comparison to the quenching of a solution of free L-tryptophan in pH 6 CBS. Both data sets are plotted as Stern-Volmer plots. In this plot there is an obvious upward curve of the free tryptophan quenching data and in fact there is a slight upward curve of the Campath-1H data too. This upwards curvature is a result of static quenching and occurs as a result of the quenching reaction produced by acrylamide and other efficient quenchers where there is a high probability of quencher and chromophore molecules being near in space at the moment the latter is excited. In such a case the probability of the reaction occurring is so high that quenching occurs almost instantaneously (statically) (Eftink and Ghiron, 1976b). Static quenching can be taken into account by plotting the data as a modified Stern-Volmer plot as described in Chapter 2. Figure 5.2b shows a modified Stern-Volmer plot for Campath-1H (pH 6 CBS) in comparison to the quenching of a solution of free L-tryptophan in identical buffer. Both datasets produce linear plots. The K_{sv} values obtained by acrylamide quenching and subsequent modified Stern-Volmer analysis for Campath-1H, pH 3.5, 5, 6, and 7.4 are presented in table 5.1. It is evident that there are no benefits to be had in using acrylamide as quencher as there is no real gain to be made in distinguishing the degree of accessibility of tryptophan exposure in each of the pH conditions tested. This and the fact that acrylamide is extremely toxic and the data obtained from quenching experiments must be corrected for

static quenching and the absorbance of acrylamide itself precluded further acrylamide quenching studies.

As mentioned previously, IgG molecules are prone to acid cleavage. In the case of Campath-1H it is the Asp-Pro bond at residues 274-275 on the heavy chain which is acid labile (Wellcome Foundation Document No: BZGA/91/0081, private communication) and cleavage at this site results in fragments of approximately 30 and 20 kDa. This cleavage pattern can be seen using reducing SDS-PAGE and the results are shown in figure 5.3. Lanes 1 and 6 are molecular weight standards (comprising phosphorylase b, bovine serum albumin, ovalbumin, carbonic anhydrase, soybean trypsin inhibitor and α -lactalbumin), lanes 2 and 3 are Campath-1H (pH 7.2 PBS) and lanes 4 and 5 are Campath-1H which has been dialysed into pH 3 CBS and stored for 13 days. Due to the reducing conditions, the molecule has been cleaved into its light and heavy chains (bands at 50 and 25 kDa) and acid cleavage has produced two further bands at approx. 30 and 23 kDa. To minimise this cleavage stability studies were carried out at pH 6 and care was taken to keep samples refrigerated at all times.

5.2.2 Short and Long-term Effect of Additives

Using a core set of nine additives/additive combinations comprising the following: 5% and 10% (w/w) mannitol, 0.01% (w/w) Poloxamer 188, 100 mM n-methylacetamide, 3% (w/w) L-histidine, 3% (w/w) L-histidine + 0.01% (w/w) Poloxamer 188, 100 mM methyl- β -cyclodextrin, 100 mM hydroxypropyl- β -cyclodextrin, and 3% (w/w) L-histidine + 100 mM methyl- β -cyclodextrin, the effects on the three mAbs Campath-1H, 4162W94 and 1209W95 were studied using DSC, fluorescence quenching techniques, visual inspection and ANS binding. Samples were studied both immediately after formulation with the additive(s) and also after two years at 4 °C. For the long-term studies, a sample of mAb in relevant buffer without any additives which was filled into vials, stoppered, and sealed at the same time and under the same conditions as the samples with additives, was used as the control.

All formulations were scanned in the DSC at a scan rate of 60 °C/hr, using identical buffer + additive in the reference cell. Each sample was subjected to two scans to check for calorimetric reversibility- none of the formulations of any of the three mAbs showed any reversibility. The DSC data was then concentration normalized, baseline subtracted and the

T_m of the main transition recorded. The short-term effects of additives on the T_m s of Campath-1H (pH 6 CBS), 4162W94 (pH 6 CBS) and 1209W95 (pH 8 TBS) are presented in table 5.2 as the change in T_m with respect to the control values of 78.2 °C, 77.1 °C and 61.3 °C for Campath-1H, 4162W94 and 1209W95 respectively. In a similar fashion, the results of the long-term effects of additives on Campath-1H and 1209W95, with respect to a control samples stored under identical conditions, are presented in table 5.3. Visual inspection revealed that all vials contained a clear bright solution. It is immediately clear from tables 5.2 and 5.3 that cyclodextrins have a strong destabilising influence on the proteins.

To monitor whether the additives affect the accessibility of the tryptophan molecules (i.e. affect the compactness of the structure), fluorescence quenching studies using succinimide as quencher were carried on long-term storage samples. The results of these studies, tabulated as K_{sv} values for each formulation, for both Campath-1H and 1209W95, are presented in table 5.4. Prior to every fluorescence experiment, the fluorescence spectrum of the buffer/additive system was recorded so that it may be subtracted from the protein/buffer/additive spectrum to leave only the protein spectrum for analysis. Significant fluorescence was observed with buffer/cyclodextrin samples on excitation at 295 nm. With control experiments we were able to show that this fluorescence could be quenched on addition of aliquots of succinimide (data not shown) and therefore the data presented in table 5.4 regarding the K_{sv} values obtained on quenching protein/buffer/cyclodextrin is invalid in the context of the other results as the data represents the quenching of both protein and cyclodextrin fluorescence. It has since been shown by colleagues that the fluorescence is due to impurities and not the cyclodextrin itself and the fluorescence can be reduced by agitating the cyclodextrin with activated charcoal prior to use. This fluorescence did not occur using an excitation wavelength of 390 nm which is the wavelength used to excite ANS and therefore ANS binding experiments using protein/buffer/cyclodextrin are valid.

The long-term effects of the additives on the hydrophobicity of the mAbs was studied by monitoring the binding of ANS to each and again comparing the results with those gained from control experiments. All experiments were performed at 25 °C and involved the addition of protein to a cuvet containing a 20 μ M solution of ANS in the relevant buffer/additive. Final protein concentration was 0.2 μ M. The excitation wavelength used was 390 nm and the emission spectrum was recorded from 400-700 nm. The wavelength of the emission maximum and the fluorescence intensity at this wavelength is recorded in table 5.5 for

Campath-1H (pH 6) and 1209W95 (pH 8) formulated in the core set of additives and stored for 2 years at 4 °C. The table also contains the data from control experiments which involved monitoring ANS binding to samples of mAb in either pH 6 CBS for Campath-1H or pH 8 TBS for 1209W95 which had been stored under identical conditions to the samples containing additives. The data contained in table 5.5 shows that the addition of 5 and 10% (w/w) mannitol, and 3% (w/w) L-histidine has no effect on the hydrophobicity of the protein surface over the testing period when compared to the control. Both the addition of 0.01% (w/w) Poloxamer 188 and the combination of 0.01% (w/w) Poloxamer 188 and 3% (w/w) L-histidine increase hydrophobicity slightly with a greater increase being observed on the addition of 0.01% (w/w) Poloxamer only. Both 100 mM n-methylacetamide and any formulations containing 100 mM cyclodextrin apparently greatly increase the hydrophobicity of the proteins over the two year period, but in fact it is the case that with cyclodextrins the results are void as the majority of the blue shift in ANS fluorescence is due to the ANS binding to the hydrophobic core of the cyclodextrins and not the proteins. So, in terms of their effect on hydrophobicity, we can order the additives as follows starting with that which shows the greatest effect: 100 mM n-methylacetamide > 0.01% (w/w) Poloxamer 188 > 3% (w/w) L-histidine + 0.01% (w/w) Poloxamer 188 > 3% (w/w) L-histidine > 5%, 10% (w/w) mannitol. It is not possible to include the cyclodextrin formulations in this list but we can see from tables 5.2 and 5.3 that the cyclodextrins and cyclodextrin/histidine formulations are least stable as analysed by the T_m obtained by DSC.

5.2.3 The Effects of Cyclodextrins

Studies of the effects of cyclodextrins on the thermal unfolding of proteins have been reported (Cooper, 1992; Cooper 1996). These studies focus on the ability of the cyclodextrins to form inclusion complexes with small nonpolar molecules and therefore bind to exposed aromatic groups on unfolded proteins. This aspect of cyclodextrin behaviour explains the results presented in tables 5.2 and 5.3 where the T_m of the mAbs is significantly reduced in the presence of both methyl- β -cyclodextrin and hydroxypropyl- β -cyclodextrin. This reduction in T_m can be attributed to the binding of cyclodextrin to the unfolded form of the protein and hence stabilizing this form, shifting the folded \leftrightarrow unfolded equilibrium in favour of the unfolded form. The question then arises whether the cyclodextrins affect the activation barrier of thermal denaturation as calculated in Chapter 4 using the method described by Sánchez-Ruiz et al. (1988a). A full kinetic analysis, as described in chapter 4

was carried out on the main endothermic transition of Campath-1H in the presence of 100 mM methyl- β -cyclodextrin at pH 4, 5 and 6. The results, tabulated as the activation energies calculated using equations 2.15-2.18 are shown in table 5.6. If we compare these results with those in the absence of cyclodextrin (see table 4.7), it is clear that methyl- β -cyclodextrin not only destabilises Campath-1H in terms of T_m but it also causes an overall reduction in the activation energy required for thermal denaturation. Again this is most likely due to the destabilisation of the folded form of protein by the cyclodextrin.

The effects of cyclodextrins on the DSC trace of Campath-1H are concentration dependent. The effects of 0, 15, 20, 30 and 40% (w/w) HPCD on the DSC trace of Campath-1H (pH 6) are shown in figure 5.4 (15% (w/w) HPCD is equivalent to 100 mM). This figure shows that as HPCD concentration increases, the T_m of the first transition stays constant, the T_m of the second transition decreases and at >30% (w/w) HPCD a third endothermic transition occurs. These T_m values are presented in table 5.7. The finding that the T_m of the first transition is independent of cyclodextrin concentration is consistent with the interpretation of this transition as a small change in tertiary structure; we can see from figure 3.10 that this tertiary structure change does not involve a great increase in the exposure of tryptophan residues and therefore there will be no significant binding of cyclodextrins to these residues. A fascinating aspect of the interaction of HPCD with Campath-1H is its apparent ability to prevent gross thermal aggregation. Figure 5.4 shows that at concentrations of 30 and 40% (w/w) HPCD, the DSC traces of Campath-1H are not prematurely distorted by exothermic aggregation events and have a smooth posttransition baseline. In addition, when such samples are removed from the DSC cell, on visual inspection they are clear and bright. Attempts were made to probe the accessibility of the tryptophan residues within this scanned Campath-1H sample but all attempts failed due to the fluorescence of impurities associated with the cyclodextrin.

The nature of the third endothermic transition of Campath-1H (pH 6) which is present at HPCD concentrations of 30 and 40% (w/w) remains unknown. Scans of Campath-1H (0.018 mM, pH 6 CBS, 40% (w/w) HPCD) were performed at six different scan rates (10.7, 17.9, 26.8, 39.8, 51.0 and 72.3 °C/hr) and the results are presented in figure 5.5. This figure illustrates not only the scan rate dependence of the main transition, that is the T_m increases with increasing scan rate (which has been discussed in some detail in Chapter 4), but also the scan rate dependence of this third transition. Scan rate dependence indicates that the process

which results in the third DSC endotherm is under kinetic control (Sánchez-Ruiz et al., 1988a; Galisteo et al., 1992). A similar transition is also observed on the DSC trace of 4162W94 (0.013 mM, pH 6 CBS, 40% (w/w) HPCD as shown in figure 5.6 where again the cyclodextrin prevents gross thermal aggregation as indicated by the absence of any exothermic events, the presence of a smooth posttransition baseline and a clear bright sample on removal from the DSC cell.

5.2.4 The Effects of DEAE-Dextran and Lactitol

The effect of DEAE-dextran and lactitol on the stability of Campath-1H (pH 6 CBS) as determined by the T_m of thermal unfolding was studied using DSC. The following additives were used (all quantities are % (w/w)): 0.5%, 1%, 5% DEAE-dextran, 1% DEAE-dextran + 1% lactitol, 1% DEAE-dextran + 5% lactitol, and 5% DEAE-dextran + 5% lactitol. Figure 5.7a presents raw DSC data illustrating the effect of 0.1 and 0.5% (w/w) DEAE-dextran on the DSC trace of Campath-1H and figure 5.7b presents raw DSC data illustrating the effect of various DEAE-dextran/lactitol combinations. The results presented in figure 5.7b show that both 5% (w/w) DEAE-dextran and the combination of 5% (w/w) DEAE-dextran + 5% (w/w) lactitol prevent exothermic aggregation of the protein on the first heating cycle though postscan visual inspection of both samples reveal that aggregation occurs on heating a second time. Neither of these samples nor any other DEAE-dextran/lactitol combination improved the calorimetric reversibility of the DSC transitions. Figure 5.7a reveals that low concentrations ($\leq 1\%$ (w/w)) of DEAE-dextran have no significant effect on the T_m of either the first or the second endotherm but, as can be seen in figure 5.7b, at higher concentrations (5% (w/w)) it has a destabilizing influence which manifests itself as a lowering of both T_m values. Figure 5.7b reveals that lactitol has a stabilizing effect on Campath-1H but this effect can be cancelled out by the destabilizing effect of 5% (w/w) DEAE-dextran. As these additives failed to improve the calorimetric reversibility of the transitions and did not exert a stabilizing effect greater than that observed on addition of mannitol, no further studies were carried out using DEAE-dextran or lactitol.

5.3 Discussion

DSC experiments with Campath-1H and 4162W94 have shown that mannitol has a stabilizing influence with respect to thermal denaturation, evidenced by increased T_m values in the presence of both 5 and 10% (w/w) mannitol. For example, the T_m of the main endothermic transition of 4162W94 increases by 1.6 and 2.5 °C on addition of 5 and 10% (w/w) mannitol respectively. Mannitol also had a stabilizing effect on 1209W95 but this effect was less pronounced. The overall stabilization effects of mannitol on the mAbs are consistent with those on antithrombin III described by Busby and Ingham (1984).

P188 has no significant effect on the T_m values of the mAbs either in the short or long-term although fluorescence quenching with succinimide suggests that in the long-term it decreases the accessibility of tryptophan residues within Campath-1H and 1209W95. Formulation of Campath-1H and 1209W95 with P188 also appears to increase the hydrophobicity of the proteins slightly. It would be expected that P188, since it is a surfactant, would have a denaturing effect on the proteins and therefore we would see a decreased T_m , increased K_{sv} values and increased hydrophobicity as it exerted its effect. The results are not in agreement with these expectations probably due to the low concentrations used (0.01%(w/w)) for the purpose of prevention of adsorption onto surfaces and denaturation at interfaces. Surfactants, by their mechanism of action, can prevent shear-induced aggregation but we have shown that they do not affect heat-induced aggregation. This emphasises the need to use several complementary techniques to assess the usefulness of formulation additives.

As expected, n-methylacetamide in protein formulation resulted in a small but significant decrease in T_m in both the short and long-term. This destabilisation is consistent with weak binding to exposed hydrogen-bonding peptide groups (Cooper and Nutley, unpublished). This destabilization effect is also suggested by increased hydrophobicity of the proteins in the presence of n-methylacetamide as shown by ANS binding experiments. L-histidine exerted no major effect on the stability of the proteins, only a very small general increase in T_m (in the order of <0.3 °C).

Cyclodextrins proved to be the most interesting additives studied. One major drawback was the fluorescent impurities within the cyclodextrins supplied as they were quenched

in addition to the proteins during fluorescence quenching experiments and hence results from these experiments were void. Also, the ability of the hydrophobic cavity of cyclodextrins to bind ANS precluded studying the hydrophobicity of the proteins in formulations containing cyclodextrins by monitoring ANS binding. DSC experiments provided a wealth of information concerning the effects of cyclodextrins on the mAbs. As expected formulations containing either MCD or HPCD resulted in a large decrease in T_m values of the mAbs both in the short and long-term. This destabilization effect is due to the cyclodextrins binding to aromatic groups on the unfolded form of the protein and hence shifting the folded \leftrightarrow unfolded equilibrium to the right (Cooper, 1992; Cooper, 1996). It was found that MCD was more effective than HPCD in reducing the T_m . In addition to lowering the T_m we have shown, using the method of activation energy calculation devised by Sánchez-Ruiz et al., (1988a), that HPCD actually decreases the activation energy required for protein thermal denaturation. If the results in table 5.6 (activation energy of thermal denaturation of Campath-1H in presence of 100 mM HPCD) are compared with those in table 4.7 (activation energy of thermal denaturation of Campath-1H without HPCD) it is seen that there is a reduction in activation energy of 71 and 43 kJ/mol, in pH 4 and 5 respectively, on addition of 100 mM HPCD.

The effects of HPCD are shown to be concentration dependent. Table 5.7 illustrates the fact that the first DSC endotherm of the thermal denaturation of Campath-1H is unaffected by the presence of HPCD whereas the T_m of the second decreases consistently on addition of increasing concentrations of HPCD. Above 30% (w/w) HPCD, the DSC of Campath-1H reveals a third endotherm, the T_m of which is seen to increase on going from 30 to 40% (w/w) HPCD. The nature of this endotherm is unknown (it is not feasible to record CD spectra at such high HPCD concentrations as the HPCD would mask the protein signal) but we have shown it to be highly scan rate dependent and therefore representative of a process under kinetic control. A similar endotherm appears when 4162W94 is subjected to the same treatment though no such effect appears with 1209W95 (data not shown).

None of the formulations tested resulted in any calorimetric reversibility of the mAbs. 30 and 40% (w/w) HPCD, 5% (w/w) DEAE-dextran, and 5% (w/w) DEAE-dextran + 5% (w/w) lactitol showed ability to prevent thermal aggregation of Campath-1H and high concentrations of HPCD also prevented thermal aggregation of both 4162W94 and 1209W95. We propose the inhibition of aggregation is a direct effect of the cyclodextrin binding to the hydrophobic residues of the unfolded protein which are involved in gross aggregation of the

unfolded protein as it is the influence of these hydrophobic regions of unfolded protein which make the protein clump together in order to hide these regions from the polar solvent. It had been hoped that although HPCD destabilized the proteins it would allow them to refold by acting as chaperone mimics, that is, in binding to hydrophobic residues and preventing aggregation, on cooling the protein sample the protein would be able to refold into its native form. As mentioned earlier, there was no evidence of chaperone mimicry as no calorimetric reversibility was observed, although it must be noted that experiments described in this thesis involve only two cyclodextrin derivatives and there are many others which may prove more suited to this purpose.

pH	K_{sv} (M^{-1}) Campath-1H, 0-0.375 M succinimide	K_{sv} (M^{-1}) 4162W94, 0-0.375 M succinimide	K_{sv} (M^{-1}) 1209W95, 0-0.375 M succinimide	K_{sv} (M^{-1}) Campath-1H, 0-1.199 M acrylamide
3	(-)	1.5 ±0.2	(-)	(-)
3.5	1.2 ±0.1	(-)	(-)	-0.7 ±0.1
4	0.7 ±0.2	(-)	(-)	(-)
5	1.6 ±0.1	0.8 ±0.2	(-)	-0.6 ±0.1
6	1.1 ±0.1	1.1 ±0.1	(-)	-0.6 ±0.1
6.6	(-)	(-)	3.2 ±0.4	(-)
7.4	1.2 ±0.2	(-)	(-)	-0.5 ±0.05
8	(-)	(-)	3.9 ±0.2	(-)

Table 5.1: Table showing the effect of buffer pH on the accessibility of tryptophan residues within the mAbs Campath-1H, 4162W94 and 1209W95, as measured by fluorescence quenching. K_{sv} represents the Stern-Volmer constant; the larger the value of this constant, the more accessible the tryptophan residues to quencher. The quencher used is either succinimide or acrylamide as indicated. (-) indicates no experiment was performed at this pH.

ADDITIVE	ΔT_m (°C)	ΔT_m (°C)	ΔT_m (°C)
	Campath-1H, pH 6	4162W94, pH 6	1209W95, pH 8
5% (w/w) mannitol	+ 1.0	+ 1.6	- 0.5
10% (w/w) mannitol	+ 2.2	+ 2.5	+ 0.7
0.01% (w/w) Poloxamer 188	0	0	0
100 mM n- methylacetamide	- 1.0	0	- 2.0
3% (w/w) L-histidine	+ 0.1	+ 0.2	- 1.1
3% (w/w) L- histidine, 0.01% (w/w) Poloxamer 188	+ 0.1	+ 0.2	- 1.0
100 mM methyl- β - cyclodextrin	- 4.8	- 3.7	- 6.0
100 mM hydroxypropyl- β - cyclodextrin	- 2.3	- 3.0	- 2.1
3% (w/w) L- histidine, 100 mM methyl- β - cyclodextrin	- 4.9	- 3.6	- 5.4

Table 5.2: Short-term effects of a range of additives on the T_m of the main endothermic transition of the three mAbs; Campath-1H (pH 6 CBS), 4162W94 (pH6 CBS) and 1209W95 (pH 8 TBS) with respect to control samples with no additives with T_m values of 78.2 °C, 77.1 °C, and 61.3 °C respectively. All data were recorded at a nominal scan rate of 60 °C/hr. Buffer baselines have been subtracted and all data concentration normalized.

ADDITIVE	ΔT_m (°C)	ΔT_m (°C)
	Campath-1H, pH 6	1209W95, pH 8
5% (w/w) mannitol	+ 1.0	+ 1.3
10% (w/w) mannitol	+ 1.8	+ 2.3
0.01% (w/w) Poloxamer 188	0	+ 0.2
100 mM n- methylacetamide	- 1.0	- 0.4
3% (w/w) L-histidine	+ 0.1	+ 0.3
3% (w/w) L- histidine, 0.01% (w/w) Poloxamer 188	+ 0.1	+ 0.3
100 mM methyl- β - cyclodextrin	- 4.8	- 3.8
100 mM hydroxypropyl- β - cyclodextrin	- 2.1	- 1.5
3% (w/w) L- histidine, 100 mM methyl- β - cyclodextrin	- 4.9	- 3.8

Table 5.3: Long-term effects (two years at 4 °C) of a range of additives on the T_m of the main endothermic transition of Campath-1H (pH 6 CBS) and 1209W95 (pH 8 TBS) with respect to long-term stored control samples with T_m values of 78.6 °C and 62.6 °C for Campath-1H and 1209W95 respectively. All data were recorded at a nominal scan rate of 60 °C/hr. Buffer baselines have been subtracted and all data concentration normalized.

ADDITIVE	K_{sv} (M^{-1})	K_{sv} (M^{-1})
	Campath-1H, long-term	1209W95, long-term
CONTROL	0.705 \pm 0.025	3.23 \pm 0.07
5% (w/w) mannitol	0.715 \pm 0.025	2.64 \pm 0.08
10% (w/w) mannitol	0.575 \pm 0.105	2.92 \pm 0.24
0.01% (w/w) Poloxamer 188	0.455 \pm 0.105	3.00 \pm 0.1
100 mM n- methylacetamide	0.480 \pm 0.060	3.34 \pm 0.06
3% (w/w) L-histidine	0.555 \pm 0.125	2.92 \pm 0.09
3% (w/w) L-histidine, 0.01% (w/w) Poloxamer 188	0.560 \pm 0.020	3.00 \pm 0.27
100 mM methyl- β - cyclodextrin	0.720 \pm 0.025	3.13 \pm 0.01
100 mM hydroxypropyl- β - cyclodextrin	0.520 \pm 0.020	2.66 \pm 0.22
3% (w/w) L-histidine, 100 mM methyl- β - cyclodextrin	0.650 \pm 0.022	2.78 \pm 0.22

Table 5.4: Table showing the effect of formulation additives on the accessibility of tryptophan residues within the mAbs Campath-1H (pH 6) and 1209W95 (pH 8) after 2 years at 4 °C, as measured by fluorescence quenching. K_{sv} represents the Stern-Volmer constant; the larger the value of this constant, the more accessible the tryptophan residues to quencher. Control samples consisted of Campath-1H (pH 6 CBS) and 1209W95 (pH 8 TBS) stored under identical conditions. The quencher used was a 2.5 M solution of succinimide.

ADDITIVE	Campath-1H λ_{\max} (nm), I (cps)	1209W95 λ_{\max} (nm), I (cps)
CONTROL	517, 9.49x10 ⁴	515, 1.11x10 ⁵
5% (w/w) mannitol	517, 1.13x10 ⁵	512, 1.18x10 ⁵
10% (w/w) mannitol	517, 1.08x10 ⁵	510, 1.25x10 ⁵
0.01% (w/w) Poloxamer 188	494, 1.49x10 ⁵	504, 1.44x10 ⁵
100 mM n- methylacetamide	442, 3.61x10 ⁵	509, 1.33x10 ⁵
3% (w/w) L-histidine	515, 1.18x10 ⁵	513, 1.28x10 ⁵
3% (w/w) L-histidine, 0.01% (w/w) Poloxamer 188	513, 1.36x10 ⁵	507, 1.60x10 ⁵
100 mM methyl- β - cyclodextrin	462, 1.51x10 ⁷	472, 1.39x10 ⁷
100 mM hydroxypropyl- β - cyclodextrin	471, 1.47x10 ⁷	471, 1.47x10 ⁷
3% (w/w) L-histidine, 100 mM methyl- β - cyclodextrin	463, 1.50x10 ⁷	471, 1.37x10 ⁷

Table 5.5: Table showing the effects of additives on the fluorescence of ANS in the presence of Campath-1H (pH 6 CBS) and 1209W95 (pH 8 TBS). Both the wavelength of the emission maximum (λ_{\max}) and the fluorescence intensity at that wavelength (I/counts per second) are tabulated. Control samples were Campath-1H in pH 6 CBS and 1209W95 in pH 8 TBS stored under identical conditions. All experiments were performed at 25 °C at a protein concentration of 0.2 μ M, ANS concentration of 20 μ M and an excitation wavelength of 390 nm was used throughout.

mAb (pH)	E_A /kJ mol ⁻¹	E_A /kJ mol ⁻¹	E_A /kJ mol ⁻¹	E_A /kJ mol ⁻¹	Average E_A /kJ mol ⁻¹
	Eq. 2.15	Eq. 2.16	Eq. 2.17	Eq. 2.18	
Campath-1H (pH 4), 2 nd transition.	321 ±3%	354 ±5%	445 ±9%	426 ±11%	386 ±9%
Campath-1H (pH 5), 2 nd transition.	455 ±9%	458 ±11%	580 ±8%	552±10%	511 ±10%
Campath-1H (pH 6), 2 nd transition.	428 ±7%	462 ±11%	665 ±8%	646 ±12%	550 ±10%

Table 5.6: Activation energies (E_A), for thermal denaturation, calculated using equations 2.15-2.18 for Campath-1H (pH 4, 5, 6) in the presence of 100 mM methyl- β -cyclodextrin.

Concentration of HPCD (% (w/w))	T _{m1} (°C)	T _{m2} (°C)	T _{m3} (°C)
0	69.4	78.2	(-)
15	69.4	76.1	(-)
20	69.4	75.3	(-)
30	69.4	74.2	81.9
40	69.4	73.5	82.5

Table 5.7: The effect of HPCD concentration on the T_m values of Campath-1H (0.013 mM, pH 6) as determined by DSC. (-) indicates the absence of a third endotherm at these HPCD concentrations. All scans were performed at a scanning rate of 60 °C/hr.

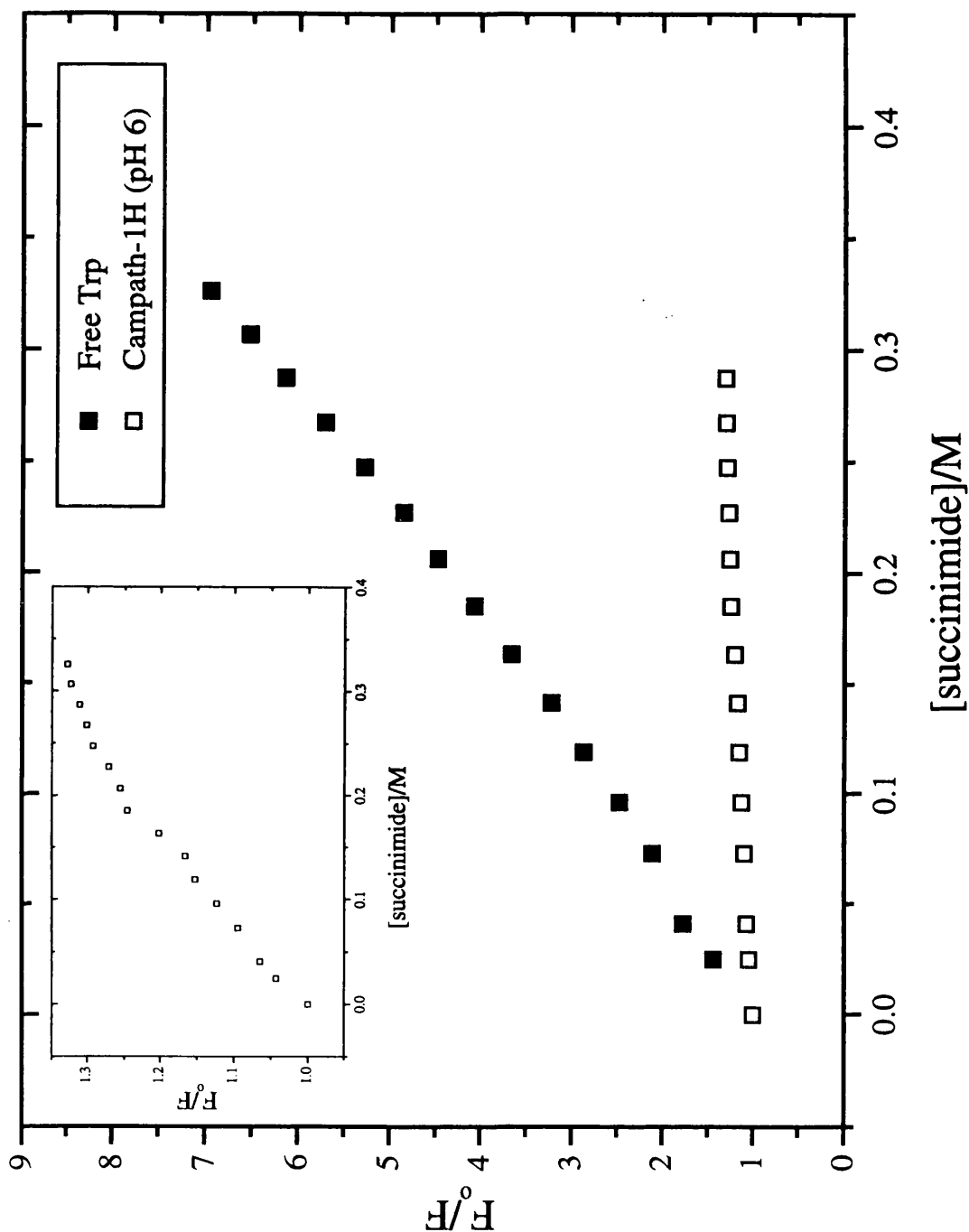


Figure 5.1: Results of succinimide quenching of Campath-1H (pH 6 CBS) plotted as a Stern-Volmer plot. Main graph shows quenching of Campath-1H in comparison to fully exposed tryptophan. K_{sv} values are 1.1 ± 0.1 and $13.9 \pm 0.3 \text{ M}^{-1}$ for Campath-1H and fully exposed tryptophan respectively. Inset shows detail of Campath-1H data showing slight negative deviation. All data recorded at $25 \text{ }^\circ\text{C}$ and using excitation wavelength of 295 nm.

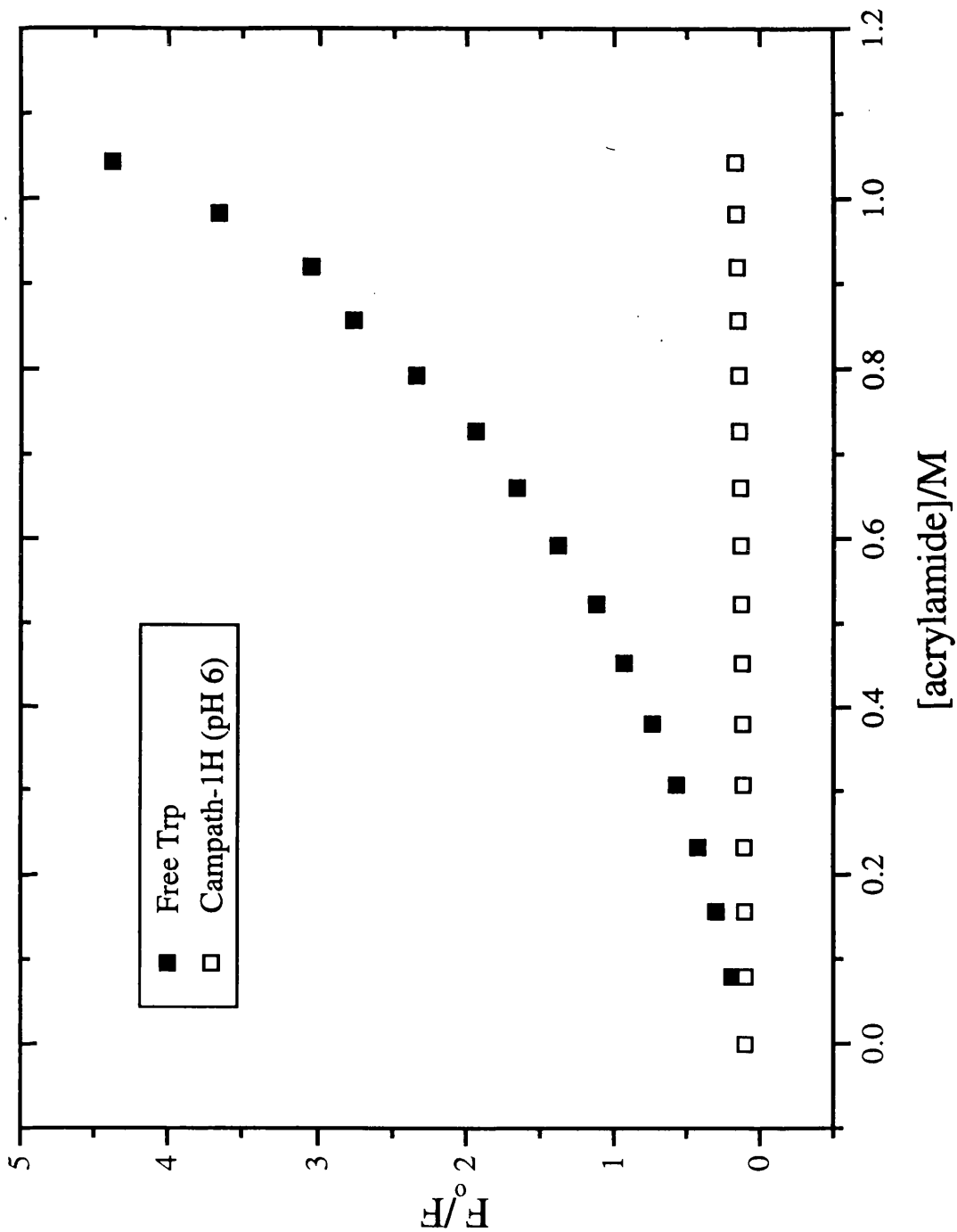


Figure 5.2a: Results of acrylamide quenching of Campath-1H (pH 6 CBS) plotted as a Stern-Volmer plot. Graph shows quenching of Campath-1H in comparison to fully exposed tryptophan and illustrates positive deviation of data obtained on quenching fully exposed tryptophan due to static quenching. All data recorded at 25 °C and using excitation wavelength of 295 nm.

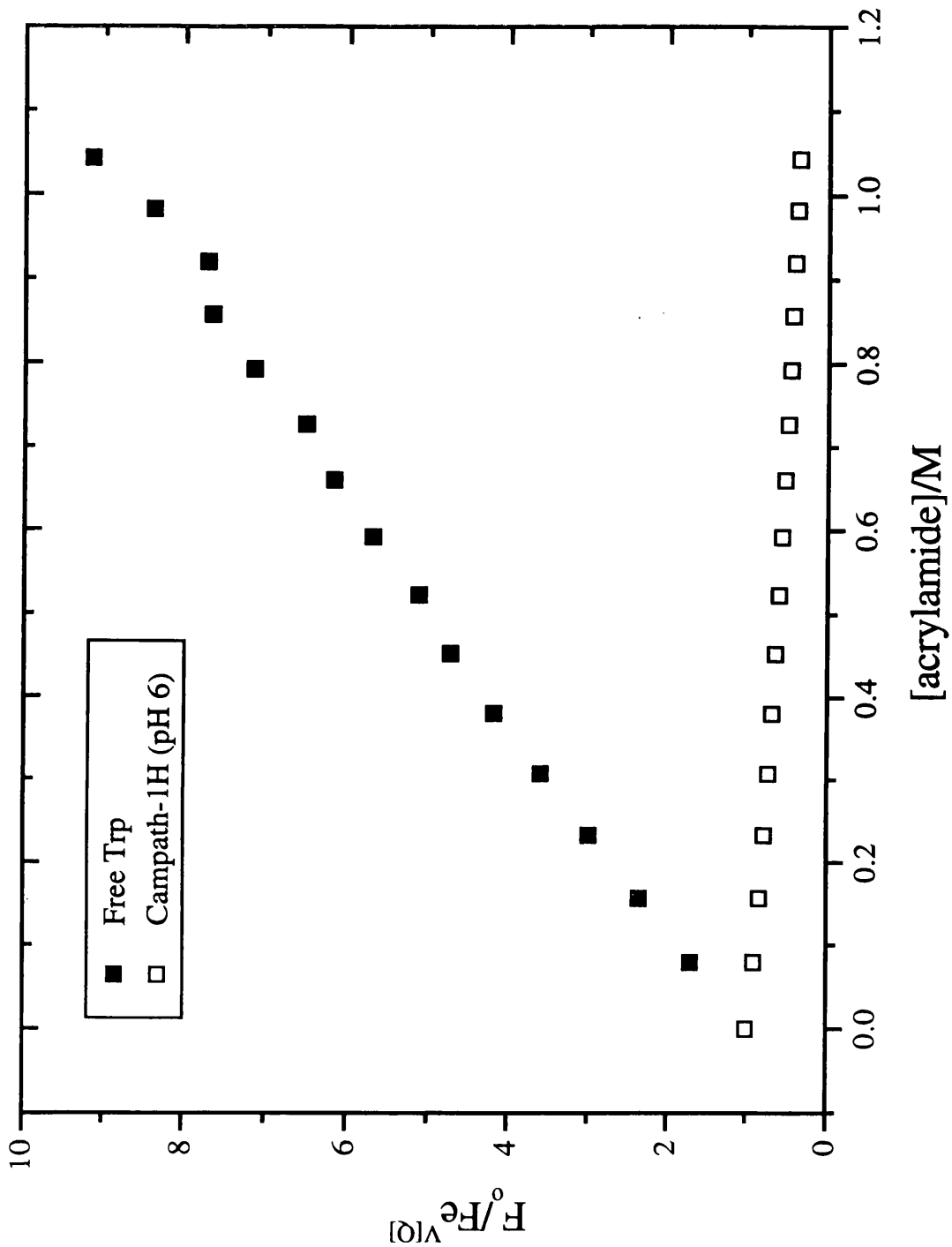


Figure 5.2b: Results of acrylamide quenching of Campath-1H (pH 6 CBS) plotted as a modified Stern-Volmer plot. Graph shows quenching of Campath-1H in comparison to fully exposed tryptophan. K_{sv} values are -0.6 ± 0.1 and $7.5 \pm 0.2 \text{ M}^{-1}$ for Campath-1H and fully exposed tryptophan respectively. All data recorded at 25°C and using excitation wavelength of 295 nm.

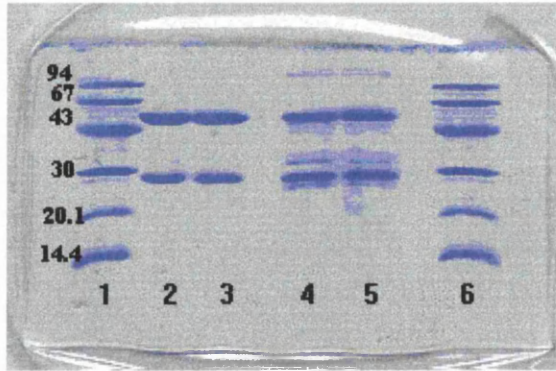


Figure 5.3: Reducing 15% SDS PAGE of equimolar amounts of **2), 3)** Campath-1H (pH 7.2 PBS) and **4), 5)** Campath-1H (pH 3 CBS). Lanes **1)** and **6)** show molecular weight standards.

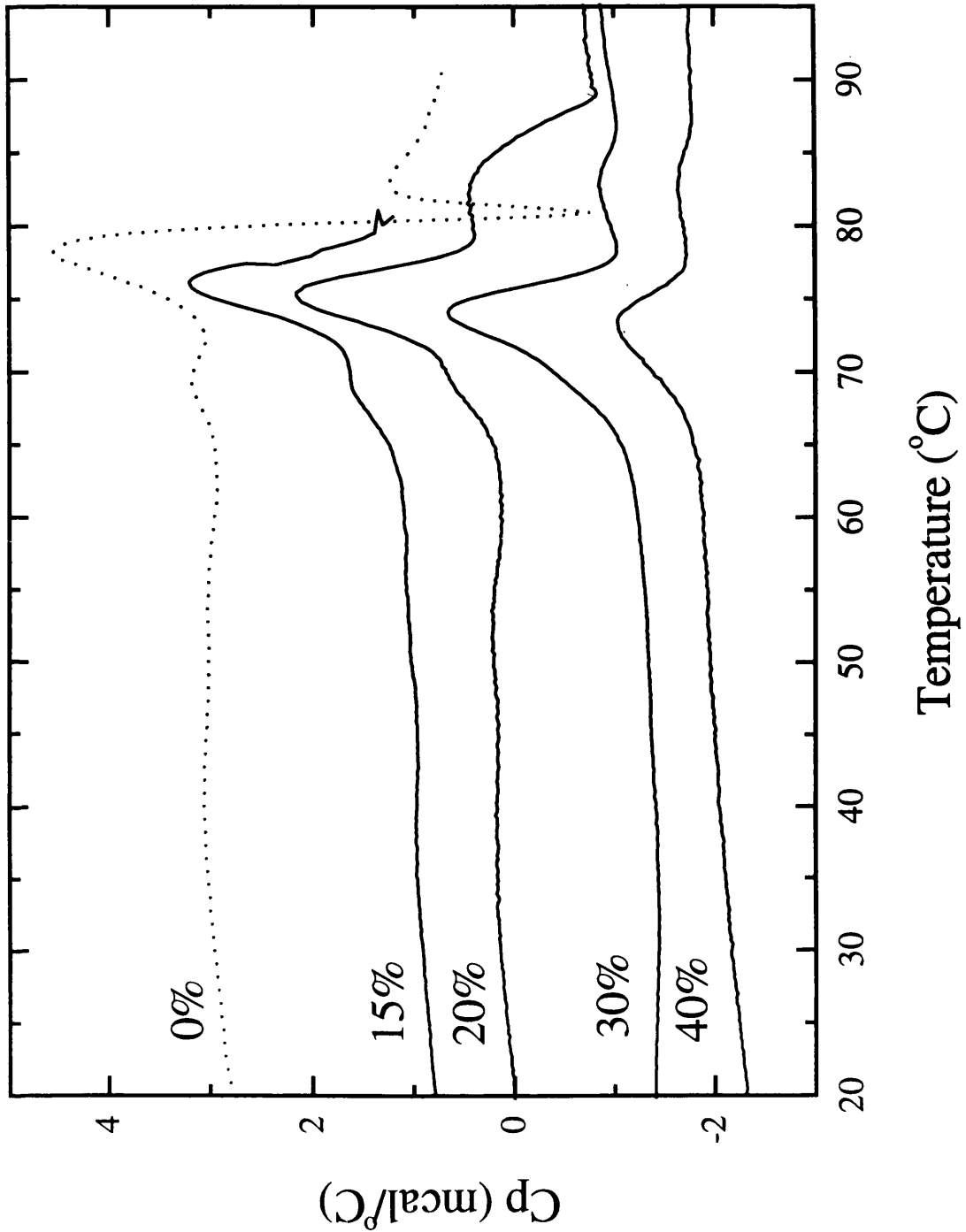


Figure 5.4: Raw DSC data showing the effects of 15, 20, 30 and 40% (w/w) HPCD on Campath-1H (0.013 mM, pH 6 CBS). Scans were performed at a nominal scan rate of 60 °C/hr, are y-offset for clarity and are shown after baseline subtraction. Graph shows 30 and 40% (w/w) HPCD results in a third endotherm and also prevents exothermic aggregation and posttransition baseline noise.

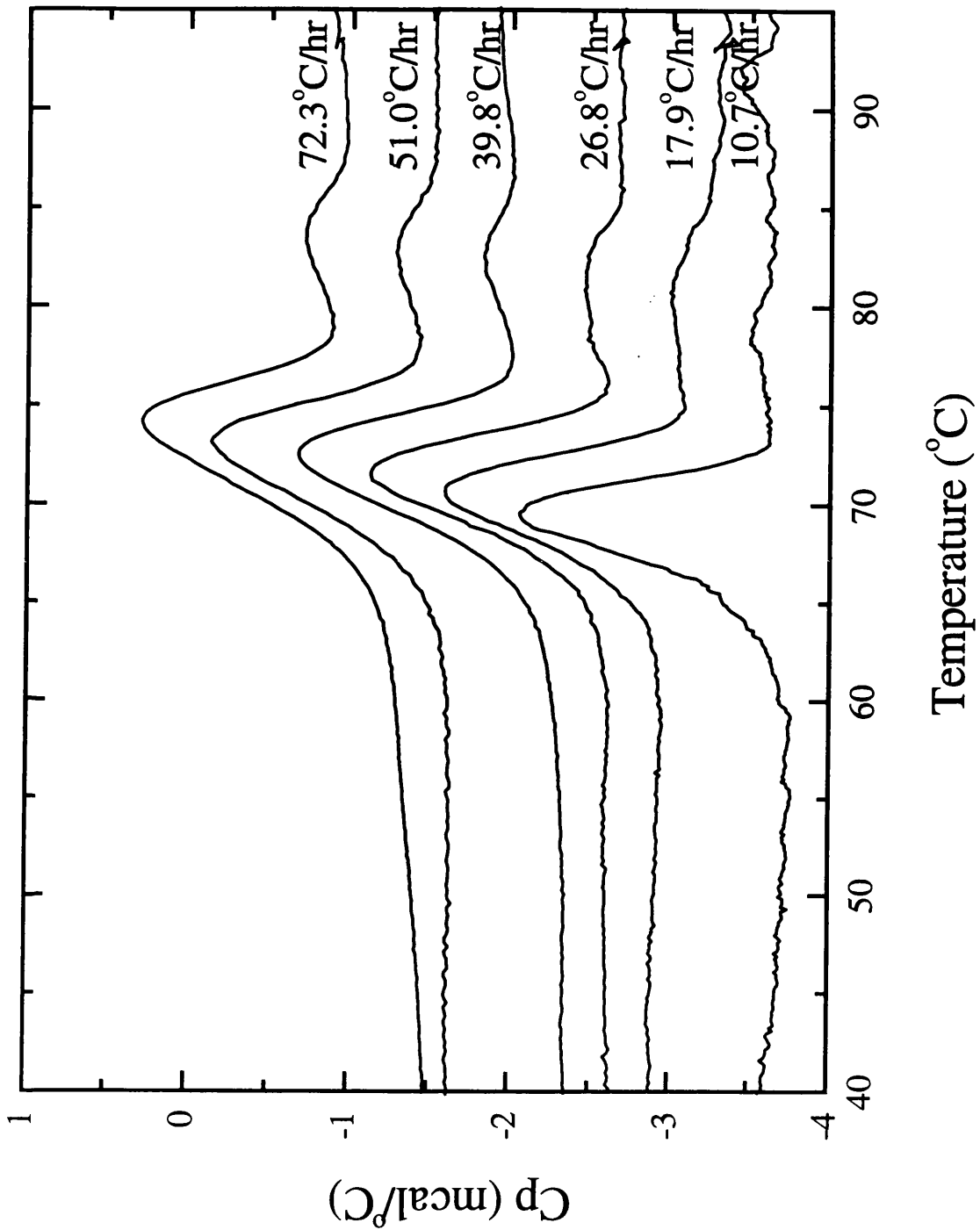


Figure 5.5: Effect of scan rate on the DSC trace of Campath-1H (0.018 mM, pH 6 CBS, 40% (w/w) HPCD). Graph shows raw data produced on scanning at six different scan rates: (a) 10.7, (b) 17.9, (c) 26.8, (d) 39.8, (e) 51.0 and (f) 72.3 $^{\circ}$ C/hr and illustrates the scan rate dependence of the T_m values of both transitions. Buffer baselines have been subtracted and scans are y-offset for clarity.

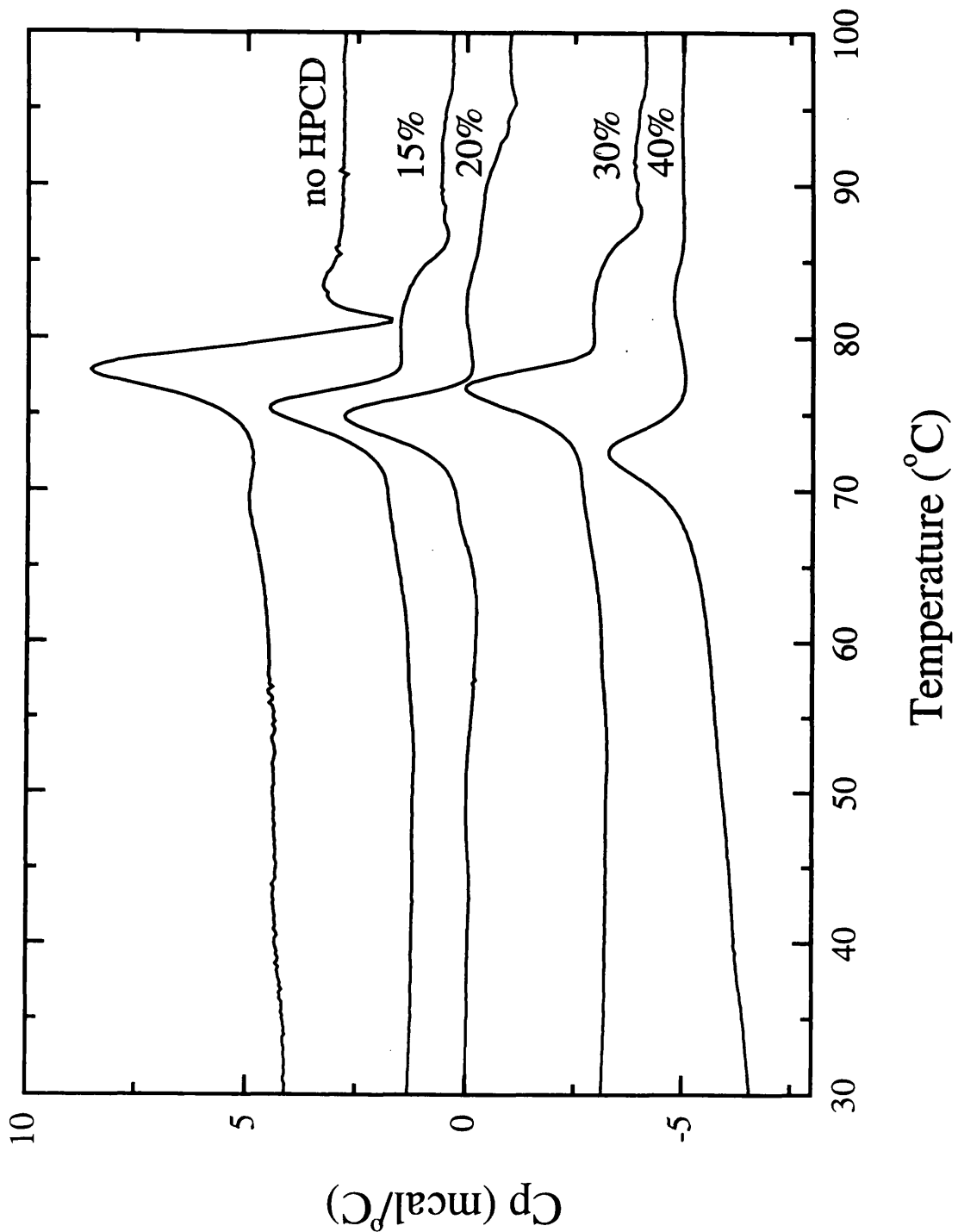


Figure 5.6: Raw DSC data showing the effects of 15, 20, 30 and 40% (w/w) HPCD on 4162W94 (0.013 mM, pH 6 CBS). Scans were performed at a nominal scan rate of 60 °C/hr, are y-offset for clarity and are shown after baseline subtraction. Graph shows 40% (w/w) HPCD results in a third endotherm and also prevents exothermic aggregation and posttransition baseline noise.

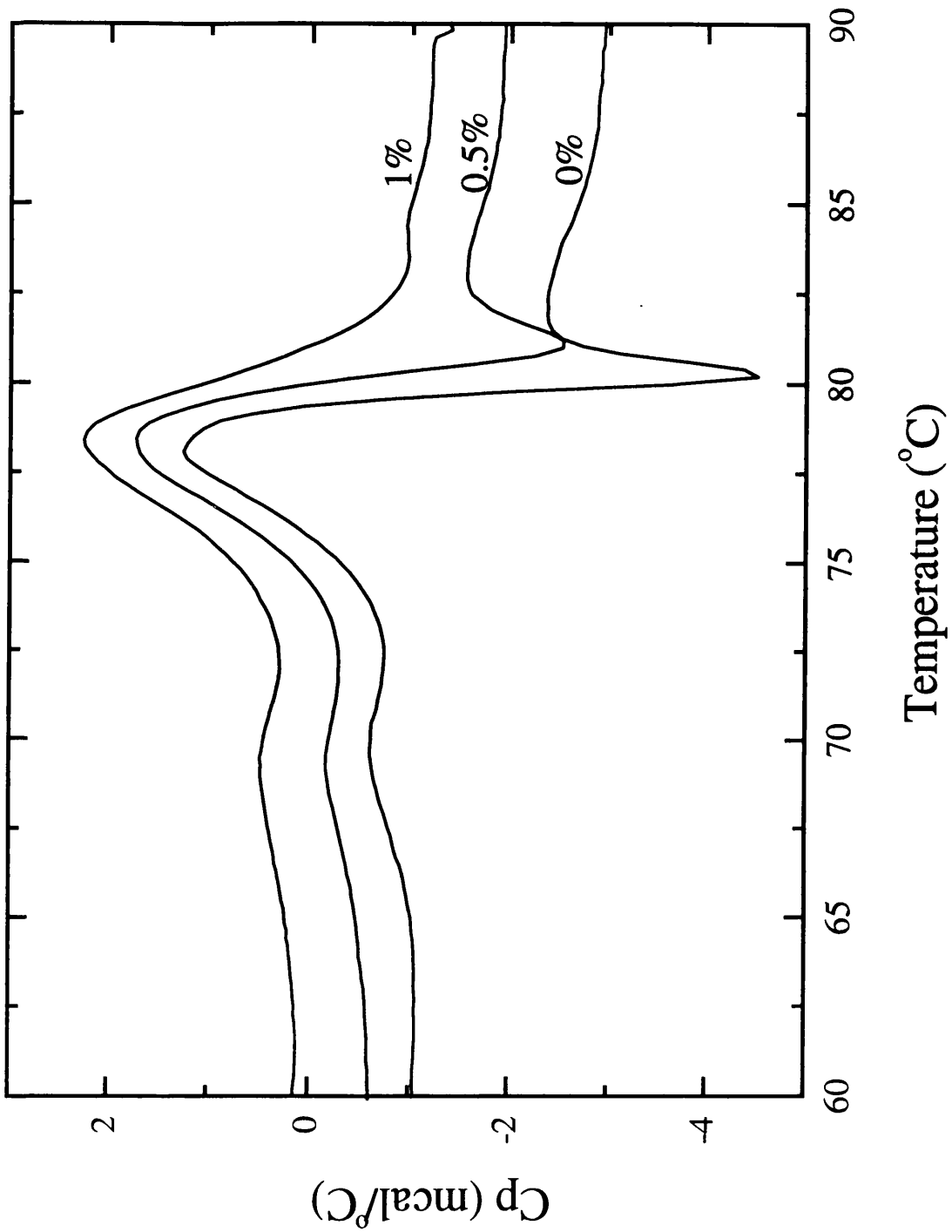


Figure 5.7a: Raw DSC data showing the effect of 0.5 and 1% (w/w) DEAE-dextran on the thermal unfolding of Campath-1H (0.0161 mM, pH6 CBS). Scans were performed at a nominal scan rate of 60 °C/hr, buffer baselines have been subtracted and data are y-offset for clarity.

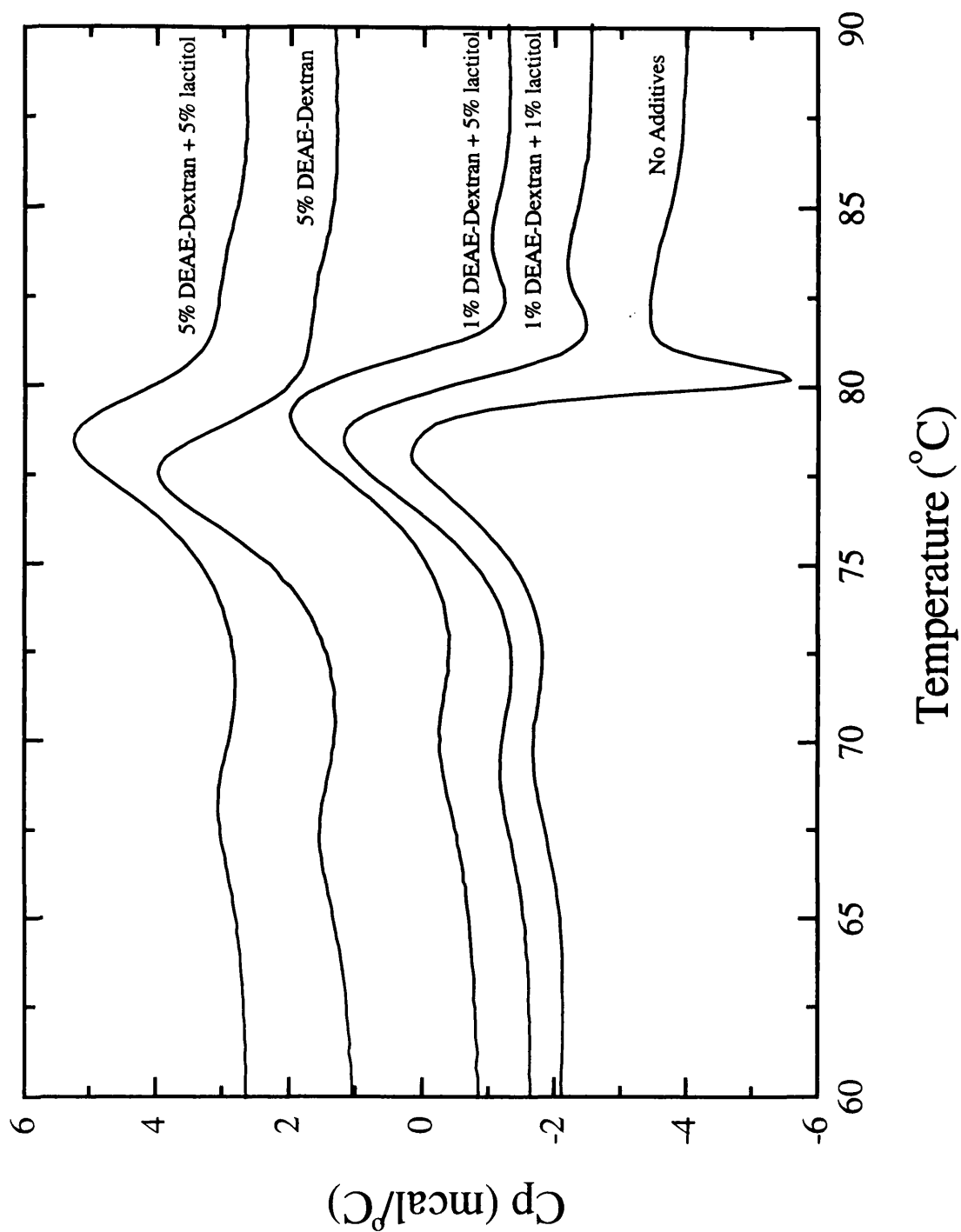


Figure 5.7b: Raw DSC data showing the effect of combinations of DEAE-dextran and lactitol on the thermal unfolding of Campath-1H (0.0196 mM, pH6 CBS). All quantities are % (w/w). Scans were performed at a nominal scan rate of 60 °C/hr, buffer baselines have been subtracted and data are y-offset for clarity.

CHAPTER 6

INDUCTION AND KINETICS OF mAb AGGREGATION

6.1 Introduction

During the formulation development of Campath-1H by Glaxo Wellcome, the formation of 'discrete macroscopic particles' in the protein solution was observed (Wellcome Company Document No: GA/LJ/027, private communication). These particles were of protein origin and it was suspected that they were either aggregates formed by denaturation of the mAb at the liquid/air interface, or some form of aggregates of Ig proteolysis fragments. Insoluble protein deposits are known to form from Ig fragments of proteolysis under acidic conditions (Glenner et al., 1971). Irrespective of the source, these fragments caused concern with respect to the long-term solution stability of the drug.

When considering the apparent spontaneous formation of macroscopic structures from solutions of Campath-1H, one can draw analogies with the formation of amyloid deposits in the various amyloidogenic disease states e.g. Alzheimer's and scrapie. Recent reports in the literature have shown that protein molecules in a particular conformational state, which is not necessarily the native one, are able to stimulate or catalyse a similar conformational transition *in vitro* (Paushkin et al., 1997). These and similar experiments with prion peptides (Kaneko et al., 1997) also indicate a possible mechanism for this conformational autocatalysis. Expansion of this theory allows for the possibility that other proteins including Campath-1H may be induced to aggregate by the addition of 'catalytic' amounts of preformed aggregate by a classic nucleation/growth mechanism (Harper and Lansbury, 1997) whereby the rate-limiting step is the initial formation of a nucleus or cluster of aggregated protein upon which subsequent growth may proceed more readily by accretion. If this is true, the rate of aggregation would increase rapidly (and non-linearly) with concentration of the unfolded protein, and, could be 'seeded' by the addition of preformed aggregates.

Despite sterile filtering of solutions of Campath-1H, denatured protein can still form at liquid/glass and liquid/air interfaces (MacRitchie, 1978). If these denatured states aggregate (it has been shown in Chapter 3 that with Campath-1H, at physiological pH, thermal denaturation coincides with thermal aggregation) they may catalyse the formation of further aggregate. Attempts to test this theory using DSC in a similar fashion to those experiments described in Chapter 4 wherein kinetic parameters were derived from DSC thermograms in accordance with the methods described by Sánchez-Ruiz et al., (1988a) were

carried out as, in the case of autocatalysis, changes in the activation energies and the rate constants for the unfolding process on adding preformed aggregate would be expected and even if the preformed aggregate was not acting as a true catalyst but was still affecting the rate of formation of subsequent aggregates, a change in the rate constant would be expected. Other methods of measuring the rate of aggregation of Campath-1H described in this chapter involve the UV/visible spectrophotometry to measure protein concentration within solutions and to measure the turbidity of protein solutions both in the presence and absence of preformed aggregate.

6.2 Results

6.2.1 Turbidity Experiments

Experiments involving the measurement of the protein concentrations of the supernatants from samples of Campath-1H seeded with preformed aggregate and then incubated at elevated temperatures were carried out over extended periods of time (typically nine days). Results from these experiments were inconsistent and irreproducible, probably due to variations in incubation temperatures caused by the removal of samples from the waterbath for UV analysis and therefore the results are not presented in this thesis. Alternatively, this may reflect the real unpredictable nature of nucleation/aggregation processes, especially in the absence of deliberate seeding. Results gained from monitoring the turbidity of Campath-1H solutions seeded with preformed aggregate were far more reproducible as these experiments were carried out over the course of some hours rather than days.

Figure 6.1a presents the data from an experiment studying the effect of the addition of 0.5 and 1% (v/v) of a dispersed solution of thermally aggregated Campath-1H (0.009 mM, pH 6 CBS), formed by heating to 85 °C in a waterbath, to samples of Campath-1H (0.009 mM, pH 6 CBS) incubated at 67 °C, on the turbidity of the samples as measured by the absorbance at 320 nm. The turbidity of each sample was recorded at regular time intervals and the data plotted as a graph of absorbance at 320 nm against time. The control experiment involved measuring the turbidity of a sample of the same solution of Campath-1H incubated under the same conditions without any added preformed aggregate. Figure 6.1b presents the data obtained by recording the absorbance of the same samples at 400 nm. The most obvious feature of both figure 6.1a and 6.1b is the long lag phase from 0 minutes to approximately 175 minutes during which time there is apparently no change in the turbidity of the solutions as measured by absorbance at either 320 or 400 nm. This feature is indicative of a nucleation/growth process as, after the lag phase, there is a steep growth period (Harper and Lansbury, 1997). It is clear that the addition of 0.5 or 1% (v/v) of preformed aggregate does not affect the rate of aggregation. These results are reproducible and repeat experiments at other temperatures between 65 and 75 °C consistently show that these low concentrations of preformed aggregate have no effect on the overall rate of thermal aggregation.

The effects of adding higher concentrations of preformed aggregate were studied using the same experimental protocol. Figures 6.2a and 6.2b show the results from experiments monitoring the effect of the addition of 5 and 10% (v/v) preformed aggregate solution on the solution turbidity as measured by solution absorbance at 320 and 400 nm respectively. Again the lag/growth phase pattern is the most obvious feature of the graphs but there is no apparent increase in the aggregation rate on addition of preformed aggregate consistent with a catalytic mechanism, in fact, there seems to be a slight reduction on aggregation rate on addition of 10% (v/v) solution of preformed aggregate.

The incubation temperature is important for the experiments described above and a range of temperatures were investigated. At 73, 74 and 75 °C, aggregation of all samples occurred within two hours and therefore not enough absorbance measurements were recorded to draw valid conclusions. At temperatures from 65-72 °C, the data were consistent with those obtained at 67 °C.

To gain a clearer insight into the effect the addition of preformed aggregate was having, experiments were attempted in which preformed aggregate was added, not at the beginning of the experiment but during the lag phase. The average duration of the lag phase was approximately 175 minutes so experiments were carried out in which small quantities (5.0, 10.0% (v/v)) of preformed aggregate were added to the samples after 70 minutes. These experiments were repeated four times and the results were inconsistent and irreproducible and therefore no data are presented. Despite the inconsistency of the data produced in these experiments, a clear lag phase was always observed when the data were plotted.

6.2.2 Effect of Preformed Aggregate on the Kinetics of Thermal Unfolding

Using the method developed by Sánchez-Ruiz et al., (1988a), as described in section 2.2.3, equations 2.16 and 2.18 were used to calculate the activation energy for the main thermal unfolding transition of Campath-1H (0.018 mM, pH 4 ABS) in the presence and absence of 1.6% (v/v) solution of dispersed preformed Campath-1H aggregate (0.018 mM, pH 4 ABS). Equations 2.15 and 2.17 were not used for these calculations as they require data collected at a range of scan rates to produce valid activation energies (see section 2.2.3). The DSC scans were performed at 10 °C/hr, the slowest rate that the machine can perform in

the hope that it would give any nucleation reaction time to proceed and also, under these pH conditions, distortion of the DSC thermograms by gross aggregation of the sample does not occur. Only a small volume of preformed aggregate was added for two reasons: firstly if autocatalysis is occurring then only a catalytic amount of preformed aggregate would be needed to 'seed' the reaction and secondly, the presence of large amounts of insoluble aggregates in the DSC cell can lead to noisy posttransition baselines as a consequence of erratic convection effects of these aggregates. The results are presented in table 6.1. The calculated activation energies are $441.0 \pm 10\%$ and $434.1 \pm 9\%$ kJ mol^{-1} in the absence and presence of preformed aggregate, respectively. These values and the value of 439 kJ mol^{-1} presented in table 4.7 (average E_A for Campath-1H (pH 4), 2nd transition as calculated using equations 2.15-2.18) reveal that there is no apparent change in E_A when catalytic amounts of preformed aggregate are present. The reduction of activation energy is not a criterion for autocatalysis but what is necessary for this process is an increase in the rate of aggregation in the presence of preformed aggregate.

Experiments carried out on solutions of Campath-1H (pH 5) in both the presence and absence of a range of concentrations of preformed aggregate (0.6, 1.0, 1.4, and 2.0% (v/v)) allowed the calculation of rate constants using equation 2.15. Again data was collected at a scan rate of $10 \text{ }^\circ\text{C/hr}$ to maximise conditions for any nucleation reaction which may take place. Figure 6.3 shows the data plotted as a graph of rate constant, k , against temperature for each of the preformed aggregate concentrations analysed. The control sample was an identical solution of Campath-1H without any added preformed aggregate. Figure 6.3 clearly shows the linear relationship between the rate constant, k , and temperature, T , and it is also clear from the graph that the addition of preformed aggregate has no significant effect on the rate of thermal denaturation.

6.3 Discussion

The experiments described in this chapter were conceived and executed in the hope that the aggregation of Campath-1H would be shown to proceed via a nucleation growth mechanism whereby a solution of Campath-1H could be induced to aggregate by the addition of a 'seed' of preformed aggregate. This seed would allow further aggregation by accretion. In fact, all experimental evidence obtained suggests that the addition of preformed aggregate has no effect whatsoever on the rate of Campath-1H aggregation. The investigation comprised a two-pronged approach: firstly solutions of Campath-1H were incubated with varying amounts of preformed aggregate and any change in the turbidity of the solutions monitored by UV-visible spectrophotometry, and secondly, the effect of adding preformed aggregate on the kinetics of the irreversible thermal denaturation of Campath-1H was studied.

By monitoring the turbidity of seeded and non-seeded Campath-1H solutions, aggregation profiles were produced which were representative of a classic nucleation/growth process in that the profiles consisted of a lag phase followed by a steep growth curve (Harper and Lansbury, 1997). The effect of adding a range of quantities of preformed aggregate and a range of incubation temperatures was studied and each experiment resulted in a reproducible lag/growth phase curve although there was no significant difference in the curves produced in the presence of aggregate when compared to the controls. In the hope that the addition of seed during the lag phase would induce a clear growth effect, aggregate was indeed added during the lag phase but no significant effect was observed suggesting that either the nucleation growth process was unaffected by preformed aggregate or the experimental set up was not suitable for studying such a system. The lag phase clearly supports a nucleation/growth mechanism- so why does preformed aggregate not act as a seed for the process? One explanation could be that the preformed aggregate undergoes some other change after formation that prevents it nucleating further aggregation or alternatively aggregate formed by thermal unfolding of protein is unsuitable as a seed.

The results of experiments monitoring the effect of preformed aggregate on the values of the kinetic parameters of the irreversible thermal denaturation of Campath-1H derived using the method developed by Sánchez-Ruiz, et al., (1988a) are more conclusive. The results show that the addition of preformed aggregate affects neither the activation energy nor the rate constants of thermal denaturation under the conditions studied. If aggregation was

Chapter 6

proceeding via a nucleation/growth mechanism one would expect to observe a significant increase in the rate of the aggregation process which would be indicated by an increase in the reaction rate.

mAb (pH)	E_A /kJ mol ⁻¹ Eq. 2.16	E_A /kJ mol ⁻¹ Eq. 2.18	Average E_A /kJ mol ⁻¹
Campath-1H (pH 4), 2 nd transition.	457 ±9%	425 ±11%	441 ±10%
Campath-1H (pH 4), 2 nd transition + 1.6% (v/v) preformed aggregate.	451 ±10%	417 ±8%	434 ±9%

Table 6.1: Activation energies (E_A) calculated using equations 2.16 and 2.18 for Campath-1H (pH 4) in the presence and absence of 1.6% (v/v) solution of preformed Campath-1H aggregate.

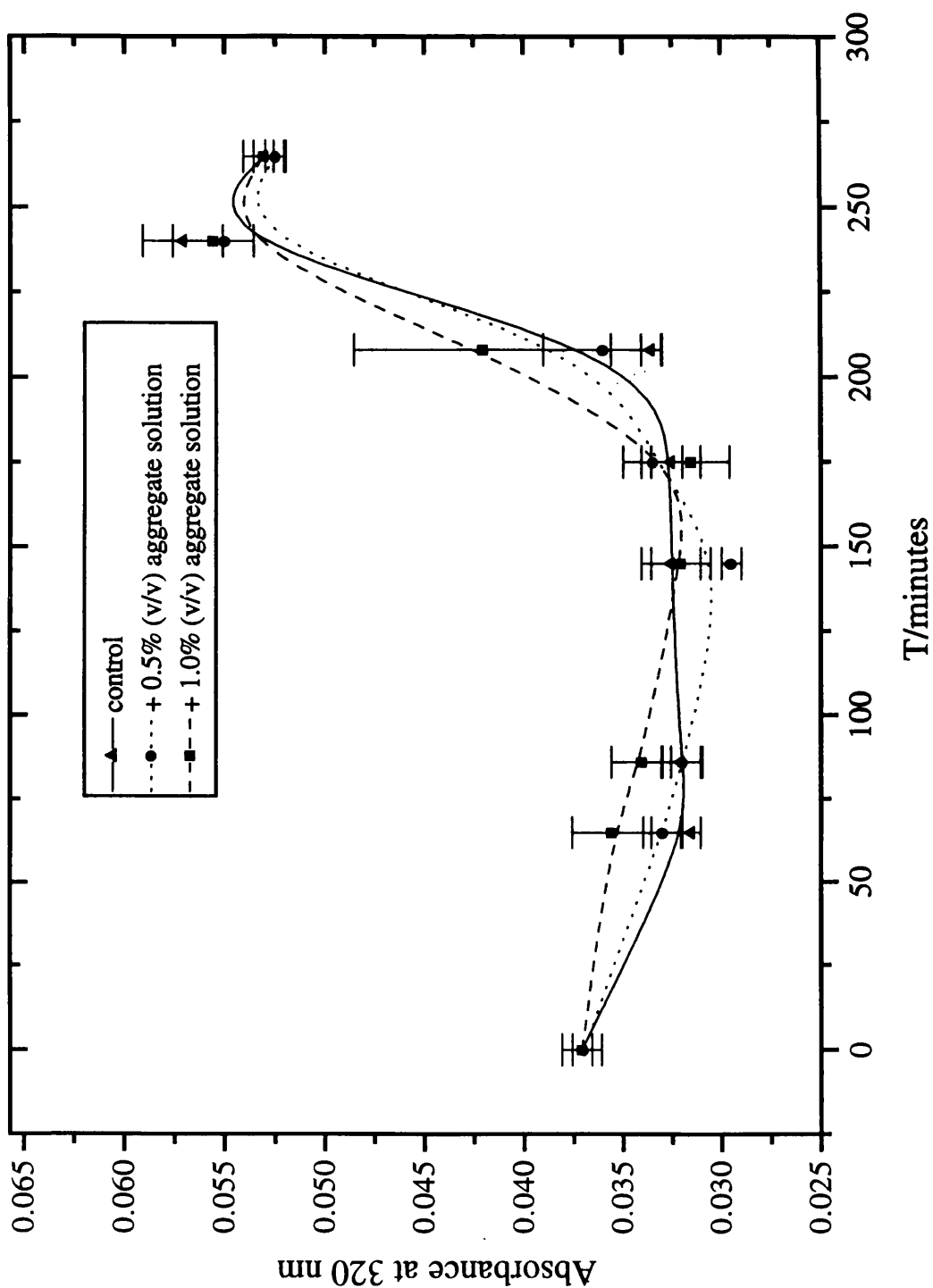


Figure 6.1a: Graph showing the effect on solution turbidity of the addition of 0.5 and 1.0% (v/v) Campath-1H aggregate solution (0.009 mM, pH 6 CBS) to samples of Campath-1H (0.009 mM, pH 6 CBS) incubated at 67 °C, with time. Solution turbidity is measured as the absorbance at 320 nm. Control samples were samples of the same Campath-1H solution incubated under identical conditions without any preformed aggregate added.

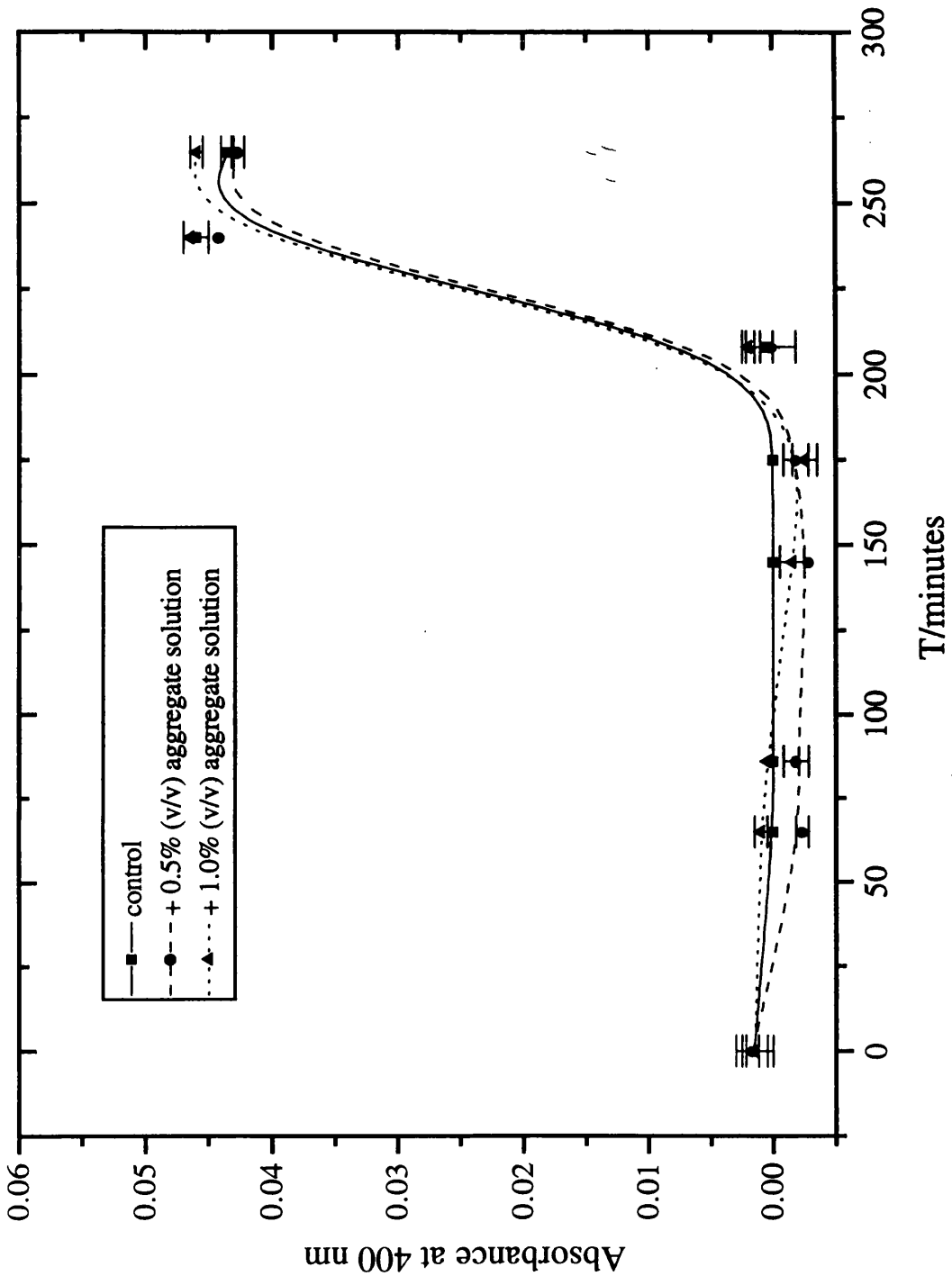


Figure 6.1b: Graph showing the effect on solution turbidity of the addition of 0.5 and 1.0% (v/v) Campath-1H aggregate solution (0.009 mM, pH 6 CBS) to samples of Campath-1H (0.009 mM, pH 6 CBS) incubated at 67 °C, with time. Solution turbidity is measured as the absorbance at 400 nm. Control samples were samples of the same Campath-1H solution incubated under identical conditions without any preformed aggregate added.

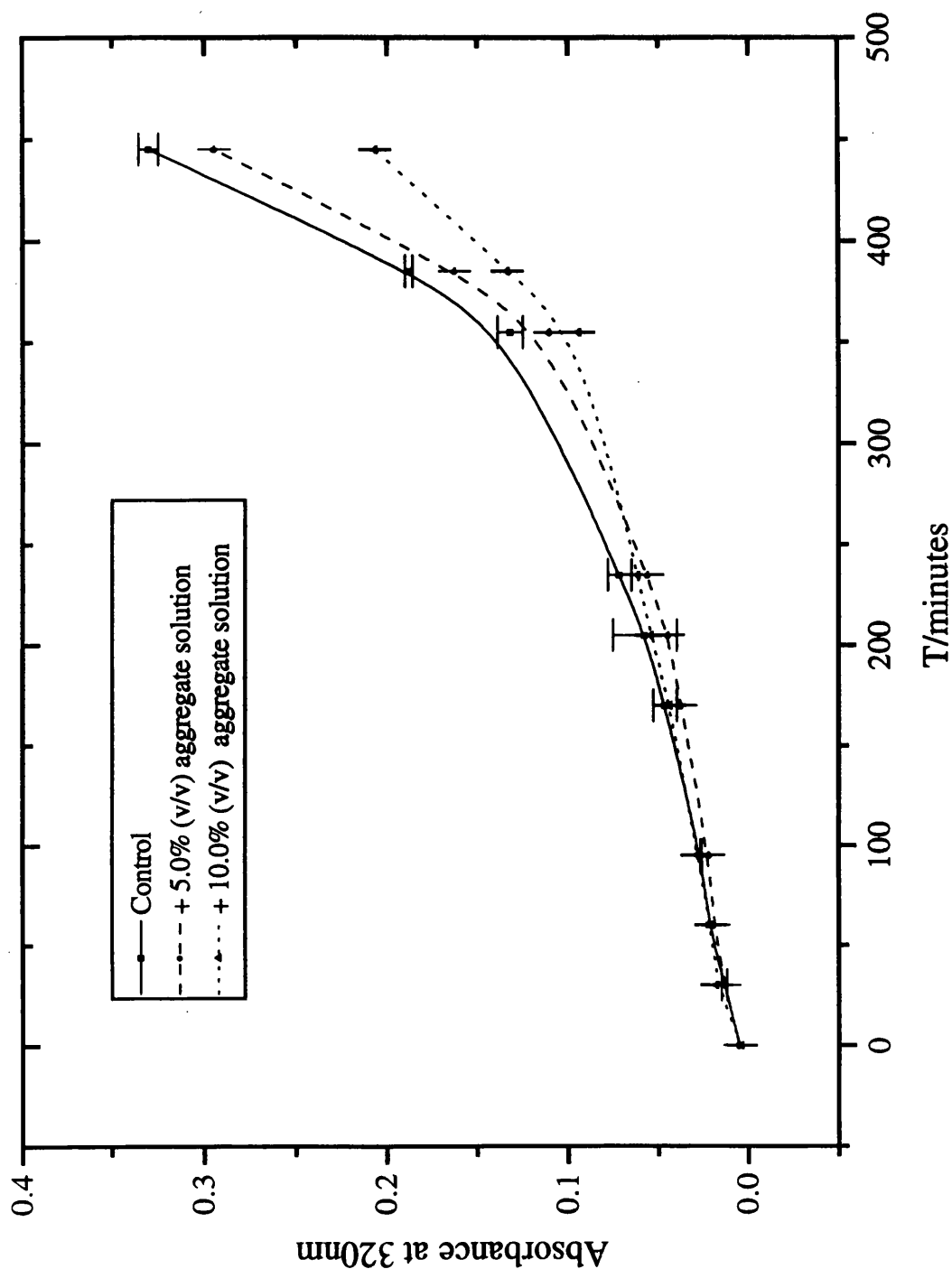


Figure 6.2a: Graph showing the effect on solution turbidity of the addition of 5.0 and 10.0% (v/v) Campath-1H aggregate solution (0.009 mM, pH 6 CBS) to samples of Campath-1H (0.009 mM, pH 6 CBS) incubated at 67 °C, with time. Solution turbidity is measured as the absorbance at 320 nm. Control samples were samples of the same Campath-1H solution incubated under identical conditions without any preformed aggregate added.

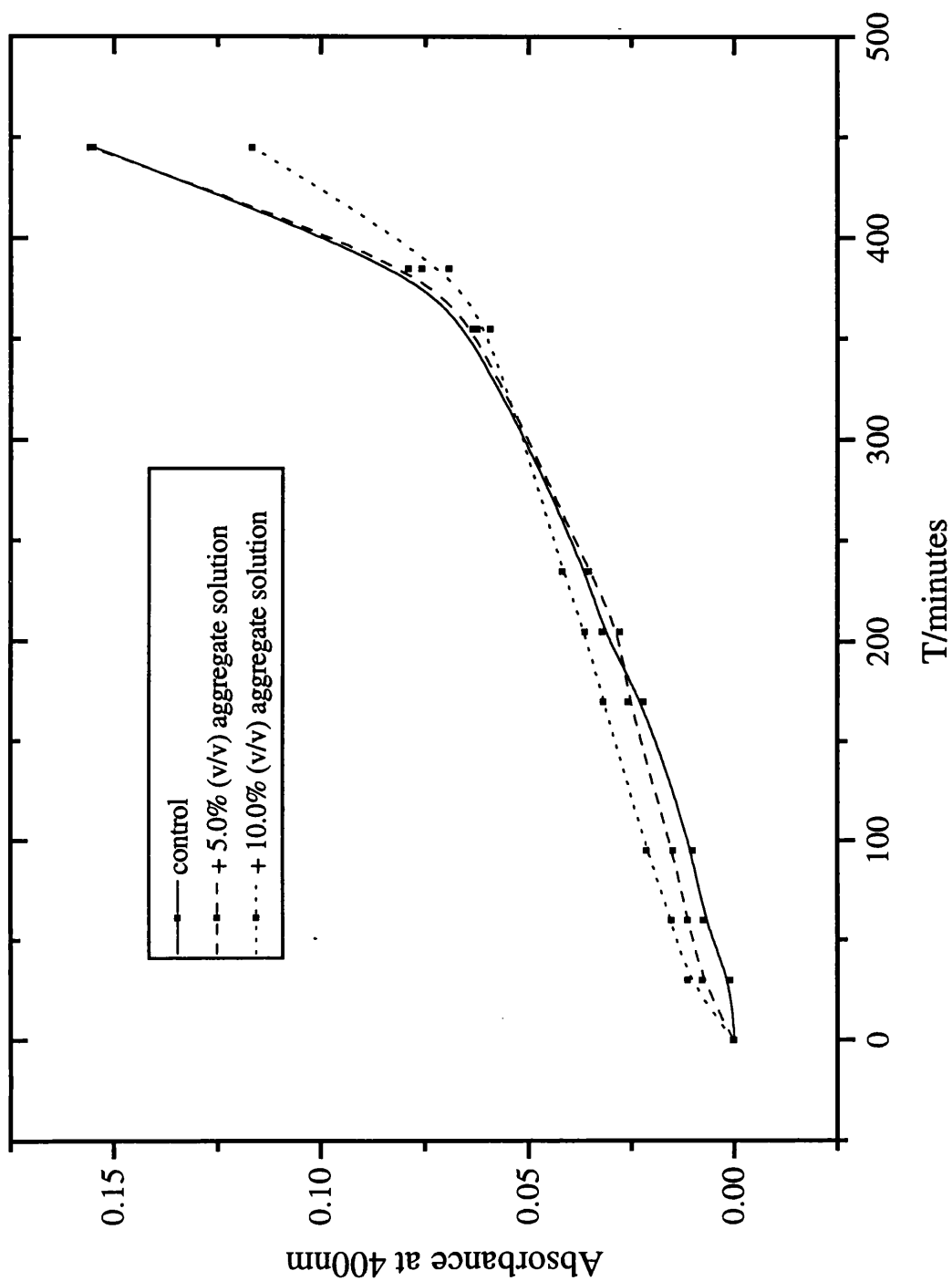


Figure 6.2b: Graph showing the effect on solution turbidity of the addition of 5.0 and 10.0% (v/v) Campath-1H aggregate solution (0.009 mM, pH 6 CBS) to samples of Campath-1H (0.009 mM, pH 6 CBS) incubated at 67 °C, with time. Solution turbidity is measured as the absorbance at 400 nm. Control samples were samples of the same Campath-1H solution incubated under identical conditions without any preformed aggregate added.

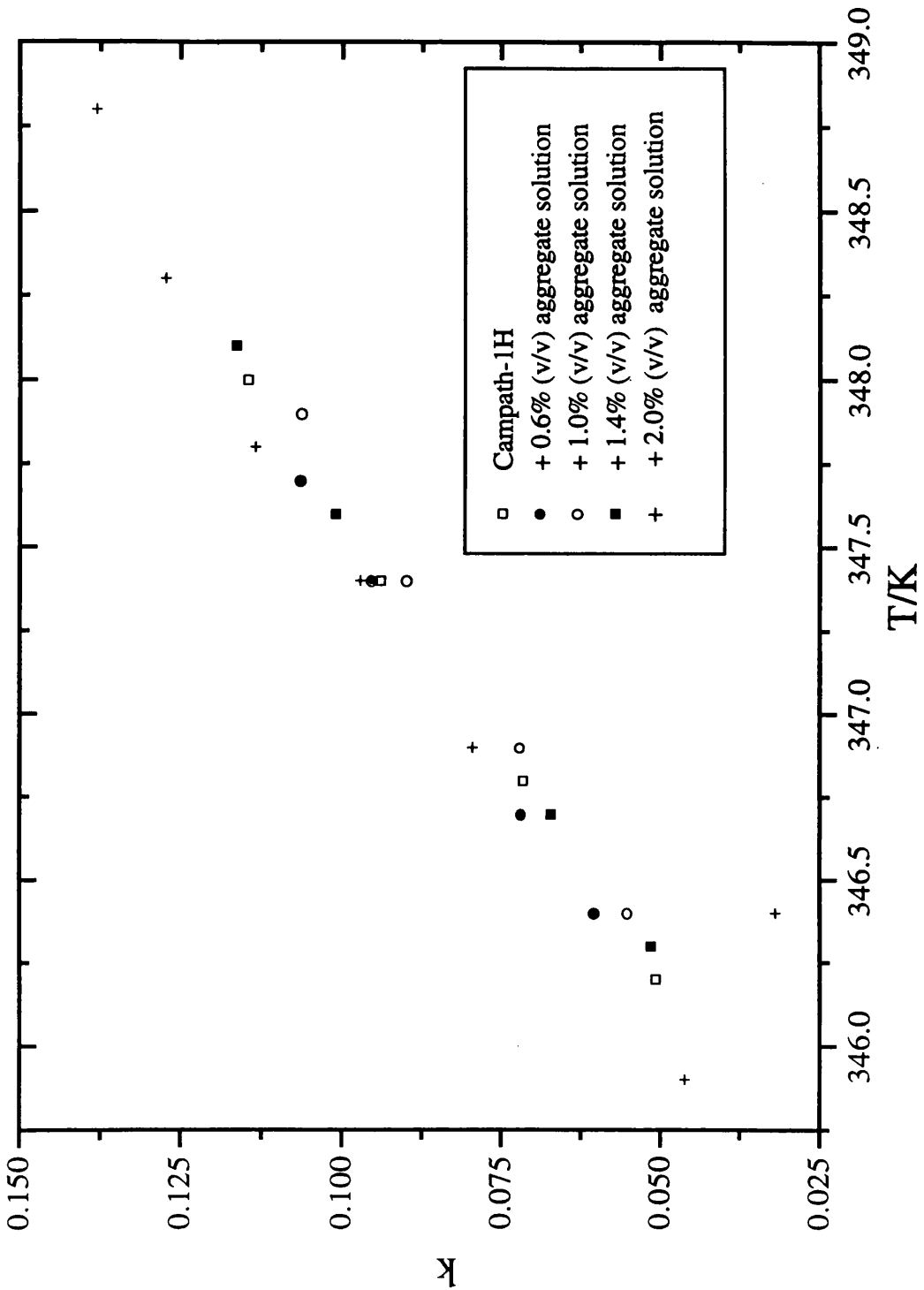


Figure 6.3: Graph of rate constants, k , calculated using equation 2.15, plotted against temperature, T , for the thermal denaturation of Campath-1H (pH 5 CBS) in the presence of 0.6, 1.0, 1.4, and 2.0% (v/v) solution of preformed Campath-1H aggregate. The control experiment was a sample of Campath-1H (pH 5 CBS) without any preformed aggregate added. DSC data were collected at a scan rate of 10 °C/hr.

CHAPTER 7

FURTHER OBSERVATIONS

7.1 Introduction

This chapter contains data relevant to the stability of mAbs which were the result of experiments which, due to time constraints, were not taken to their natural conclusion and therefore do not justify a unique chapter to themselves. The experiments were designed to investigate two broad areas of mAb stability: firstly the effect of low concentrations of denaturants such as urea and guanidine hydrochloride (GdmHCl) on their behaviour and secondly the usefulness of isothermal calorimetry for studying mAb thermal denaturation. A brief introduction to the reasoning behind these areas of study follows.

7.1.1 The Effects of Low Concentrations of Denaturants

Monitoring changes in protein structure with fluorescence spectroscopy and/or CD as a function of denaturant concentration is a common method of measuring the folding stability of the protein (Wong and Tanford, 1973; Vuilleumier, et al., 1993; Kelly and Price, 1997; Freskgård, et al., 1998). This technique can also be applied to investigate the existence of folding intermediates if the unfolding curves as monitored by fluorescence spectroscopy and CD are noncoincident (Matthews and Crisanti, 1981; Van Mierlo et al., 1998). Contained in this chapter are the results of such unfolding experiments for Campath-1H, 4162W94 and 1209W95 and some preliminary conclusions are drawn.

7.1.2 Isothermal Calorimetry

While DSC measures the heat uptake of a sample over a specified temperature range, isothermal calorimetry measures the heat uptake over a specified time period at a constant temperature and in the past has been used mainly to measure the kinetics of the decomposition of traditional organic drug molecules (Hansen, et al., 1989; Angberg et al., 1993). DSC is by far the most common method of measuring thermal denaturation of proteins, but, as discussed in chapter 4, the thermodynamic analysis of DSC curves relies on the assumption that equilibrium exists throughout the temperature-induced unfolding process (Privalov and Khechinashvili, 1974) and when used to study irreversible processes DSC data cannot be analysed in terms of equilibrium thermodynamics; only kinetic data can be obtained (Lepock, et al., 1992; Sánchez-Ruiz, 1992). Accurate kinetic data can be obtained from DSC traces if the DSC signal is split up into the separate contributions of the denaturation and aggregation

processes (Sandu and Singh, 1990) but most DSC instruments do not have the ability to scan at slow enough rates to achieve this separation and frequently only one peak is observed with very little fine structure. Also, at temperatures below the T_m , the processes involved in protein denaturation and aggregation will take place on a much larger timescale than a DSC experiment making the calculation of accurate kinetic parameters difficult.

True isothermal calorimetry can be helpful in these situations as, since the heat uptake of a sample is measured at a fixed temperature, one fewer variable is introduced into any subsequent analysis (Waters and Paddy, 1988). Because of the need for extremely sensitive instrumentation, especially when the sample being studied is a protein, very little published work is available, however Hoffmann et al., (1997) have studied the denaturation and aggregation of β -lactoglobulin using isothermal calorimetry utilising a denaturation and aggregation model derived by Roefs and de Kruif (1994). In an attempt to use this method of calorimetry to gain a better understanding of the processes involved in mAb denaturation and aggregation, preliminary experiments with Campath-1H were carried out and the results presented in this chapter.

7.2 Results

7.2.1 Unfolding with Denaturants

All three mAbs: Campath-1H (pH 6 citrate), 4162W94 (pH 6 citrate) and 1209W95 (pH 8 Tris) were unfolded using GdmHCl from 0-6 M and monitored by CD (ellipticity at 210 nm) and fluorescence spectroscopy (emission at 360 nm). The CD results are shown in figure 7.1 plotted as the percentage change in ellipticity at 210 nm versus GdmHCl concentration. The midpoint of the unfolding curves are 2.5, 3.0 and 1.9 M GdmHCl for Campath-1H, 4162W94 and 1209W95 respectively. It is interesting that 1209W95 which is the least thermally stable of the three mAbs is also the least chemically stable in addition to having the most accessible tryptophan residues as shown by succinimide quenching. Figure 7.2 presents the data from the GdmHCl unfolding as monitored by fluorescence spectroscopy. The data are plotted as fluorescence intensity at 360 nm versus GdmHCl concentration and the midpoints of these unfolding curves are 3.5, 2.8 and 2.6 M GdmHCl for Campath-1H, 4162W94 and 1209W95 respectively. 1209W95 is unique in this respect as it does not follow a classical unfolding curve in that significant structural changes occur even at the lowest concentrations of GdmHCl. It is clear from the midpoints of the unfolding curves that all three mAbs unfolding curves as determined from CD are noncoincident with those obtained by fluorescence measurements which suggests the chemical unfolding is a multistate process which is consistent with the conclusions drawn from DSC experiments concerning the thermal unfolding as discussed in chapter 4.

During these experiments it was noticed that the fluorescence intensity (at 360 nm) of Campath-1H significantly decreased on going from 0-2.5 M GdmHCl due to a blue shift of the emission spectrum which is indicative of the tryptophan residues within the molecule becoming less exposed to the solvent. This would seem to suggest that the molecule is becoming more tightly packed and rigid- the opposite of what one expects during chemical denaturation. This apparent reduction in protein mobility has been reported within crystalline proteins with bound denaturant at low (<1 M) concentrations where the decrease in mobility is detected as a decrease in the temperature factor (B-factor) of the protein crystals (Dunbar, et al., 1997). To probe the accessibility of the tryptophan residues at these low GdmHCl concentrations, succinimide quenching experiments were carried out and results, presented as Stern-Volmer plots, are given in figure 7.3. K_{sv} for Campath-1H in the presence of 0.5 M

GdmHCl is $0.98 \pm 0.03 \text{ M}^{-1}$ compared to $1.20 \pm 0.08 \text{ M}^{-1}$ at 0 M GdmHCl. These K_{sv} values support the hypothesis that the molecule does indeed become more rigid and tightly packed in the presence of low GdmHCl concentrations and the implications of this finding will be discussed later. DSC experiments were carried out to study whether 0.5 M GdmHCl affected the T_m of Campath-1H (pH 6) and a reduction to $70.3 \text{ }^\circ\text{C}$ from $78.2 \text{ }^\circ\text{C}$ was observed for the main transition and the sample had aggregated when removed from the cell.

DSC experiments were carried out to investigate whether low concentrations of urea, a weaker denaturant than GdmHCl, had any effect on the thermal unfolding of Campath-1H. Some of the data produced is presented in figure 7.4. This figure presents the raw DSC data obtained on scanning Campath-1H (0.0201 mM, pH 6 CBS) and Campath-1H (0.0201 mM, pH 6 CBS, 0.5 M urea). The baseline scans have been subtracted and scans are y-offset for clarity. The presence of the urea increases the T_m of the main unfolding transition by $11 \text{ }^\circ\text{C}$ and also the ΔH_{cal} for the transition is also greatly increased (data could not be fitted using Origin software and therefore values for ΔH_{cal} are not reported). Successive scanning in the presence of 0.5 M reveals a degree of reversibility and sees both the T_m and ΔH_{cal} decrease. Gross aggregation of the sample is also prevented. To probe whether 0.5 M urea disrupts the structure of Campath-1H, the urea unfolding curve was recorded using CD and the results, plotted as the percentage change in ellipticity at 210 nm as a function of urea concentration, are presented in figure 7.5. The urea unfolding curve has its midpoint at 6.8 M urea. From figure 7.5 it is clear that 0.5 M urea has no apparent effect on the structure of the antibody.

7.2.1 Isothermal Calorimetry

The results of preliminary isothermal calorimetry experiments using Campath-1H are presented in this chapter. Once temperature and concentration trials were performed data were collected revealing the high quality of data that can be obtained and both the temperature and concentration dependence of the traces. Figure 7.6 presents the raw data from isothermal measurements of Campath-1H (0.1054 mM, pH 6 CBS) performed at 67.5, 68.5, 69.5, 70.5 $^\circ\text{C}$. This temperature range was chosen as it is below the T_m of the main transition as defined by DSC, and therefore the sample would not aggregate immediately, and data could be collected. It is also a temperature range where unfolding reaction would be occurring on a reasonable timescale for data collection. The data reveal obvious temperature dependence of

the scans. Figure 7.7 comprises the raw isothermal data collected from scans carried out at 70.5 °C on Campath-1H (pH 6 CBS) at 0.023, 0.412, 0.054, 0.063 and 0.1054 mM concentrations. The concentration dependence of the traces is evident. These data were then normalized and the data presented in figure 7.8 and again the concentration dependence of the traces is evident. Figures 7.6-7.8 show how, when held at constant temperature close to the unfolding transitions, heat uptake is observed. This heat uptake gradually decays over a period of time, presumably as all the protein in the cell irreversibly unfolds.

7.3 Discussion

By monitoring the unfolding behaviour of Campath-1H, 4162W94 and 1209W95 in increasing concentrations of GdmHCl, using both CD and intrinsic tryptophan fluorescence spectroscopy, we can draw two conclusions. Firstly, both techniques reveal that the least chemically stable antibody is 1209W95 which is also the least thermally stable ($T_m = 61.3 \pm 0.1$ °C at pH 8) and also the antibody with the highest Stern-Volmer constant ($K_{sv} = 3.9 \pm 0.2$ M⁻¹). This is probably due to the fact that 1209W95 is an antibody-TMT conjugate and the TMT moiety may cause a disruption in the antibody structure which makes the molecule less tightly packed than either Campath-1H or 4162W94 and therefore the thermal stability is decreased and also the tryptophan residues within the molecule will be more accessible to solvent and hence the large K_{sv} value. The second conclusion is drawn from the fact that the Campath-1H and 1209W95 unfolding curves, as monitored by CD and by fluorescence spectroscopy are noncoincident, and therefore the unfolding of these two mAbs involves folding intermediates (Matthews and Crisanti, 1981; Van Mierlo, et al., 1998). This is in agreement with conclusions from chapter 4 which suggested that the thermal unfolding of both Campath-1H and 1209W95 involved at least one significantly populated intermediate phase as the ratio of the calorimetric and van't Hoff enthalpies of the unfolding transitions, as determined by DSC ($\Delta H_{vH}/\Delta H_{cal}$), are less than unity (Sturtevant, 1987).

The GdmHCl unfolding curve as monitored by fluorescence spectroscopy also revealed that at low concentrations of denaturant ($[GdmHCl] < 2.5$ M) the Campath-1H molecule is more tightly packed and rigid than at zero denaturant concentration. This was revealed by the fact that the emission spectrum is blue shifted at these low GdmHCl concentrations. Further proof of this phenomenon was obtained by succinimide quenching techniques which resulted in a K_{sv} of 0.98 ± 0.03 M⁻¹ for Campath-1H (pH 6, 0.5 M GdmHCl) compared to a K_{sv} of 1.20 ± 0.08 M⁻¹ in the absence of GdmHCl indicating the tryptophan residues are less accessible when the molecule is exposed to 0.5 M GdmHCl. This finding is in agreement with studies on the effects of GdmHCl on the crystal structure of ribonuclease A by Dunbar et al., (1997). However, this increase in rigidity and mobility is not mirrored by an increase in the T_m as measured by DSC.

0.5 M urea has an unusual effect on the DSC thermogram of Campath-1H (pH 6) as shown in figure 7.4. The urea increases the reversibility of unfolding, causes an apparent

increase in the ΔH_{cal} , and also causes a large decrease in the T_m . The urea unfolding curve obtained by CD suggests that 0.5 M urea exerts no significant structural effects and time constraints prevented further investigation which may have led to a conclusion.

Preliminary isothermal calorimetry results with Campath-1H show the high temperature and concentration dependence of the traces. Our results show that isothermal calorimetry is a valid technique to use to investigate the thermal denaturation of mAbs and, since it offers the advantage of greater simplicity of interpretation of data over DSC it is possible it may lead to greater confidence in the values of the derived kinetic parameters. The main disadvantages though are the necessity for protein solutions of high concentration and also the time involved in carrying out a single experiment and for some workers these disadvantages may prove inhibitory.

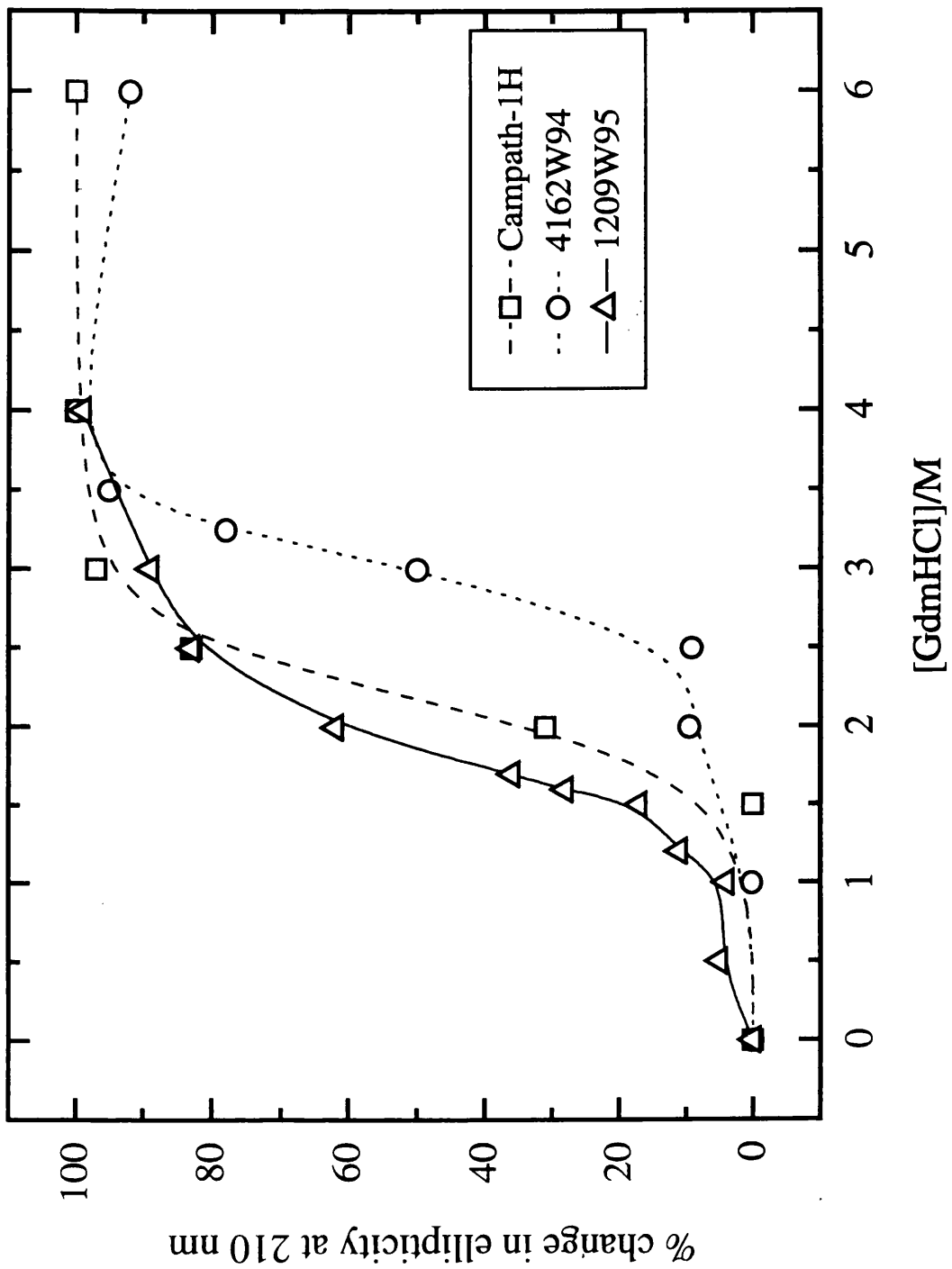


Figure 7.1: GdmHCl unfolding curves for Campath-1H (pH 6), 4162W94 (pH 6) and 1209W95 (pH 8) as monitored by CD. Graph is plotted as the percentage change in ellipticity at 210 nm versus GdmHCl concentration and the midpoints of the curves are 2.5, 3.0, and 1.9 M GdmHCl for Campath-1H, 4162W94 and 1209W95 respectively.

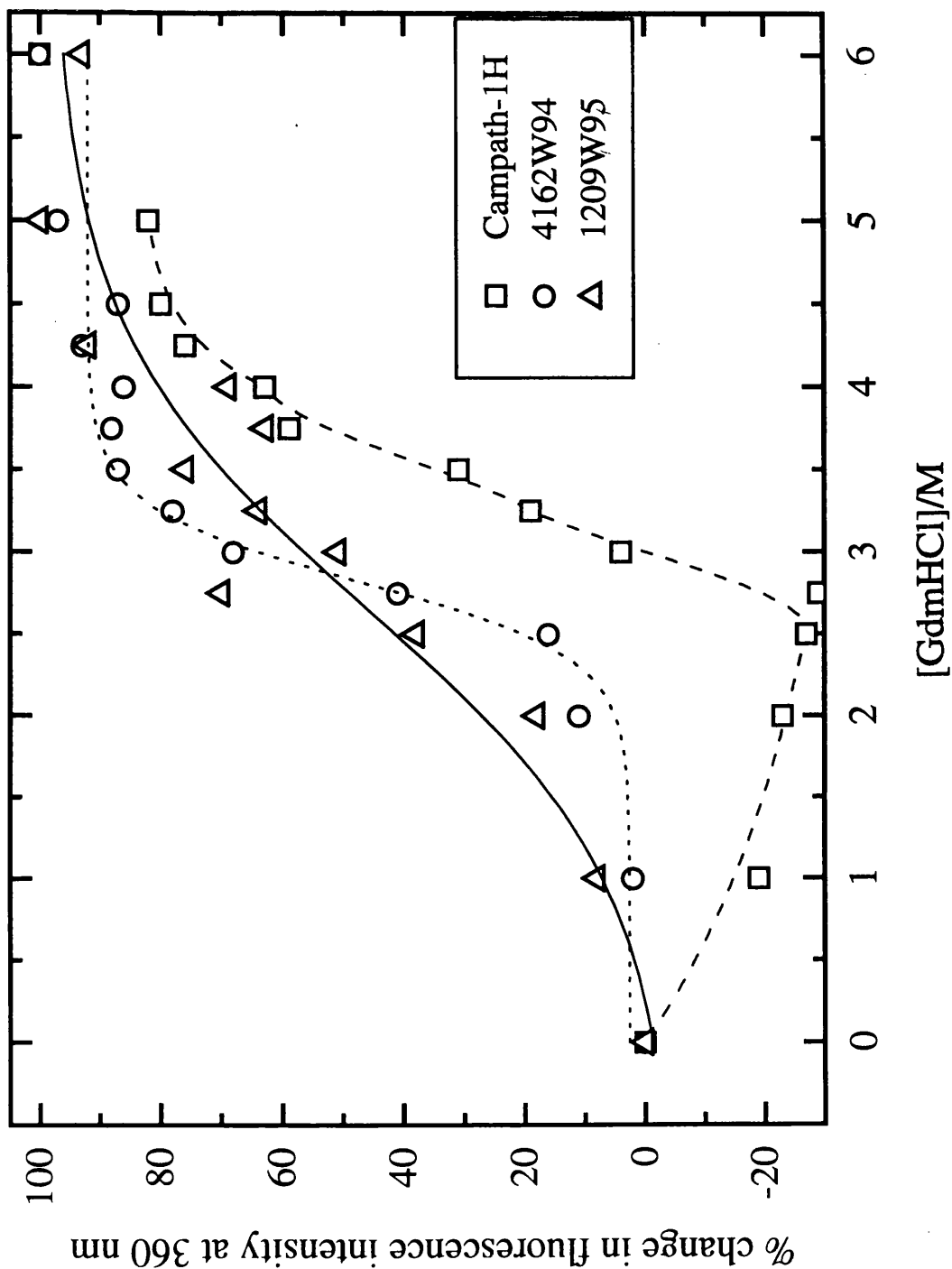


Figure 7.2: GdmHCl unfolding curves for Campath-1H (pH 6), 4162W94 (pH 6) and 1209W95 (pH 8) as monitored by fluorescence spectroscopy. Graph is plotted as the percentage change in fluorescence intensity at 360 nm versus GdmHCl concentration and the midpoints of the curves are 3.5, 2.8, and 2.6 M GdmHCl for Campath-1H, 4162W94 and 1209W95 respectively.

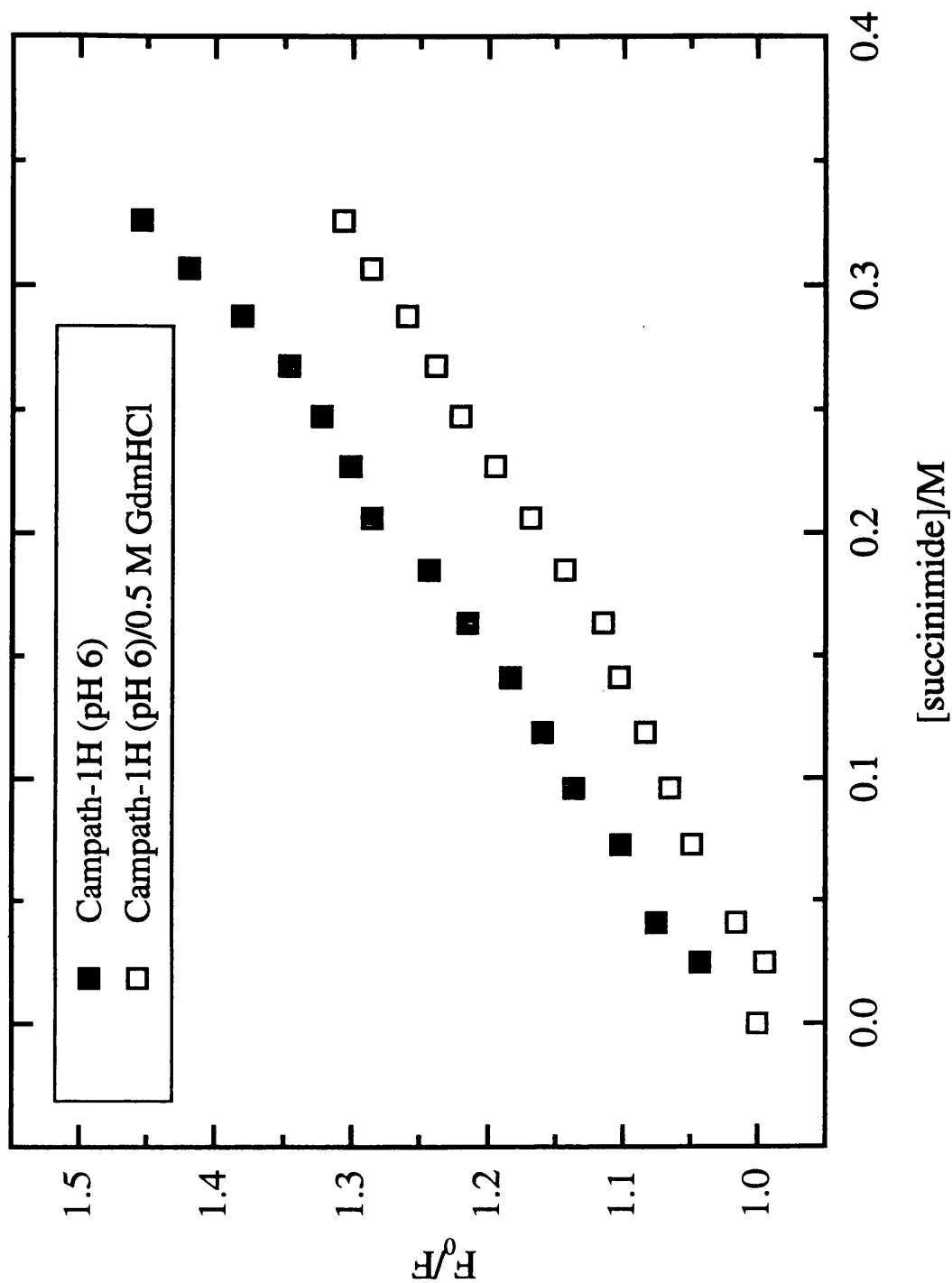


Figure 7.3: Results of succinimide quenching of Campath-1H (pH 6 CBS) and Campath-1H (pH 6 CBS/0.5 M GdmHCl) plotted as a Stern-Volmer plot. K_{sv} values are 1.20 ± 0.08 and $0.98 \pm 0.03 \text{ M}^{-1}$ in the absence and presence of 0.5 M GdmHCl respectively. All data were recorded at 25 °C using an excitation wavelength of 295 nm.

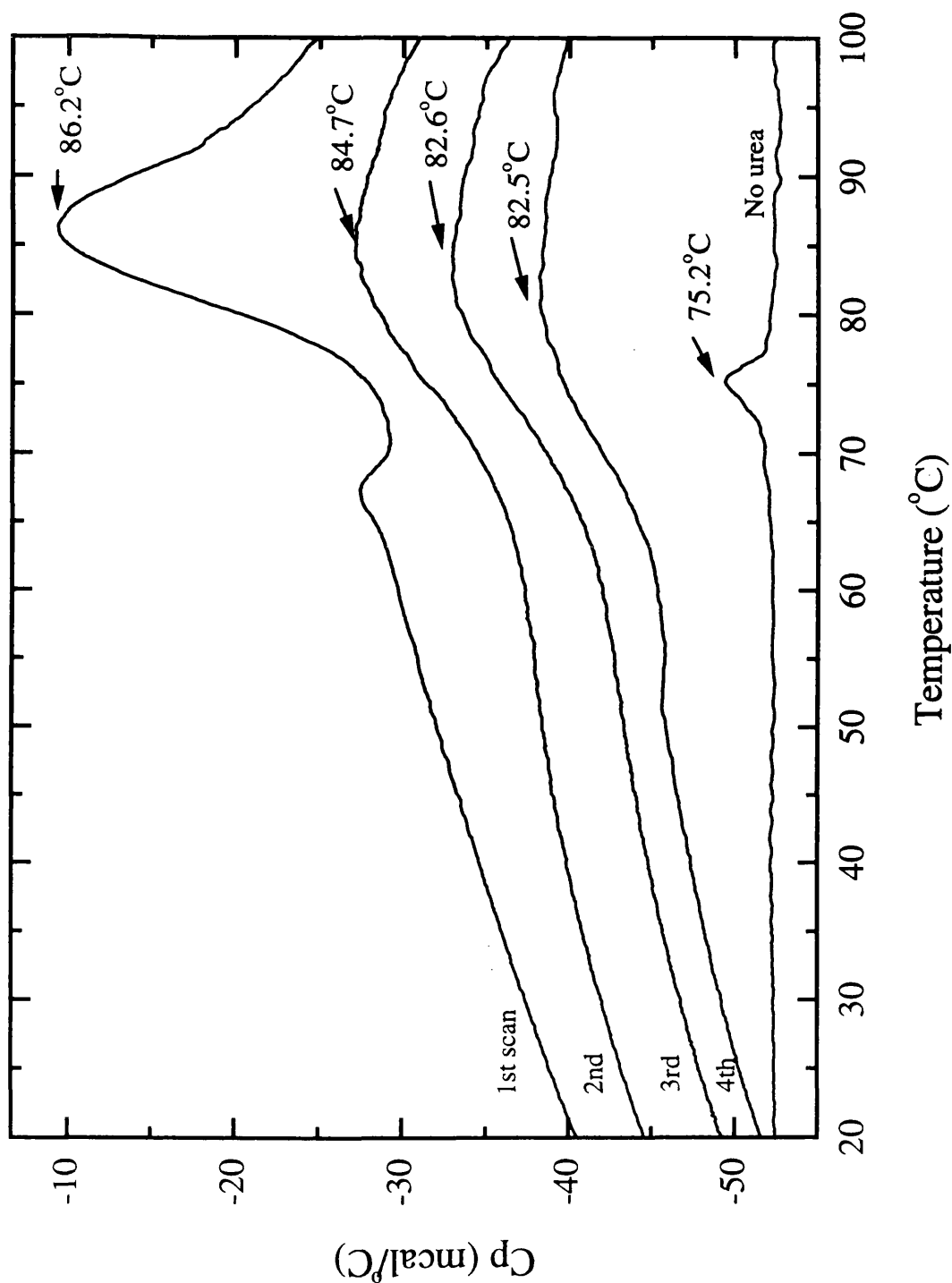


Figure 7.4: Raw DSC data showing effect of 0.5 M urea on the T_m of the main endothermic transition of Campath-1H (pH 6 CBS). Data from four successive scans are shown to illustrate the partial calorimetric reversibility of the transition. A scan performed in the absence of urea is shown on the same scale for comparison.

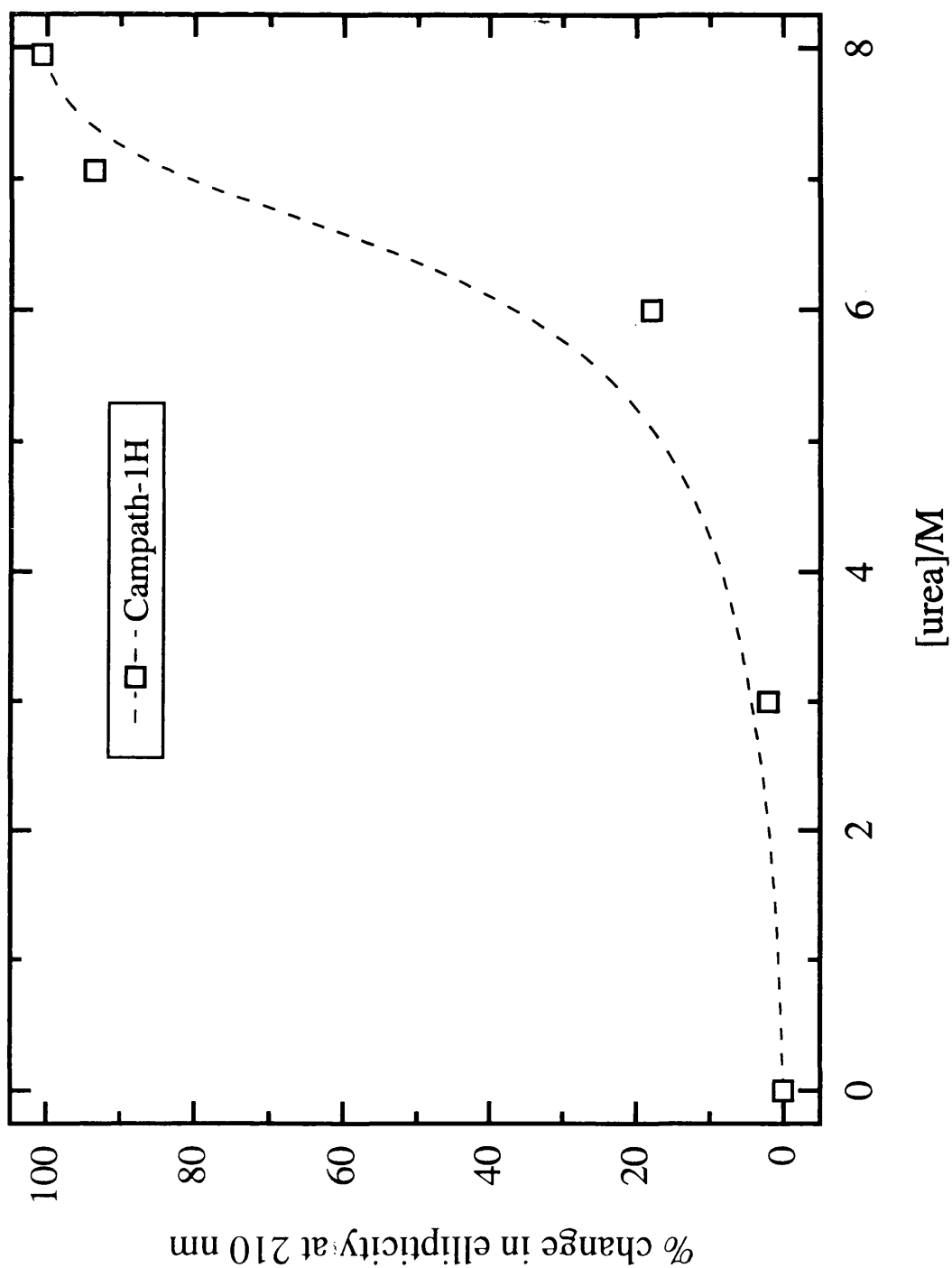


Figure 7.5: Urea unfolding curve for Campath-1H (pH 6) as monitored by CD. Graph is plotted as the percentage change in ellipticity at 210 nm versus urea concentration and the midpoint of the curve is 6.8 M urea.

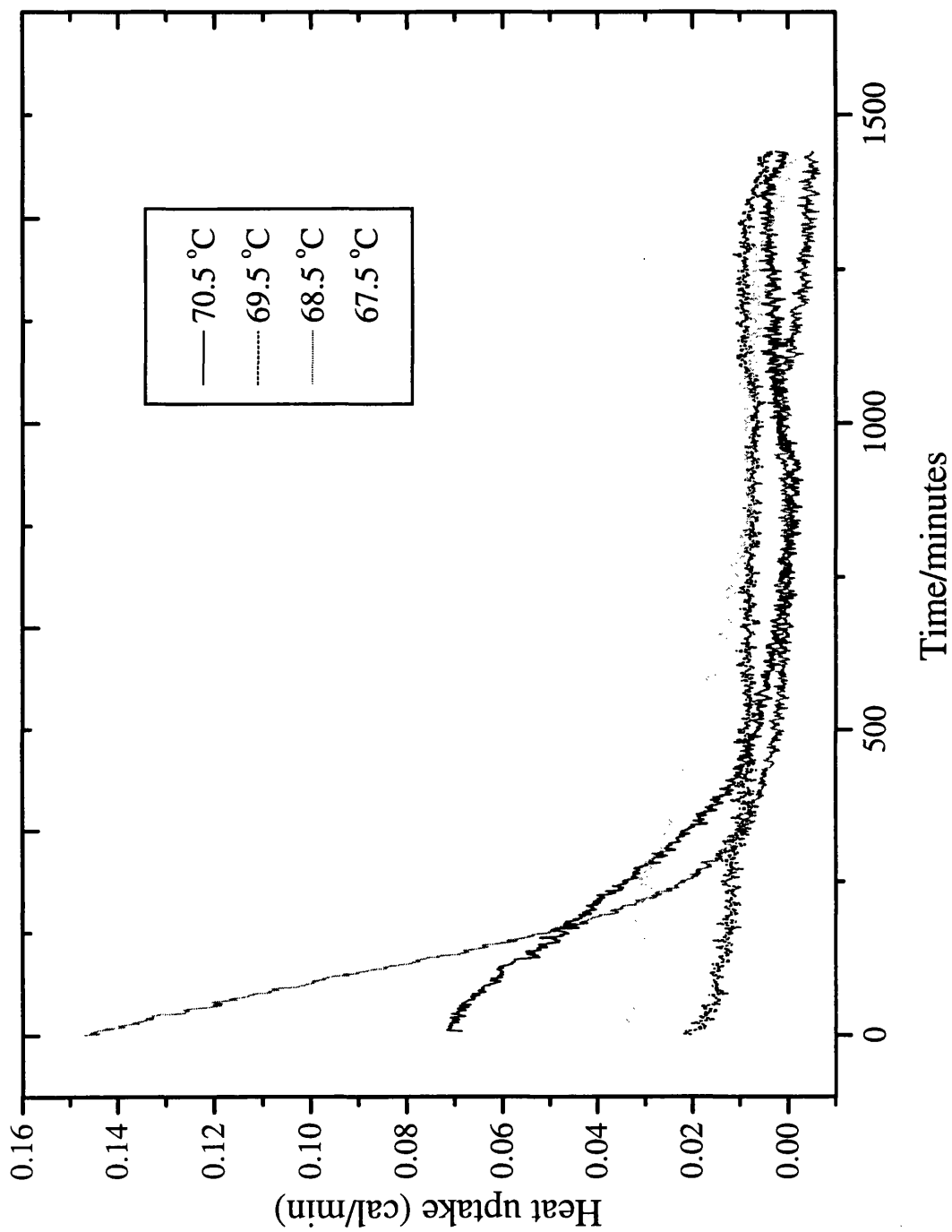


Figure 7.6: Raw isothermal calorimetry data for Campath-1H (0.1054 mM, pH 6 CBS) showing temperature dependence of scans. Four separate traces at 67.5, 68.5, 69.5 and 70.5 °C are shown.

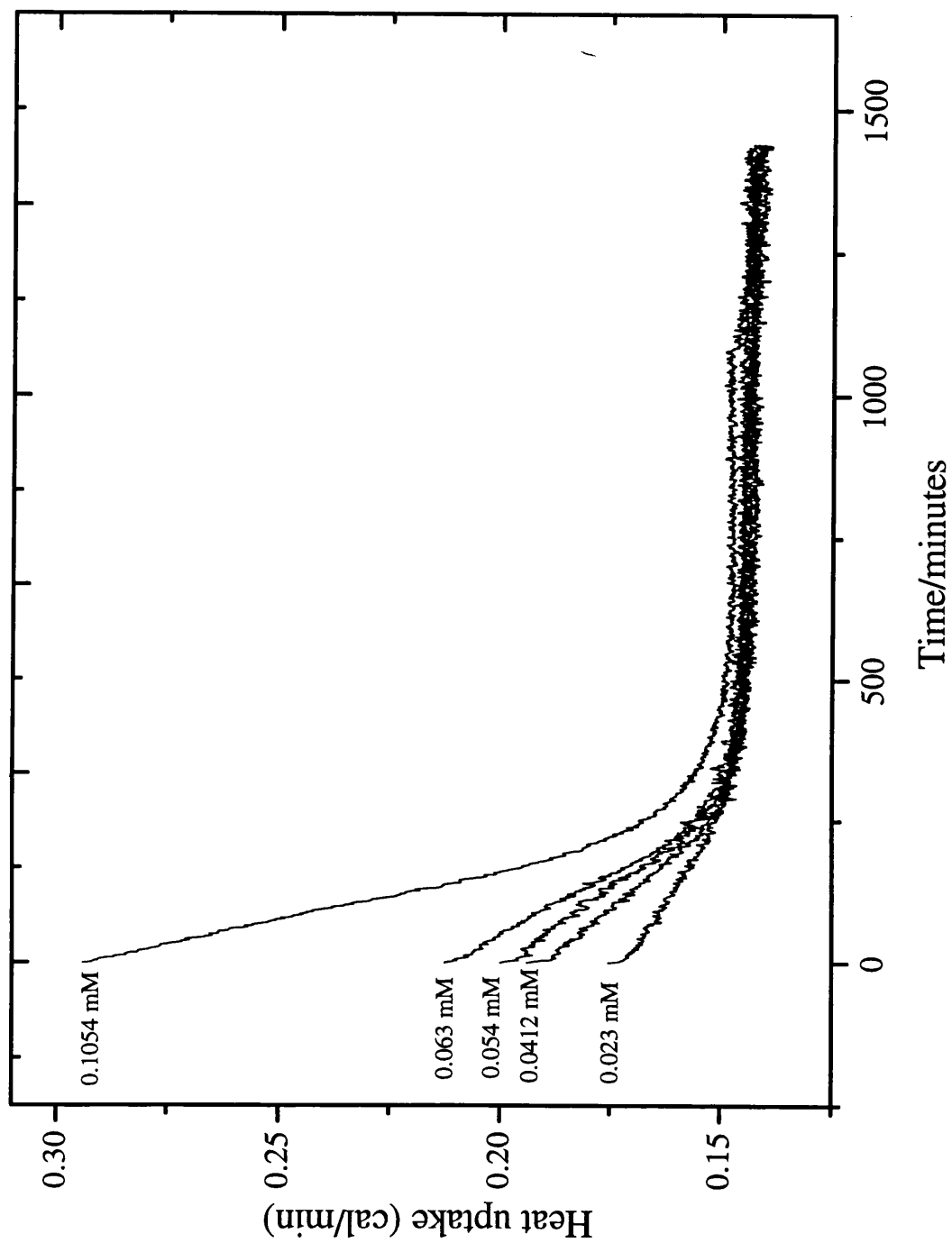


Figure 7.7: Raw isothermal calorimetry data for Campath-1H (pH 6 CBS) at a range of concentrations (0.023, 0.0412, 0.054, 0.063, and 0.1054 mM) showing concentration dependence of data. Data for all traces were collected at 70.5 °C.

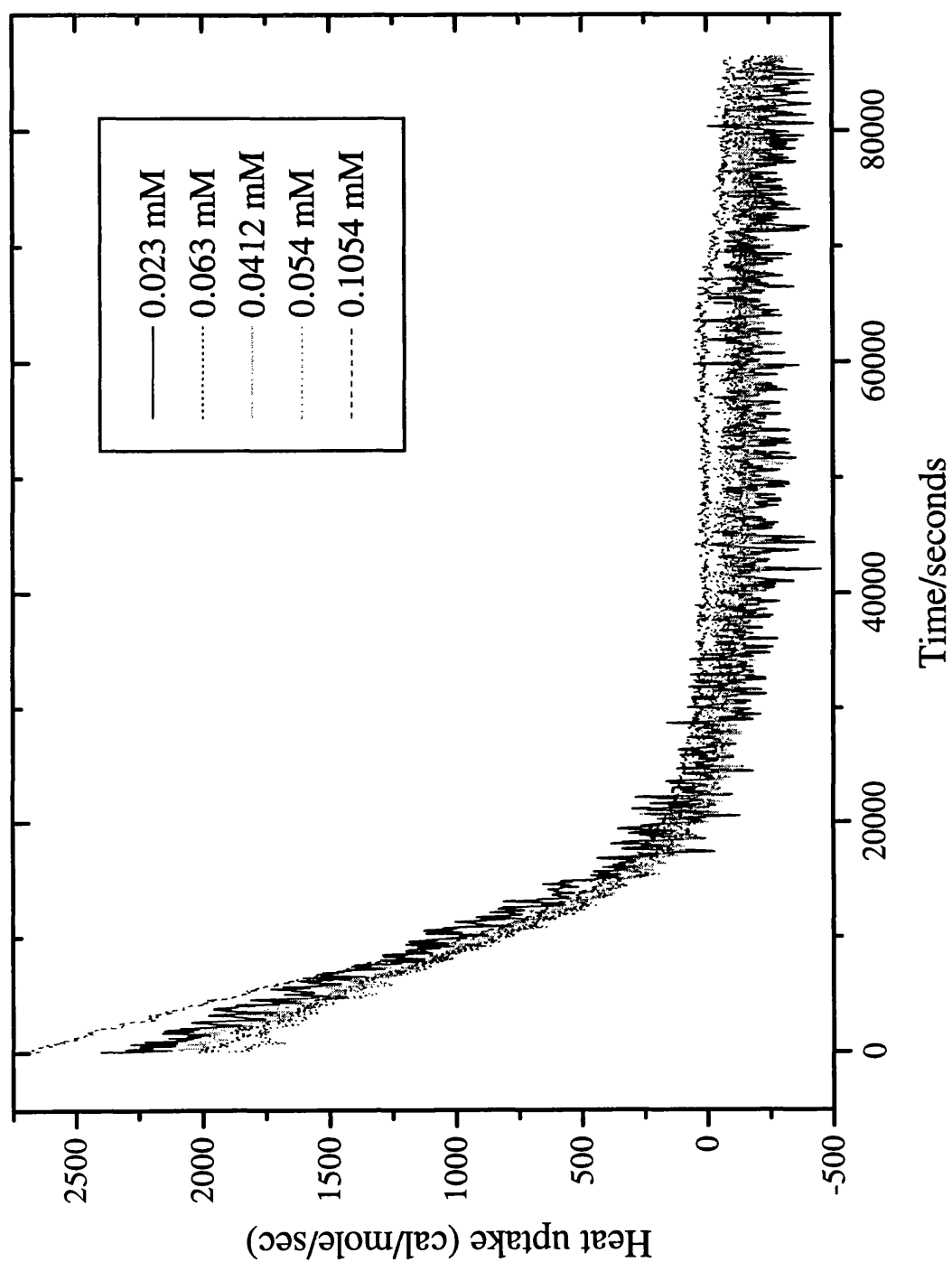


Figure 7.8: Normalized isothermal calorimetry data for Campath-1H (pH 6 CBS) at a range of concentrations (0.023, 0.0412, 0.054, 0.063, and 0.1054 mM) illustrating the concentration dependence of the trace profiles. All data were collected at 70.5 °C.

CHAPTER 8

GENERAL CONCLUSIONS

This thesis has: investigated the stability of mAbs in terms of their thermal characteristics in solution using DSC, CD and fluorescence spectroscopy; compared the effects of pH and additives on the reversibility of thermal denaturation and aggregation; studied the dynamic accessibility of protein groups using fluorescence quenching techniques; related calorimetric and kinetic parameters to the long-term storage properties of these proteins, and applied these techniques to aged samples to examine the long-term effects of additives. A summary of the findings is given below:

- The three mAbs Campath-1H, 4162W94 and 1209W95 thermally unfold in two main steps, both endothermic. The first step involves a small change in tertiary structure, probably some minor domain rearrangement, which is reversible under certain conditions. The second step involves major irreversible changes in both tertiary and secondary structure which is immediately followed by loss of all structure.
- Analysis of the irreversible thermal unfolding of the mAbs allows the calculation of the activation energies and rate constants for the unfolding reaction. These rate constants can then be extrapolated back to physiological conditions and the shelf-life of the protein under these conditions calculated. This half-life is relevant when thermal unfolding is the only mechanism of protein degradation at work.
- The thermal stability of the mAbs can be significantly increased by the addition of mannitol. The cyclodextrins, methyl- β - and hydroxypropyl- β -cyclodextrin both reduce the thermal stability and activation energy required to thermally unfold Campath-1H by binding to residues on the unfolded form of the protein and shifting the equilibrium in favour of this form. The cyclodextrins also have the ability, at high concentrations, to prevent the gross thermal aggregation of the mAbs, probably by masking hydrophobic patches on the unfolded protein.
- The addition of preformed aggregate has no significant effect on either the rate of aggregation or the activation energy of unfolding of Campath-1H which suggests if the formation of Campath-1H aggregate proceeds via a classic nucleation/growth mechanism, then the preformed aggregate used is not suitable as a seed for this process.

This current research updates previous work on the thermal unfolding of mAbs and makes attempts to apply recent work on the kinetic analysis of irreversible protein denaturation to mAbs which are very complex model systems. This thesis sets limits on the usefulness of deriving kinetic data for the purpose of shelf-life calculation and also presents valuable data on the effects of various commonly used and novel formulation additives on the unfolding of these proteins. This work shows the complementary nature of DSC, CD and

Chapter 8

fluorescence spectroscopy as tools for studying protein unfolding, and in terms of protein drug formulation development, shows how these techniques afford data which cannot be arrived at by traditional assays of bioactivity.

REFERENCES

References

Adamson, A.W., *Physical Chemistry of Surfaces*, 2nd edition, 1960, Interscience Publishers, New York, p. 174.

Ahmad, F., and Bigelow, C.C., Thermodynamic Stability of Proteins in Salt Solutions: A Comparison of the Effectiveness of Protein Stabilizers, *Journal of Protein Chemistry*, 1986, **5**, 355-367.

Alexander, A.J., and Hughes, D.E., Monitoring of IgG Antibody Thermal Stability by Micellar Electrokinetic Capillary Chromatography and Matrix-Assisted Laser Desorption/Ionization Mass Spectrometry, *Analytical Chemistry*, 1995, **67**, 3626-3632.

Angberg, M., Nyström, C., and Castensson, S., Evaluation of Heat-Conduction Microcalorimetry in Pharmaceutical Stability Studies VII. Oxidation of Ascorbic Acid in Aqueous Solution, *International Journal of Pharmaceutics*, 1993, **90**, 19-33.

Arriaga, P., Menéndez, M., Villacorta, J.M., and Laynez J., Differential Scanning Calorimetric Study of the Thermal Unfolding of β -Lactamase I from *Bacillus cereus*, *Biochemistry*, 1992, **31**, 6603-6607.

Baker, D., and Agard, D.A., Kinetics versus Thermodynamics in Protein Folding, *Biochemistry*, 1994, **33**, 7505-7509.

Biltonen, R.L., and Freire, E., Thermodynamic Characterization of Conformational States of Biological Macromolecules Using Differential Scanning Calorimetry, *Critical Reviews in Biochemistry*, 1978, **5**, 85-124.

Borrebaeck, C.A.K., 'Antibody Engineering- A Practical Guide', 1992, W.H. Freeman, San Francisco.

Brewster, M.E., Estes, K.S., and Bodor, N., An Intravenous Toxicity Study of 2-hydroxypropyl- β -cyclodextrin, a Useful Drug Solubilizer, in Rats and Monkeys, *International Journal of Pharmaceutics*, 1990, **59**, 231-243.

References

- Brewster, M.E., Hora, M.S., Simpkins, J.W., and Bodor, N., Use of 2-Hydroxypropyl- β -cyclodextrin as a Solubilizing and Stabilizing Excipient for Protein Drugs, *Pharmaceutical Research*, 1991, **8**, 792-795.
- Brewster, M.E., Simpkins, J.W., Hora, M.S., Stern, W.C., and Bodor, N., The Potential Use of Cyclodextrins in Parenteral Formulations, *Journal of Parenteral Science and Technology*, 1989, **43**, 231-240.
- Brouillette, C.G., Tendian, S.W., Heard, B.C., Dunleavy, D., Shorter, A.L., Myszka, D.G., and Chaiken, I.M., Storage Stability of the Solution Formulation of sCD4 Determined by DSC in Comparison with Two Functional Assays, *Journal of Thermal Analysis*, 1996, **47**, 1597-1609.
- Buckton, G., and Beezer, A.E., The Application of Microcalorimetry in the Field of Physical Pharmacy, *International Journal of Pharmaceutics*, 1991, **72**, 181-191.
- Busby, T.F., and Ingham, K.C., Calcium-Sensitive Thermal Transitions and Domain Structure of Human Complement Subcomponent C1r, *Biochemistry*, 1987, **26**, 5564-5571.
- Busby, T.F., and Ingham, K.C., Thermal Stabilization of Antithrombin III by Sugars and Sugar Derivatives and the Effects of Nonenzymatic Glycosylation, *Biochimica et Biophysica Acta*, 1984, **799**, 80-89.
- Carroll, A.R., Rowlands, D.J., and Clarke, B.E., Synthesis and Secretion of a Functional Antibody in a Vaccinia Virus Expression System, *Molecular Immunology*, 1992, **29**, 821-827.
- Chang, B.S., Randall, C.S., and Lee, Y.S., Stabilization of Lyophilized Porcine Pancreatic Elastase, *Pharmaceutical Research*, 1993, **10**, 1478-1483.
- Cheetham, G.M.T., Hale, G., Waldmann, H., and Bloomer, A.C., Crystal Structures of a Rat Anti-CD52 (Campath-1) Therapeutic Antibody Fab Fragment and its Humanized Counterpart, *Journal of Molecular Biology*, 1998, **284**, 85-99.

References

Choy, E.H.S., Clinical Pharmacology and Therapeutic Potential of Monoclonal Antibody Treatment in Rheumatoid Arthritis, *Drugs and Aging*, 1998, **12**, 139-148.

Conejero-Lara, F., Mateo, P.L., Aviles, F.X., and Sánchez-Ruiz, J.M., Effect of Zn²⁺ on the Thermal Denaturation of Carboxypeptidase B, *Biochemistry*, 1991a, **30**, 2067-2072.

Conejero-Lara, F., Sánchez-Ruiz, J.M., Mateo, P.L., Burgos, F.J., Vendrell, J., and Avilés, F.X., Differential Scanning Calorimetric Study of Carboxypeptidase B, Procarboxypeptidase B and its Globular Activation Domain, *European Journal of Biochemistry*, 1991b, **200**, 663-670.

Cooper, A., Effect of Cyclodextrins on the Thermal Stability of Globular Proteins, *Journal of the American Chemical Society*, 1992, **114**, 9208-9209.

Cooper, A., Lovatt, M., and Nutley, M.A., Energetics of Protein-Cyclodextrin Interactions, *Proceedings of the Eighth International Symposium on Cyclodextrins*, 1996, 189-192.

Creighton, T.E., *Proteins: Structures and Molecular Properties*, 2nd edition, W.H. Freeman and Company, New York, 1993.

Crowe, J.S., Hall, V.S., Smith, M.A., Cooper, H.J., and Tite, J.P., Humanized Monoclonal Antibody Campath-1H: Myeloma Cell Expression of Genomic Constructs, Nucleotide Sequence of cDNA Constructs and Comparison of Effector Mechanisms of Myeloma and Chinese Hamster Ovary Cell-Derived Material, *Clin. exp. Immunol.*, 1992, **87**, 105-110.

Dai, H.J., and Krull, I.S., Thermal Stability Studies of Immunoglobulins using Capillary Isoelectric Focusing and Capillary Zone Electrophoretic Methods, *Journal of Chromatography A*, 1998, **807**, 121-128.

Davoodi, J., Wakarchuk, W.W., Surewicz, W.K., and Carey, P.R., Scan-Rate Dependence in Protein Calorimetry: The Reversible Transitions of *Bacillus circulans* Xylanase and a Disulfide-bridge Mutant, *Protein Science*, 1998, **7**, 1538-1544.

References

- Dunbar, J., Yennawar, H.P., Benerjee, S., Luo, J., and Farber, G.K., The Effect of Denaturants on Protein Structure, *Protein Science*, 1997, **6**, 1727, 1733.
- Eftink, M.R., and Ghiron, C.A., Exposure of Tryptophanyl Residues in Proteins. Quantitative Determination by Fluorescence Quenching Studies, *Biochemistry*, 1976a, **15**, 672-680.
- Eftink, M.R., and Ghiron, C.A., Fluorescence Quenching of Indole and Model Micelle Systems, *The Journal of Physical Chemistry*, 1976b, **80**, 486-493.
- Eftink, M.R., and Ghiron, C.A., Fluorescence Quenching Studies with Proteins, *Analytical Biochemistry*, 1981, **114**, 199-227.
- Eftink, M.R., and Ghiron, C.A., Indole Fluorescence Quenching Studies on Proteins and Model Systems: Use of the Inefficient Quencher Succinimide, *Biochemistry*, 1984, **23**, 3891-3899.
- Farah, R.A., Clinchy, B., Herrera, L., and Vitetta, E.S., The Development of Monoclonal Antibodies for the Therapy of Cancer, *Critical Reviews in Eukaryotic Gene Expression*, 1998, **8**, 321-356.
- Fatouros, A., Österberg, T., and Mikaelsson, M., Recombinant Factor VIII SQ—Inactivation Kinetics in Aqueous Solution and the Influence of Disaccharides and Sugar Alcohols, *Pharmaceutical Research*, 1997a, **12**, 1679-1684.
- Fatouros, A., Österberg, T., and Mikaelsson, M., Recombinant Factor VIII SQ—Influence of Oxygen, Metal Ions, pH and Ionic Strength on Its Stability in Aqueous Solution, *International Journal of Pharmaceutics*, 1997b, **155**, 121-131.
- Freire, E., and Biltonen, R.L., Statistical Mechanical Deconvolution of Thermal Transitions in Macromolecules. 1. Theory and Application to Homogeneous Systems, *Biopolymers*, 1978, **17**, 436-479.

References

Freire, E., van Osdol, W.W., Mayorga, O.L., and Sánchez-Ruiz, J.M., Calorimetrically Determined Dynamics of Complex Unfolding Transitions in Proteins, *Ann. Rev. Biophys. Biophys. Chem.*, 1990, **19**, 159-188.

Freskgård, P.-O., Petersen, L.C., Gabriel, D.A., Li, X., and Persson, E., Conformational Stability of Factor VIIa: Biophysical Studies of Thermal and Guanidine Hydrochloride-Induced Denaturation, *Biochemistry*, 1998, **37**, 7203-7212.

Galisteo, M.L., and Sánchez-Ruiz, J.M., Kinetic Study into the Irreversible Thermal Denaturation of Bacteriorhodopsin, *European Biophysics Journal*, 1993, **22**, 25-30.

Galisteo, M.L., Conejero-Lara, F., Núñez, J., Sánchez-Ruiz, J.M., and Mateo, P.L., A Calorimetric Approach to the Kinetics of the Irreversible Denaturation of Proteins, *Thermochimica Acta*, 1992, **199**, 147-157.

Galisteo, M.L., Mateo, P.L., and Sánchez-Ruiz, J.M., Kinetic Study on the Irreversible Thermal Denaturation of Yeast Phosphoglycerate Kinase, *Biochemistry*, 1991, **30**, 2061-2066.

Garda-Salas, A.L., Santamariá, R.I., Marcos, M.J., Zhadan, G.G., Villar, E., and Shnyrov, V.L., Differential Scanning Calorimetry of the Irreversible Thermal Denaturation of Cellulase from *Streptomyces halstedii* JM8, *Biochemistry and Molecular Biology International*, 1996, **38**, 161-170.

Giancola, C., De Sena, C., Fessas, D., Graziano, G., and Barone, G., DSC Studies on Bovine Serum Albumin Denaturation. Effects of Ionic Strength and SDS Concentration, *International Journal of Biological Macromolecules*, 1997, **20**, 193-204.

Gill, S.C., and von Hippel, P.H., Calculation of Protein Extinction Coefficients from Amino Acid Sequence Data, *Analytical Biochemistry*, 1989, **182**, 319-326.

Glennner, G.G., Ein, D., Eanes, E.D., Bladen, H.A., Terry, W., and Page, D.L., Creation of "Amyloid" Fibrils from Bence Jones Proteins *In Vitro*, *Science*, 1971, **174**, 712-714.

References

- Goding, J.W., 'Monoclonal Antibodies: Principles and Practice', 3rd edition, 1996, Academic Press, New York.
- Gombotz, W.R., Pankey, S.C., Phan, D., Drager, R., Donaldson, K., Antonsen, K.P., Hoffman, A.S., and Raff, H.V., The Stabilization of a Human IgM Monoclonal Antibody with Poly(vinylpyrrolidone), *Pharmaceutical Research*, 1994, **11**, 624-632.
- Guha, S., and Bhattacharyya, B., A Partially Unfolded Intermediate During Tubulin Unfolding: Its Detection and Spectroscopic Characterization, *Biochemistry*, 1995, **34**, 6925-6931.
- Hale, G., Bright, S., Chumbley, G., Hoang, T., Metcalf, D., Munro, A.J., and Waldmann, H., Removal T-Cells from Bone Marrow for Transplantation- A Monoclonal Anti-Lymphocyte Antibody that Fixes Human Complement, *Blood*, 1983, **62**, 873-882.
- Hale, G., Rye, P.D., Warford, A., Lauder, I., and Britobabapulle, A., The Glycosylphosphatidylinositol-Anchored Lymphocyte Antigen CDw52 is Associated with the Epididymal Maturation of Human Spermatozoa, *Journal of Reproductive Immunology*, 1993, **23**, 189-205.
- Hansen, L.D., Lewis, E.A., Eatough, D.J., Bergstrom, R.G., and DeGraft-Johnson, D., Kinetics of Drug Decomposition by Heat Conduction Calorimetry, *Pharmaceutical Research*, 1989, **6**, 20-27.
- Harper, J.D., and Lansbury, P.T., Models of Amyloid Seeding in Alzheimer's Disease and Scrapie: Mechanistic Truths and Physiological Consequences of the Time-Dependent Solubility of Amyloid Proteins, *Ann. Rev. Biochem.*, 1997, **66**, 385-407.
- Harris, L.J., Larson, S.B., Hasel, K.W., Day, J., Greenwood, A., and McPherson, A., The Three-Dimensional Structure of an Intact Monoclonal Antibody for Canine Lymphoma, *Nature*, 1992, **360**, 369-372.

References

- Hoffmann, M.A.M., van Miltenburg, J.C., van der Eerden, J.P., van Mil, P.J.J.M., and de Kruif, C.G., Isothermal and Scanning Calorimetry Measurements on β -Lactoglobulin, *Journal of Physical Chemistry B*, 1997, **101**, 6988-6994.
- Ingham, K.C., Brew, S.A., Migliorini, M.M., and Busby, T.F., Binding of Heparin by Type-III Domains and Peptides from the Carboxy-Terminal Hep-2 Region of Fibronectin, *Biochemistry*, 1993, **32**, 12548-12553.
- Inglis, A.S., Cleavage at Aspartic Acid, *Methods in Enzymology*, 1983, **91**, 324-332.
- Isaacs, J.D., Watts, R.A., Hazleman, B.L., Hale, G., Keogan, M.T., Cobbold, S.P., and Waldmann, H., Humanised Monoclonal Antibody Therapy for Rheumatoid Arthritis, *Lancet*, 1992, **340**, 748-752.
- Jackson, W.M., and Brandts, J.F., Thermodynamics of Protein Denaturation. A Calorimetric Study of the Reversible Denaturation of Chymotrypsinogen and Conclusions Regarding the Accuracy of the Two-State Approximation, *Biochemistry*, 1970, **9**, 2294-2301.
- Jiskoot, W., Beuvery, E.C., de Koning, A.A.M., Herron, J.N., and Crommelin, D.J.A., Analytical Approaches to the Study of Monoclonal Antibodies, *Pharmaceutical Research*, 1990, **7**, 1234-1241.
- Johnson, D.M., Pritchard, R.A., Taylor, W.F., Conley, D., Zyniga, G., and McGreevy, K.G., Degradation of the LH-RH Analog Nafarelin Acetate in Aqueous Solution, *International Journal of Pharmacy*, 1986, **31**, 125.
- Kaneko, K., Wille, H., Melhorn, I., Zhang, H., Ball, H., Cohen, F.E., Baldwin, M.A., and Prusiner, S.B., Molecular Properties of Complexes Formed Between the Prion Protein and Synthetic Peptides, *Journal of Molecular Biology*, 1997, **270**, 574-586.
- Kats, M., Richberg, P.C., and Hughes, D.E., Conformational Diversity and Conformational Transitions of a Monoclonal Antibody Monitored by Circular Dichroism and Capillary Electrophoresis, *Analytical Chemistry*, 1995, **67**, 2943-2948.

References

Kats, M., Richberg, P.C., and Hughes, D.E., pH-Dependent Isoform Transitions of a Monoclonal Antibody Monitored By Micellar Electrokinetic Capillary Chromatography, *Analytical Chemistry*, 1997, **69**, 338-343.

Kelly, S.M., and Price, N.C., The Application of Circular Dichroism to Studies of Protein Folding and Unfolding, *Biochimica et Biophysica Acta*, 1997, **1338**, 161-185.

Koenigbauer, M.J., Pharmaceutical Applications of Microcalorimetry, *Pharmaceutical Research*, 1994, **11**, 777-783.

Köhler, G., and Milstein, C., Continuous Cultures of Fused Cells Secreting Antibody of Predefined Specificity, *Nature*, 1975, **256**, 495-497.

Kravchuk, Z.I., Chumanevich, A.A., Vlasov, A.P., and Martsev, S.P., Two High-Affinity Monoclonal IgG2a Antibodies with Differing Thermodynamic Stability Demonstrate Distinct Antigen-Induced Changes in Protein A-binding Affinity, *Journal of Immunological Methods*, 1998, **217**, 131-141.

Kreimer, D.I., Shnyrov, V.L., Villar, E., Silman, I., and Weiner, L., Irreversible Thermal Denaturation of *Torpedo californica* Acetylcholinesterase, *Protein Science*, 1995, **4**, 2349-2357.

Laemmli, U.K., Cleavage of Structural Proteins During the Assembly of the Head of Bacteriophage-T4, *Nature*, 1970, **227**, 680-685.

La Rosa, C., Milardi, D., Grasso, D., Guzzi, R., and Sportelli, L., Thermodynamics of the Thermal Unfolding of Azurin, *Journal of Physical Chemistry*, 1995, **99**, 14864-14870.

Landon, M., Cleavage at Aspartyl-Prolyl Bonds, *Methods in Enzymology*, 1977, **47**, 145-149.

Le Bihan, T., and Gicraud, C., Kinetic Study of the Thermal Denaturation of G Actin Using Differential Scanning Calorimetry and Intrinsic Fluorescence Spectroscopy, *Biochemical and Biophysical Research Communications*, 1993, **194**, 1065-1073.

References

- Lee, J.C., and Timasheff, S.N., The Stabilization of Proteins by Sucrose, *Journal of Biological Chemistry*, 1981, **256**, 7193-7201.
- Lehrer, S.S., Solute Perturbation of Protein Fluorescence. The Quenching of the Tryptophyl Fluorescence of Model Compounds and of Lysozyme by Iodide Ion, *Biochemistry*, 1971, **10**, 3254-3263.
- Lepock, J.R., Ritchie, K.P., Kolios, M.C., Rodahl, A.M., Heinz, K.A., and Kruuv, J., Influence of Transition Rates and Scan Rate on Kinetic Simulations of Differential Scanning Calorimetry Profiles of Reversible and Irreversible Protein Denaturation, *Biochemistry*, 1992, **31**, 12706-12712.
- Lepock, J.R., Rodahl, A.M., Zhang, C., Heynen, M.L., Waters, B., and Cheng, K.-H., Thermal Denaturation of the Ca²⁺-ATPase of Sarcoplasmic Reticulum Reveals Two Thermodynamically Independent Domains, *Biochemistry*, 1990, **29**, 681-689.
- Li, S. and Purdy, W.C., Cyclodextrins and Their Applications in Analytical Chemistry, *Chemical Reviews*, 1992, **92**, 1457-1470.
- Lim, S.H., Davey, G., and Marcus, R., Differential Response in a Patient Treated with Campath-1H Monoclonal Antibody for Refractory non-Hodgkin Lymphoma, *Lancet*, 1993, 432-433.
- Lin, T., and Timasheff, S.N., Why Do Some Organisms Use a Urea-Methylamine Mixture as Osmolyte? Thermodynamic Compensation of Urea and Trimethylamine *N*-Oxide Interactions with Protein, *Biochemistry*, 1994, **33**, 12695-12701.
- Loseva, O.I., Tischenko, V.M., Olsovská, Z., Franek, F., and Zav'yalov, V.P., Correlation of the Character of Intramolecular Melting with Digestibility by Pepsin in Precipitating and Non-Precipitating Pig Anti-Dnp Antibodies, *Molecular Immunology*, 1986, **23**, 743-746.
- Lumry, R., and Eyring, H., Conformation Changes of Proteins, *Journal of Physical Chemistry*, 1953, **58**, 110-120.

References

- Ma, C.-Y., and Harwalkar, V.R., Effects of Medium and Chemical Modification on Thermal Characteristics of β -Lactoglobulin, *Journal of Thermal Analysis*, 1996, **47**, 1513-1525.
- MacRitchie, F., Proteins at Interfaces, *Advances in Protein Chemistry*, 1978, **32**, 283.
- Manly, S.P., Matthews, K.S., and Sturtevant, J.M., Thermal Denaturation of the Core Protein of *lac* Repressor, *Biochemistry*, 1985, **24**, 3842-3846.
- Manning, M.C., Patel, K., and Borchardt, R.T., Stability of Protein Pharmaceuticals, *Pharmaceutical Research*, 1989, **6**, 903-918.
- Matthews, C.R., and Crisanti, M.M., Urea-Induced Unfolding of the α Subunit of Tryptophan Synthase: Evidence for a Multistate Process, *Biochemistry*, 1981, **20**, 784-792.
- Milardi, D., La Rosa, C., Grasso, D., Guzzi, R., Sportelli, L., and Fini, C., Thermodynamics and Kinetics of the Thermal Unfolding of Plastocyanin, *European Biophysics Journal*, 1998, **27**, 273-282.
- Morin, P.E., Diggs, D., and Freire, E., Thermal Stability of Membrane-Reconstituted Yeast Cytochrome *c* Oxidase, *Biochemistry*, 1990, **29**, 781-788.
- Nisonoff, A., Hopper, J.E., and Spring, S.B., 'The Antibody Molecule', 1975, Academic Press, New York.
- Nozaki, Y., The Preparation of Guanidine Hydrochloride, *Methods in Enzymology*, 1972, **26**, 43-50.
- Page, M.J., and Sydenham, M.A., High Level Expression of the Humanized Monoclonal Antibody Campath-1H in Chinese Hamster Ovary Cells, *Biotechnology*, 1991, **9**, 64-68.
- Panchal, R.G., Novel Therapeutic Strategies to Selectively Kill Cancer Cells, *Biochemical Pharmacology*, 1998, **55**, 247-252.

References

- Paushkin, S.V., Kushnirov, V.V., Smirnov, V.N., and Ter-Avanesyan, M.D., *In Vitro* Propagation of the Prion-Like State of Yeast Sup35 Protein, *Science*, 1997, **277**, 381-383.
- Picó, G.A., Thermal Stability of Human Serum Albumin by Sodium Halide Salts, *Biochemistry and Molecular Biology International*, 1996, **38**, 1-6.
- Plaza del Pino, I.M., and Sánchez-Ruiz, J.M., An Osmolyte Effect on the Heat Capacity Change for Protein Folding, *Biochemistry*, 1995, **34**, 8621-8630.
- Poljak, R.J., Amzel, L.M., Avey, H.P., Chen, B.L., Phizackerley, R.P., and Sau, F., Three-Dimensional Structure of the Fab' Fragment of a Human Immunoglobulin at 2.8 Å Resolution, *Proc. Natl Acad. Sci. USA*, 1973, **70**, 3305-3310.
- Privalov, P.L., and Gill, S.J., Stability of Protein Structure and Hydrophobic Interaction, *Advances in Protein Chemistry*, 1988, **39**, 191-234.
- Privalov, P.L., and Khechinashvili, N.N., A Thermodynamic Approach to the Problem of Stabilization of Globular Protein Structure: A Calorimetric Study, *Journal of Molecular Biology*, 1974, **86**, 665-684.
- Privalov, P.L., and Potekhin, S.A., Scanning Microcalorimetry in Studying Temperature-Induced Changes in Proteins, *Methods in Enzymology*, 1986, **131**, 4-51.
- Privalov, P.L., Scanning Microcalorimeters for Studying Macromolecules, *Pure and Applied Chemistry*, 1980, **52**, 479-497.
- Privalov, P.L., Stability of Proteins: Proteins Which Do Not Present a Single Cooperative System, *Advances in Protein Chemistry*, 1982, **35**, 1-104.
- Privalov, P.L., Thermal Investigations of Biopolymer Solutions and Scanning Microcalorimetry, *FEBS Letters*, 1974, **40**, S140-S153.

References

- Ptitsyn, O.B., Pain, R.H., Semisotnov, G.V., Zerovnik, E., and Razgulyaev, O.I., Evidence for a Molten Globule State as a General Intermediate State in Protein Folding, *FEBS Letters*, 1990, **262**, 20-24.
- Reichmann, L., Clarke, M., Waldmann, H., and Winter, G., Reshaping Human Antibodies for Therapy, *Nature*, 1988, **332**, 323-327.
- Remmele, R.L., Nightlinger, N.S., Srinivasan, S., and Gombotz, W.R., Interleukin-1 Receptor (IL-1R) Liquid Formulation Development Using Differential Scanning Calorimetry, *Pharmaceutical Research*, 1998, **15**, 200-208.
- Ritter, M.A., and Ladyman, H.M., 'Monoclonal Antibodies. Production, Engineering and Clinical Application, 1995, Cambridge University Press, Cambridge.
- Roefs, S.P.F.M., and de Kruif, K.G., A Model for the Denaturation and Aggregation of β -Lactoglobulin, *European Journal of Biochemistry*, 1994, **226**, 883-889.
- Rowan, W., Tite, J., Topley, P., and Brett, S.J., Cross-linking of the Campath-1 Antigen (CD52) Mediates Growth Inhibition in Human B- and T-lymphoma Cell Lines, and Subsequent Emergence of CD52-deficient Cells, *Immunology*, 1998, **95**, 427-436.
- Ryazantsev, S., Tishchenko, V., Vasiliev, V., Zav'yalov, V., and Abramov, V., Structure of Human Myeloma IgG3 K κ , *European Journal of Biochemistry*, 1990, **190**, 393-399.
- Sánchez-Ruiz, J.M., López-Lacomba, J.L., Cortijo, M., and Mateo, P.L., Differential Scanning Calorimetry of the Irreversible Thermal Denaturation of Thermolysin, *Biochemistry*, 1988a, **27**, 1648-1652.
- Sánchez-Ruiz, J.M., Lopez-Lacomba, J.L., Mateo, P.L., Vilanova, M., Serra, M.A., and Aviles, F.X., Analysis of the Thermal Unfolding of Porcine Procarboxypeptidase A and its Functional Pieces by Differential Scanning Calorimetry, *European Journal of Biochemistry*, 1988b, **176**, 225-230.

References

- Sánchez-Ruiz, J.M., Theoretical Analysis of Lumry-Eyring Models in Differential Scanning Calorimetry, *Biophysical Journal*, 1992, **61**, 921-935.
- Sandu, C., and Singh, R.K., Modeling Differential Scanning Calorimetry, *Thermochimica Acta*, 1990, **159**, 267-298.
- Santoro, M.M., Liu, Y., Khan, S.M.A., Hou, L., and Bolen., D.W., Increased Thermal Stability of Proteins in the Presence of Naturally Occurring Osmolytes, *Biochemistry*, 1992, **31**, 5278-5283.
- Shnyrov, V.L., and Mateo, P.L., Thermal Transitions in the Purple Membrane from *Halobacterium halobium*, *FEBS Letters*, 1993, **324**, 237-240.
- Shnyrov, V.L., Marcos, M.J., and Villar, E., Kinetic Study on the Irreversible thermal Denaturation of Lentil Lectin, *Biochemistry and Molecular Biology International*, 1996, **39**, 647-656.
- Shnyrov, V.L., Sánchez-Ruiz, J.M., Boiko, B.N., Zhadan, G.G., and Permyakov, E.A., Applications of Scanning Microcalorimetry in Biophysics and Biochemistry, *Thermochimica Acta*, 1997, 165-180.
- Stern, O., and Volmer, M., *Physikalische Zeitschrift*, 1919, **20**, 183.
- Sturtevant, J.M., Biochemical Applications of Differential Scanning Calorimetry, *Annual Reviews of Physical Chemistry*, 1987, **38**, 463-488.
- Sturtevant, J.M., Some Applications of Calorimetry in Biochemistry and Biology, *Annual Reviews of Biophysics and Bioengineering*, 1974, **3**, 35-51.
- Szejtli, J., Cyclodextrins in Drug Formulations: Part II, *Pharmaceutical Technology*, August 1991, 24-28.
- Teale, F.W.J., and Badley, R.A., Depolarization of the Intrinsic and Extrinsic Fluorescence of Pepsinogen and Pepsin, *Biochemistry Journal*, 1970, **116**, 341-348.

References

- Tenold, R.A., Intravenously Injectable Immune Serum Globulin, *U.S. Patent 4,396,608*, (1983).
- Timasheff, S.N. and Arakawa, T., in *Protein Structure: A Practical Approach*, Ed. Creighton, T.E., IRL Press, Oxford, (1989).
- Tischenko, V.M., Zav'yalov, V.P., Medgyesi, G.A., Potekhin, S.A., and Privalov, P.L., A Thermodynamic Study of Cooperative Structures in Rabbit Immunoglobulin G, *European Journal of Biochemistry*, 1982, **126**, 517-521.
- Trail, P.A., Willner, D., Knipe, J., Henderson, A.J., Lasch, S.J., Zoeckler, M.E., *et al*, Effect of Linker Variation on the Stability, Potency, and Efficacy of Carcinoma-Reactive BR64-Doxorubicin Immunoconjugates, *Cancer Research*, 1997, **57**, 100-105.
- Treumann, A., Lifely, M.R., Schneider, P., and Ferguson, M.A.J., Primary Structure of CD52, *The Journal of Biological Chemistry*, 1995, **270**, 6088-6099.
- Underwood, P.A., and Bean, P.A., The Influence of Methods of Production, Purification and Storage of Monoclonal Antibodies Upon Their Observed Specificities, *Journal of Immunological Methods*, 1985, **80**, 189-197.
- Usami, A., Ohtsu, A., Takahama, S., and Fujii, T., The Effect of pH, Hydrogen Peroxide and Temperature on the Stability of Human Monoclonal Antibody, *Journal of Pharmaceutical and Biomedical Analysis*, 1996, **14**, 1133-1140.
- Van Mierlo, C.P.M., Van Dongen, W.M.A.M., Vergeldt, F., Van Berkel, W.J.H., and Steensma, E., The Equilibrium Unfolding of *Azotobacter vinelandii* Apoflavodoxin II Occurs via a Relatively Stable Folding Intermediate, *Protein Science*, 1998, **7**, 2331-2344.
- Vogl, T., Jatzke, C., and Hinz, H.-J., Thermodynamic Stability of Annexin V E17G: Equilibrium Parameters from an Irreversible Unfolding Reaction, *Biochemistry*, 1997, **36**, 1657-1668.

References

Vuilleumier, S., Sancho, J., Loewenthal, R., and Fersht, A.R., Circular Dichroism Studies of Barnase and Its Mutants: Characterization of the Contribution of Aromatic Side Chains, *Biochemistry*, 1993, **32**, 10303-10313.

Wang, Y.-C.J., and Hanson, M.A., Parenteral Formulations of Proteins and Peptides: Stability and Stabilizers, *Journal of Parenteral Science and Technology*, 1988, **42** (supplement), S4-S26.

Waters, D.N., and Paddy, J.L., Equations for Isothermal Differential Scanning Calorimetric Curves, *Analytical Chemistry*, 1988, **60**, 53-57.

Weinblatt, M.E., Maddison, P.J., Bulpitt, K.J., Hazleman, B.L., Urowitz, M.B., Sturrock, R.D., Coblyn, J.S., Maier, A.L., Spreen, W.R., Manna, V.K., and Johnston, J.M., Campath-1H, a Humanized Monoclonal Antibody, in Refractory Rheumatoid Arthritis, *Arthritis and Rheumatism*, 1995, **38**, 1589-1594.

Wong, K.-P., and Tanford, C., Denaturation of Bovine Carbonic Anhydrase B by Guanidine Hydrochloride, *The Journal of Biological Chemistry*, 1973, **248**, 8518-8523.

Xia, M.-Q., Hale, G., Lively, M.R., Ferguson, M.A.J., Campbell, D., Packman, L., and Waldmann, H., Structure of the Campath-1H Antigen, a Glycosylphosphatidylinositol-Anchored Glycoprotein which is an Exceptionally Good Target for Complement Lysis, *Biochemistry Journal*, 1993, **293**, 633-640.

Zhadan, G.G., and Shnyrov, V.L., Differential Scanning Calorimetric Study of the Irreversible Thermal Denaturation of 8 kDa Cytotoxin from the Sea Anemone *Radianthus macrodactylus*, *Biochemistry Journal*, 1994, **299**, 731-733.

